universität wien

MASTERARBEIT / MASTER'S THESIS

Titel der Masterarbeit / Title of the Master's Thesis

„Notum is probably not a Wnt-signaling antagonist in *Nematostella vectensis*"

verfasst von / submitted by

Magdalena Schatka, BSc

angestrebter akademischer Grad / in partial fulfilment of the requirements for the degree of

Master of Science (MSc)

Wien, 2021 / Vienna, 2021

Studienkennzahl lt. Studienblatt / degree programme code as it appears on the student record sheet:	UA 066 877
Studienrichtung lt. Studienblatt / degree programme as it appears on the student record sheet:	Masterstudium Genetik und Entwicklungsbiologie
Betreut von / Supervisor:	Mag. Dr. Grigory Genikhovich, Privatdoz.
Mitbetreut von / Co-Supervisor:	

Acknowledgments

I have had the pleasure working with wonderful people and I am grateful for all the support and help that I got during this time. Firstly, I want to thank my parents, Kurt and Claudia for always being there for me. Not only did they support me financially during this time, but also encouraged me in every decision I made during my studies. I also want to thank my siblings Simon and Sarah, for being wonderfully annoying and providing me with moral support along the way. Moreover, I want to thank my friends, especially my roommate (wifey) Annika, who all were incredibly patient when I underestimated my experiments and had to postpone our arrangements. Also thanks to Juno for her fluffy support and feline perspective.

I am also extremely thankful for the professional environment I got to join. Thanks to Ulrich Technau for allowing me to work in his lab and the Technau group, consisting of many inspiring and loving people. A special shout out to Malte, our in-house genius. It was a pleasure to work with them and they provided a welcoming work environment and lots of expertise.

Most importantly, I want to thank my supervisor Grigory Genikhovich, who not only provided me with this interesting project, but has proven to be extremely patient and helpful at every step of the way. Not only is he a walking lexicon, but also supplied everyone with jokes, memes, and an excellent sticker collection. I am especially grateful for having been part of the Genikhovich group and all its members. Thanks to David Mörsdorf, for his constructive input. Isabell Niedermoser is one of the most helpful and funniest people I have ever had the pleasure to work with, being incredibly supportive whenever I was struggling. Tatiana Lebedeva is and will forever be my lab sensei, being amazingly knowledgeable and caring. Paul Knabl was also there, causing a lot of “bottomless” situations (less inappropriate than it sounds).

Lastly, I want to thank the Core Facility for Cell Imaging and Ultrastructure Research (University of Vienna) for the access to the confocal microscope and Stephanie Wienkoop (University of Vienna) with her help with mass spectrometry. Special thanks to Stanislav Kremnyov (Lomonosov Moscow State University) for sharing unpublished data on *Dynamena pumila* Notum and Jochen Rink (MPI) for supplying the *Schmidtea mediterranea*.

Table of Content

1 Introduction

1.1 The establishment of body axes and patterning

One of the most fascinating processes during the embryonic development of multicellular organisms is the formation of body plans and the patterning of body axes. This highly regulated mechanism establishes the body symmetry, thus a framework for cell differentiation and morphogenesis (Capron et al., 2009). The body axes allow for pattern formation, a process where a fertilized egg divides and over time, gives rise to cells with distinct cellular identities. These differentiated cells then cooperate forming different germ layers, which ultimately result in a functional organ system and eventually a fully developed organism (Christian, 2012).

In Metazoa, there are two main types of body symmetries – the radial and the bilateral (Holló, 2015). A radial body symmetry only has one body axis, which allows for an oral- aboral organization and is represented in ctenophores and cnidarians as well as larval sponges (Ryan & Baxevanis, 2007). The majority of animals, however, belong to the Bilateria, having 3 germ layers (endoderm, mesoderm and ectoderm) and a bilateral body symmetry, meaning that their body is organized using two orthogonal body axes. This allows for not only an anterior-posterior organization but also the differentiation between a dorsal and a ventral side of an organism (Genikhovich & Technau, 2017). Many interpret body axes as a system of molecular coordinates, which assign different cellular identities depending on where in this coordinate system a cell is located (Niehrs, 2010). Having two body axes greatly increases the amount of positional information available, which also allows for the development of more complex organisms (Genikhovich & Technau, 2017; Hill & Petersen, 2018).

1.2 Positional information and the role of morphogen gradients

Scientists have long been speculating, what underlying mechanisms establish our body axes and pattern the body accordingly. Starting in the late nineteenth and early twentieth centuries, it was already suggested that there are substances in our bodies, which are capable of generating gradients patterning the body axes (Green & Sharpe, 2015). The concept of gradients became a highly debated topic in 1952, when Alan Turing suggested a reaction-diffusion (RD) model of biological pattern formation. In RD, a weakly diffusing “Activator” is activating its own production as well as the production of an “Inhibitor”, which diffuses well and suppresses the production of the second activator peak close to the original activator

source. Once the concentration of the inhibitor falls below a certain threshold, another activator peak can emerge generating a regular pattern of activator production peaks and valleys. Importantly, every activator peak is generated anew from a noisy homogenous state rather than from any sort of pre-pattern (Gierer & Meinhardt, 1972; Green & Sharpe, 2015). Lewis Wolpert argued that RD was too random to be reliable and proposed an alternative model of positional information (PI), which concentrated on explaining how an existing pattern can generate a more complex pattern (Green & Sharpe, 2015).

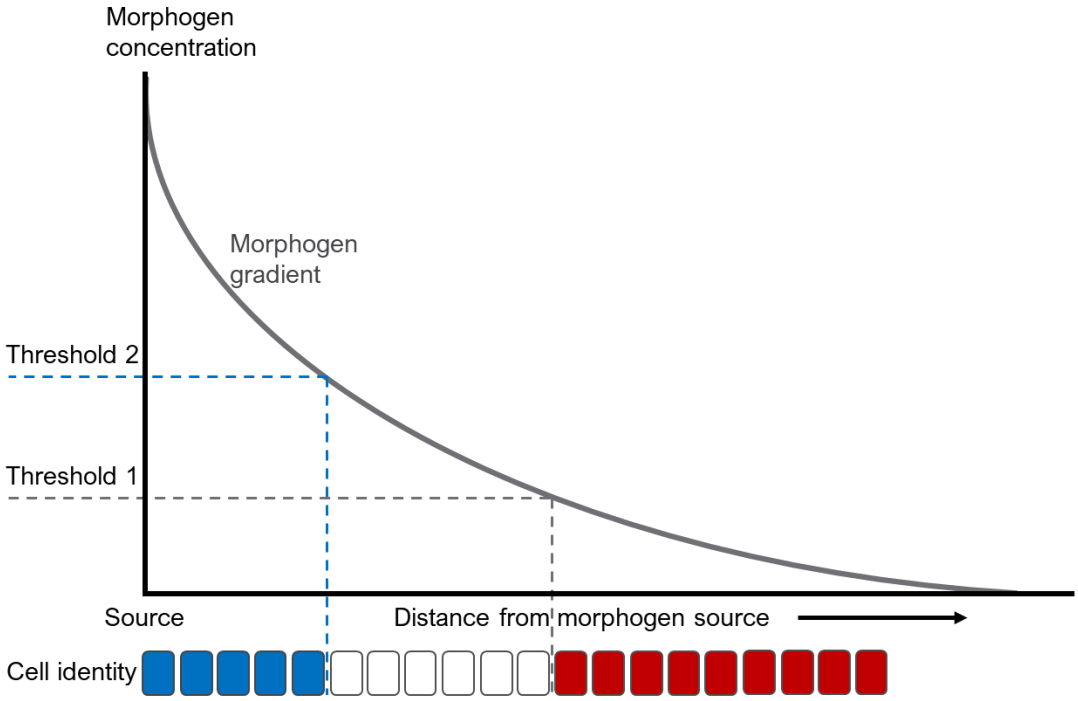

Figure 1 French flag model as proposed by Lewis Wolpert, 1969*. The morphogen concentration is plotted in relation to the distance from the morphogen source. Below the diagram there is a sketch of the assigned cell identity marked in blue, white and red. Above Threshold 2, the cells acquire blue identity. Between Thresholds 2 and 1, the cells acquire white identity. Below Threshold 1, the cells acquire a red identity.*

Wolpert's "French flag" model (see fig.1) suggests that the morphogens are produced at a source and diffuse throughout the tissue. While the concentration of morphogens is obviously highest at the source, its concentration decreases as the distance to the source increases, generating a gradient. By cells responding to different thresholds of activation concentrations, boundaries of target gene expression are established. This allows to differentiate between cells and set boundaries between varying cellular fates (Restrepo et al., 2014) as illustrated in figure 1, where threshold 2 requires a high morphogen concentration, which assigns a blue identity

close to the source. Threshold 1 is lower and patterns the white cells which are located farther from the source. Lastly, all cells which are furthest from the source, require low morphogen concentrations and take on a red identity.

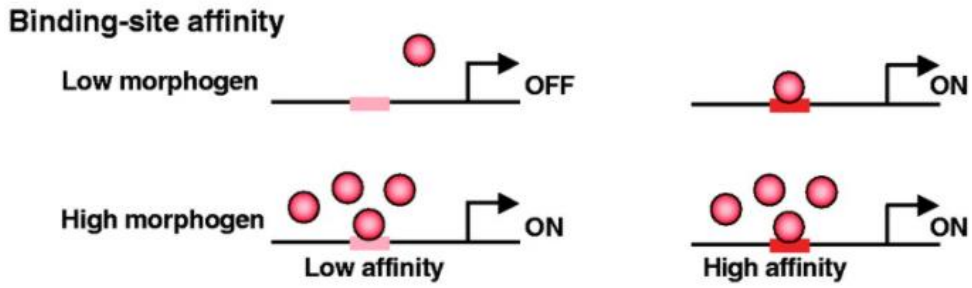

Figure 2 Scheme of binding site affinity theory. *Shown are low and high affinity binding sites in a low morphogen and high morphogen concentration. When morphogen concentration is low, only the high affinity sites are bound, and gene transcription is activated. In a high morphogen environment, all sites are bound and transcription is activated either way* (Ashe & Briscoe, 2006).

The different concentrations are then interpreted by a cell through specific signal transduction mechanisms. Varying amounts of morphogens or ligands bind the receptors on the cell surface, which triggers an intracellular response, leading to the target gene transcription (Sagner & Briscoe, 2017). Depending on the amount of ligand activated- receptors, the degree of target gene activation or repression varies (Rogers & Schier, 2011). This means that the initial difference in morphogen concentration has to be interpreted accordingly and lead to differential target gene expression (Gurdon & Bourillot, 2001). A possibility to explain this mechanism is through the concept of binding site affinity of transcription factors. Assuming that transcription factors are activated upon receptor binding by the morphogen, they can directly affect gene transcription in the nucleus, by binding *cis*- regulatory elements. The binding site affinity theory suggests that different genes have enhancer regions with a high or low affinity for transcription factors (Ashe & Briscoe, 2006; Rogers & Schier, 2011). This means, that if there is a high concentration of morphogens present, then there are proportionally more activated transcription factors that can bind the high and low affinity sites, initiating gene transcription (see fig.2). In contrast, if there are only low amounts of activated transcription factors present, then the low affinity sites are not bound, while the concentration is sufficient to activate the high affinity binding sites and initiate transcription for those genes. This means that the same morphogen can induce different cell fates in various contexts (Sagner & Briscoe, 2017).

The concept of positional information assigned by morphogen concentrations has been criticized in recent years. For instance, one point of criticism has been that embryos vary in size, meaning that the gradient cannot be fixed and has to be scaled accordingly (Fried & Iber, 2014). Furthermore, there is no explanation regarding the influence of proliferation within growing tissue on the morphogen gradient formation (Kutejova et al., 2009). Yet, the model provides a useful framework in understanding how body axes are patterned. A growing body of molecular data shows, however, that the RD and the PI are not mutually exclusive and often act in parallel or in a sequence to pattern structures during development (Green and Sharpe, 2015)

1.3 The origin of bilaterality and the model system *Nematostella vectensis*

Cnidarians, the phylogenetic sister group to all Bilateria, are of particular interest for investigating the evolutionary origin of bilaterality. Four out of five cnidarian classes (Hydrozoa, Scyphozoa, Cubozoa, Staurozoa), have a single body axis and radially symmetric bodies, while class Anthozoa comprising sea anemones, sea pens, hard and soft corals, are bilaterally symmetric (Genikhovich & Technau, 2017).

The anthozoan *Nematostella vectensis* is a brackish water polyp, which belongs to the family of *Edwardsiidae*. In the last decades, this sea anemone has been established as an essential model system in evolutionary developmental biology. Its life cycle starts off as a fertilized egg, undergoing cleavage until it reaches the blastula stage. It then enters the gastrula stage, which is coined by the invagination of the pre-endodermal plate, followed by the freely swimming planula stage. The planula then settles and forms a primary polyp (PP) which over time develops into mature adult animals (Genikhovich & Technau, 2017).

Apart from having a simple body plan, allowing for easy manipulation, it can be maintained and spawned under laboratory conditions, which is one of its most practical features (Genikhovich & Technau, 2009). Moreover, a variety of single cell analyses and other molecular techniques have been established (Ikmi et al., 2014; Karabulut et al., 2019; Layden et al., 2013; Sebé-Pedrós et al., 2017). In spite of simple morphology of *Nematostella*, its genome has a gene number as well as a genomic organization comparable to that in bilaterians making it an even more interesting model organism (Putnam et al., 2007; Schwaiger et al., 2014).

1.4 The canonical Wnt- signaling pathway and its role in *Nematostella*

The primary body axis of *Nematostella*, also called the oral- aboral axis (see fig.3A) spans the body column from the mouth to the foot of the polyp. The second body axis is the directive axis, which can only be morphologically distinguished when analysing a cross section. The directive axis is indicated by the orientation of the retractor muscles on the mesenteries (marked with black and yellow arrows) and the siphonoglyph, which is a ciliated groove on one side of the pharynx (see fig.3B) (Genikhovich & Technau, 2017).

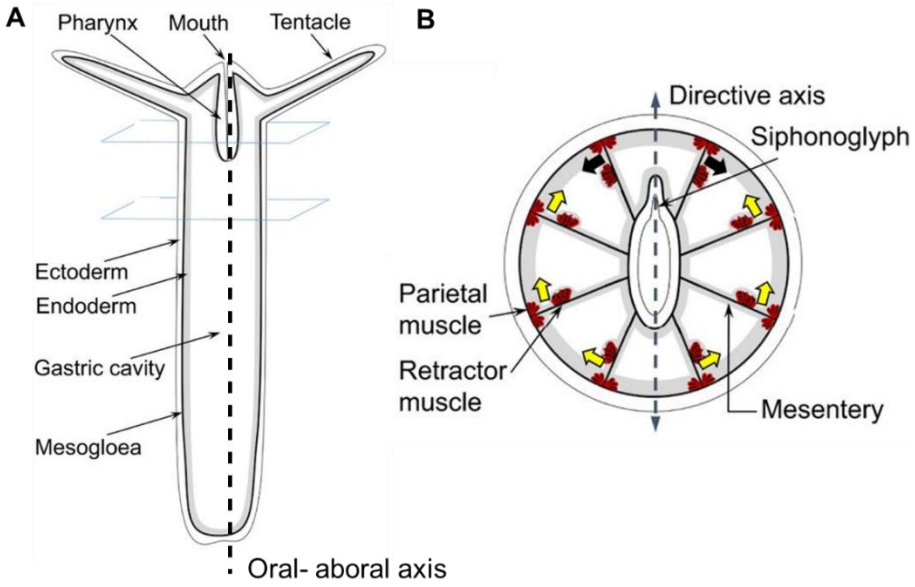

Figure 3 Scheme of the body plan of Nematostella vectensis*. (A) Side view of a Nematostella polyp with the oral-aboral axis indicated as a dashed line. (B) Cross section of the polyp in the pharynx region. One can see the directive axis, indicated by the dashed line. The orientation of the retractor muscles is market with yellow and black arrows.*

These body axes are patterned by morphogen gradients as discussed in 1.2. While the primary body axis is established by the canonical Wnt-signaling pathway, the directive axis depends on the bone morphogenetic protein (BMP) signaling pathway. In this Master thesis, we will mainly focus on components regarding the primary body axis, thus the canonical Wnt-signaling pathway.

The canonical Wnt- signaling pathway is an ancient, highly conserved pathway which is found in all Metazoa including vertebrates, where it plays a major role in cell-fate specification, proliferation, and differentiation (Komiya & Habas, 2008). In *Nematostella*, there are 11 of the

12 known Wnt- gene subfamilies (Guder et al., 2006). One of its major roles is patterning the primary body axis, which is further supported by the staggered expression of Wnt- genes in both ectodermal and endodermal epithelia along this axis (Guder et al., 2006; Kusserow et al., 2005). Apart from that Dishevelled, a component of the Wnt pathway, is localized at the animal pole from the oocyte until the gastrula (Layden et al., 2016; Lee et al., 2007) marking the point of invagination, and β-catenin is also stabilized in the oral region of the blastula (Wikramanayake et al., 2003). Morpholino knockdown of β-catenin results in the failure of the *Nematostella* embryo to gastrulate and, intriguingly, also to form its aboral domain (Leclère et al., 2016; Röttinger et al., 2012).. The oralizing activity of Wnt was also shown during regeneration (Trevino et al., 2011).

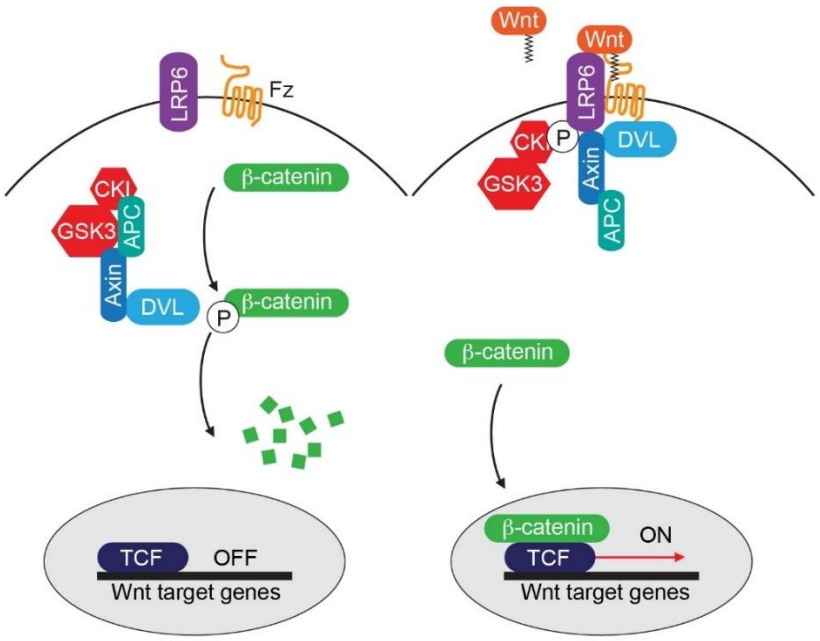

Figure 4 Scheme of the canonical Wnt-signaling pathway (Sawa & Korswagen, 2013)*. Inactive (left) and active (right) Wnt signaling.*

In principle, when the Wnt- pathway is inactive, no Wnt ligands bind to the receptor proteins Frizzled and LRP5/6 (see fig.4). This means that the ß-catenin concentration in the cytoplasm is controlled by the destruction complex consisting of Axin, APC, GSK3ß and CK1α. This complex phosphorylates ß-catenin, which is subsequently ubiquitinated and then proteasomally degraded (García de Herreros & Duñach, 2019). On the other hand, the pathway is activated when a Wnt ligand binds to the Frizzled receptor, which recruits LRP5/6. This leads to the binding of Axin to LRP5/6 which is mediated by Dishevelled, inhibiting the formation of the ß-catenin degradation complex. Therefore, ß-catenin is no longer degraded,

it can accumulate in the cytoplasm and go into the nucleus where it interacts with members of the TCF/LEF protein family to regulate target gene expression (MacDonald et al., 2009). Consequently, the phosphorylation of ß-catenin is one of the main factors controlling canonical Wnt- signaling. The amino-terminal region is especially important, in particular the four highly conserved serine/threonine residues (S33, S37, T41, and S45), that form the GSK3ß phosphorylation site (Peifer et al., 1994). Previous studies have shown that these phospho-serine/threonine residues are critical for β- catenin recognition by the ubiquitin ligase β-TrCP and its subsequent ubiquitination and degradation, thus regulating the stability of β-catenin protein (Winston et al., 1999).

1.5 Regulatory mechanisms of canonical Wnt-signaling

Wnt-pathway is crucial for embryonic development and adult tissue homeostasis in all multicellular animals (Jiang & Cong, 2016). In vertebrates, aberrant Wnt/β-catenin signaling is the cause of numerous malignancies, including cancers (White et al., 2012). There are several different methods how Wnt-signaling is regulated to maintain appropriate intensities, most of which includes control at the membrane-proximal level. One regulatory method is adjusting the responsiveness of a Wnt target cell to Wnt-signaling. This includes the modulation of the receptors and co-receptors, as well as the availability of receptors in general (Jiang & Cong, 2016). In mice for example, the transmembrane E3 ubiquitin ligases ZNRF3 and RNF43, which are antagonised by R-spondin, promote the degradation of receptors and thus inhibit Wnt signaling (Hao et al., 2016). Another example is the protein DKK1, a negative Wnt/ß-catenin regulator that plays a crucial role in head formation in vertebrate development. It acts by binding a receptor Kremen and forming a complex with LRP5/6, followed by the endocytosis of this complex, reducing the number of LRP5/6 receptors on the cell membrane (Niida et al., 2004). Another mechanism uses specific co-activators for instance GPR124 and TSPAN12, which are ligand specific and enhance the cell responsiveness to Wnt-signaling (Zhou & Nathans, 2014). Additionally, there are also extracellular processes that target the ligands themselves. This includes Tiki, a Wnt-modifier that cleaves the N-terminal region of the Wnt-ligands. The proteins Cerberus and Frzb can also directly target Wnt ligands, by binding them and thus inhibiting Wnt-signaling (Bouldin & Kimelman, 2012).

1.6 Notum, the extracellular Wnt signaling antagonist

Notum was also identified as a Wnt-dependent antagonist of Wnt signaling. Acting outside the cell, Notum was first identified as a negative feedback regulator of Wnt signaling patterning the imaginal discs in *Drosophila* (Giráldez et al., 2002). It is also crucial for neural tube development in zebrafish and the main Wnt-signaling antagonist in planarians where it is required for head regeneration (Flowers et al., 2012; Petersen & Reddien, 2011). Notum proteins carry a characteristic Ser-His-Asp catalytic triad with similarities to pectin acetylesterases, making it part of the α/β-hydrolase superfamily (Kakugawa et al., 2015). Due to this catalytic site, it was first assumed that Notum affects the *Drosophila* glypicans Dally or Dally-like protein by cleaving off their N-acetylglucosamine residues and decreasing their ability to bind Wnt-ligands (Giráldez et al., 2002). Another theory proposed that Notum can switch Dally-like protein from an activator to an antagonist, by cleaving of its GPI anchor (Kreuger et al., 2004). However, in recent years new structural analyses suggested that Notum does not target glypicans. It was found that in Notum, the lipase consensus sequence (GxSxG motif) which is part of the Ser-His-Asp catalytic triad is situated in a hydrophobic cavity where only palmitoleic acids and myristoleic acids can sterically fit inside. These fatty acids are exactly the type of fatty acid tails that are attached to Wnt-ligands. Human Notum was found to act as a carboxylesterase that can cleave off these fatty acid tails, preventing Wnt ligands from receptor binding (Kakugawa et al., 2015; Zhang et al., 2015).

Interestingly, there is also a *Notum* ortholog found in *Nematostella vectensis,* which was described by a previous Master student (Schauer, 2016). *Nematostella Notum* was identified in a Linear DNA Amplification-ChIP, and also carries the conserved GxSxG active site motive of carboxylesterases. Moreover, *Nematostella Notum* is mainly expressed in the blastoporal region (fig. 5) and is highly Wnt-signaling dependent (Schauer, 2016).

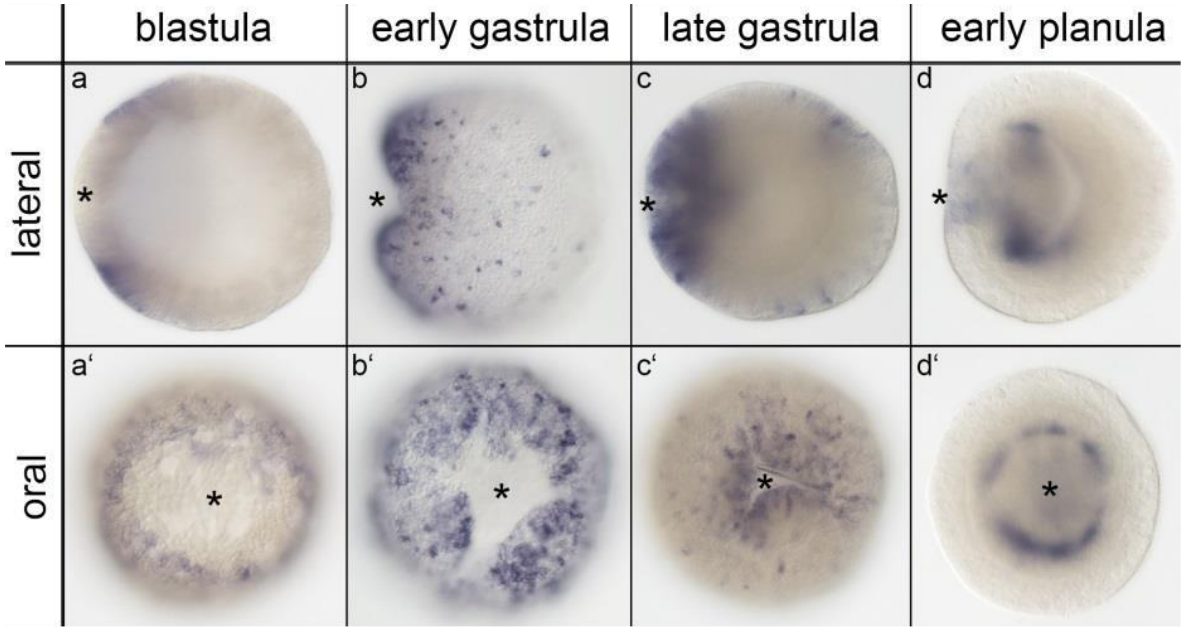

Figure 5 Wild type expression of Notum in Nematostella vectensis (Schauer, 2016). *Notum is mainly located in the oral ectoderm which later (early planula) becomes restricted to a ring around the blastopore. At this stage, expression also starts in the endoderm close to the pharynx and is asymmetrical along the directive axis. The oral opening is marked with an asterisk and shown are lateral and oral views of each embryo.*

1.7 Hypothesis and aims of this project.

The canonical Wnt-signaling pathway is a crucial component of embryonic development and the establishment of the primary body axis in *Nematostella*. Overactivation of Wnt-signaling can result in the formation of ectopic heads or the complete oralization, meaning that this pathway has to be highly regulated to maintain appropriate levels (Kraus et al., 2016; Marlow et al., 2013; Trevino et al., 2011). As the deacylase Notum was identified as a Wnt-signaling antagonist in many different organisms, and since a Notum homolog was also found in the *Nematostella* genome, we perform a functional analysis of *Notum* and investigate whether its role as a Wnt-signaling antagonist is conserved in *Nematostella vectensis*.

2 Materials and Methods

2.1 Animal husbandry and induction of spawning

2.1.1 *Nematostella vectensis*

Female and male adult polyps were maintained in separate boxes in 16‰ artificial sea water (*Nematostella* medium, NM) at 18°C in the dark. The animal culture was fed five times per week using *Artemia salina* larvae. To induce spawning, the animal boxes were moved to an incubator where they were incubated at 25°C and constant illumination for 10 hours. Afterwards, they were moved back to 18°C. Usually within 2- 4.5h after the incubation period, most animals had spawned and could be fertilized in- vitro. For this, egg packages were placed into the NM containing sperm, in the male boxes for at least 30 min. To remove the jelly surrounding the fertilized oocytes, the egg packages were transferred into 3% cysteine/NM, pH 7.5 and placed on a shaker for 30-40min. Afterwards, the eggs were washed five times in fresh NM. Eggs could be de-jellied prior to or following fertilization, depending on what was needed for further manipulation. (Genikhovich & Technau, 2009). The incubation temperature for experimental embryos was 21°C.

2.1.2 *Schmidtea mediterranea*

The asexual *Schmidtea mediteranea* strain was kept in boxes in Planarian Medium (PM)/ Montjuic salt solution (see table on the right) and fed blended chicken or calf liver weekly (Sánchez & Howard, 2008). After feeding, the boxes were carefully cleaned, first washed with tap water, then 70% EtOH, followed by another tap water and Elix rinse. The medium was exchanged weekly after feeding.

1x stock of Planarian Medium	
NaCl	1.6mM
CaCl2	1mM
MgSO4	1mM
MgCl2	0.1mM
KCl	0.1mM
NaHCO3	12mM
pH to 7.0 using HCL (12M)	
Elix water	To 1L

2.2 Standard molecular cloning

2.2.1 Amplification of gene fragments using PCR

To amplify a DNA sequence of interest (for probes, mRNA templates, etc.), sequences were obtained from transcriptomes sequenced in the Technau lab or from GenBank®, the NIH genetic sequence database (https://www.ncbi.nlm.nih.gov/genbank/). Specific primers were generated using the online tool (https://bioinfo.ut.ee/primer3-0.4.0/) and checked using the Primer Stats application of the Sequence Manipulation Suit (SMS) (https://www.bioinformatics.org/sms2/pcr_primer_stats.html). A list of qPCR primers can be seen in 6.2. The annealing temperature (Ta) for each reaction was checked using the NEB Tm calculator (https://tmcalculator.neb.com/), depending on whether Q5® High-Fidelity (NEB) or Tag® DNA Polymerase (ThermoScientific) was used (see standard PCR mix and programs below). The volume of each reaction was scaled according to further processing (10µl-50µl). Volume of DNA templates was adjusted: for plasmids around 0.5µl of plasmid dilution (~1-2ng/µl), for cDNA or genomic DNA (2µl, independent of the concentration).

Q5 Polymerase Mix		Taq Polymerase Mix	
5X Q5 Reaction Buffer	4µl	5x Green Taq Buffer	4µl
10 mM dNTPs	0.3µl	10 mM dNTPs	0.3µl
10 µM Forward Primer	1µl	10 µM Forward Primer	1µl
10 µM Reverse Primer	1µl	10 µM Reverse Primer	1µl
Template DNA	0.5-2µl	Template DNA	0.5-2µl
Q5 Polymerase (5U/µl)	0.1µl	Taq Polymerase (5U/µl)	0.1µl
Nuclease-Free Water	x µl	Nuclease-Free Water	x µl
Total volume	20µl	Total volume	20µl

PCR programs used:

	Q5® High Fidelity Polymerase			Taq® DNA Polymerase		
Phase	Temp.	Time	Cycles	Temp.	Time	Cycles
Initial Denaturation	98C°	30sec		95C°	30sec	
Denaturation	98C°	10sec	30-40	95C°	30sec	30-40
Annealing	Ta	10–30sec		Ta	15-30sec	
Elongation	72C°	30sec/kb		72C°	1min/kb	
Final Extension	72C°	2min		72C°	3min	
Pause	4C°	∞		4C°	∞	

After the PCR, the product was loaded on a gel (1-2% in TAE/SYBR safe), which was run for ~20-40 min at 120V. If the entire product was loaded it was purified using peqGOLD Gel Extraction Kit (VWR) or Monarch® DNA Gel Extraction Kit (NEB) (the elution step was repeated using the initial flow-through for both columns). This was the case for clone checks or ligation into a cloning vector. If only a fraction of the product was loaded (~3µl) to check the efficiency, the rest was PCR purified using the QIAquick PCR Purification Kit (QIAGEN) (elution step also repeated using flow-through), which was the case for fragments used as transcription templates. Afterwards, the DNA concentration was measured using the Thermo Scientific™ NanoDrop™ 2000/2000c Spectrophotometer and, if not immediately used, stored at -20°C.

2.2.2 Double Restriction Digestion

When DNA fragments were ligated into a specific backbone, both fragments (insert and backbone) were digested using standard restriction enzymes from NEB. The double digestion mix is shown below.

Double restriction digestion standard mix	
Plasmid	1µg (if possible)
10x CutSmart Buffer	3µl
Restriction Enzyme 1 (20,000 U/ml)	0.5µl (0.25µl if High Fidelity HF®)
Restriction Enzyme 2 (20,000 U/ml)	0.5µl (0.25µl if High Fidelity HF®)
Nuclease-Free Water	Xµl
Total volume	30µl

The reaction was incubated at 37°C between 1h to 8h. After the incubation period, the entire reaction was loaded on a gel, followed by a gel extraction (see 2.2.1). The NEBBioCalculator (https://nebiocalculator.neb.com/) was used to calculate the needed concentrations of each fragment for the ligation (protocol using T4 DNA Ligase (NEB) is shown below). The reaction was mixed by pipetting and centrifuged. Then it was incubated for 1-2h at RT, and lastly 5µl of this reaction mix (see 2.2.3) were transformed.

Ligation reaction using 2 gel extracted fragments	
2X Ligation Buffer	2.5µl
Vector fragment	Xµl
Insert fragment	Xµl
T4 Ligase	0.2µl
Total volume	5µl

2.2.3 Cloning and transformation

For standard cloning of PCR fragments, pJET1.2 (Thermo Scientific) was used as a cloning vector. While Q5 polymerase creates blunt ends, Taq polymerase creates 3'-A overhangs, that do not ligate into the blunt pJET1.2 vector of the CloneJET PCR Cloning Kit. Therefore, Taq amplified products, were blunted before the ligation reaction. Following mixes were used for ligation (prepared on ice):

Blunt- end cloning	
2X Reaction Buffer	5µl
PCR product	1µl
pJET1.2 vector (50ng/µl)	0.5µl
Nuclease-free Water	Xµl
T4 DNA ligase	0.5µl
Total volume	10µl

TA cloning	
2X Reaction Buffer	10µl
PCR product	1µl
Nuclease-free Water	Xµl
DNA Blunting Enzyme	0.5µl
Total volume	19µl
Vortex briefly, then centrifuge (few sec).	
Incubate at 70°C for 5min, chill on ice.	
Add following:	
pJET1.2 vector (50ng/µl)	0.5µl
T4 DNA ligase	0.5µl
Total volume	20µl

The reaction mix was vortexed, followed by a quick centrifugation. To ligate, the reaction was kept at RT for at least 5 min (up to 30 min). This was immediately followed by a transformation (~3µl of the ligation reaction) or was stored at -20°C. To transform the ligation product, 50µl aliquots of competent TOP10 *Escherichia coli* cells were thawed for 5 min. Depending on the ligation, different volumes of ligation mix were added to each aliquot. The cells were then heat shocked at 42°C for 1min and afterwards placed back on ice. 100µl of LB Medium without antibiotics was added and gently tapped to mix. This mix was then spread on pre-heated LB-plates with Antibiotics (Ampicillin) using glass beads and incubated ON at 37°C.

2.2.4 Colony Check and MiniPrep

To check, which vector carried the correct insert, 8 colonies per plate were checked performing a colony PCR (standard Taq reaction mix, scaled to 10µl reaction volume). As primers, the standard pJet1.2F and pJet1.2R primers were used for checking the pJET1.2 clones and any vector-specific primers for other plasmids. Each clone was picked using a

pipette tip and added to the reaction mix. The residue left on the tip, was spread on a second pre-warmed and marked LB-AMP plate. While the second plate was incubated at 37°C for at least 5h, the standard PCR program for Taq Polymerase was used (cycles reduced to 25). The products were loaded on a gel (1% TAE) and the clones that gave band of expected sizes, were used to inoculate 5ml LB medium+ AMP and incubated ON in a shaker at 37°C. The next day, the plasmids were purified using the innuPREP Plasmid Mini Kit (Analytik Jena) according to the manufacturer's protocol. The concentration was measured, and the plasmids were sent for Sanger sequencing at Microsynth.

2.3 Gene knock-down using short hairpin RNAs

2.3.1 shRNA preparation

The shRNAs used were designed by Grigory Genikhovich and synthesized as described (Karabulut et al., 2019). The shRNA primers (6.1) were dissolved to a final concentration of 50µM in DEPC water. 3µl of the T7 forward and 3µl of the gene specific reverse primers were mixed, quickly centrifuged and denatured for 5min at 98°C, followed by a 5min annealing step at 24°C. Of this mixture, 2µl were used for in vitro transcription using the AmpliScribe™ T7-Flash™ Transcription Kit (Lucigen) following the protocol (see on the right). The mix was incubated ON at 37°C, then the DNA template was digested by adding 1µl RNAse-free DNase and incubating it for 15 min at 37°C. Then the shRNAs were purified using the Direct-zol™ RNA MiniPrep Plus (ZYMO Research) according to the supplied protocol, the concentration was measured using Nanodrop, and shRNA was stored at -20°C.

T7 IVT mix	
DEPC water	4.5µl
10xT7 reaction buffer	2µl
DTT	2µl
ATP	2µl
CTP	2µl
GTP	2µl
UTP	2µl
RNase Inhibitor	0.5µl
T7 RNA Polymerase	2µl
DNA template	1µl
Final volume	20µl

2.3.2 Electroporation procedure

To electroporate the shRNAs, unfertilized eggs, were de-jellied as described in 2.1.1. Per shRNA, approximately 100µl of 15% Ficoll in 12‰ NM were pipetted into a 2ml Eppendorf tube. Then embryos in NM were added on top. The embryos could settle, and the NM

supernatant was removed, then new embryos were added etc. until all the embryos were in the tube with as little NM as possible. Then the embryos and Ficoll were slowly mixed. For each shRNA, a 2ml Eppendorf tube was prepared containing 300ng/µl of shRNA. The ratio between the volumes of embryos to shRNA solution should be around 70:30 maximum (less shRNA volume is preferred) in a total volume of 100µl of electroporation mix. This was mixed and transferred to 4 mm gap electroporation cuvette (Bio-Rad) using cut pipette tips. Before starting, dishes with sperm water were prepared (one for each shRNA) and labeled. Afterwards the cuvettes were gently flicked and placed into the Bio-Rad Gene-Pulser-Xcell Electroporation System and electroporated with a single 25 ms square pulse of ~50V. The cuvette was then filled up with NM and the embryos quickly transferred into the prepared Petri dishes. The embryos were then incubated at 21°C until ready for fixation. For each experiment, a batch of embryos was electroporated with shmOrange as control.

2.3.3 Validation of Knock-down using Quantitative Real-Time PCR

The efficiency of the shRNA knockdown (KD) was validated using quantitative real-time PCR (qPCR). For this, a fraction of the electroporated embryos (~100 embryos) were used for RNA extraction. The total RNA was extracted using the phenol-chloroform method with the TRIzol® Reagent (Life Technologies) according to the manufacturer's protocol. The DNA was removed using TURBO™ DNase treatment (Thermo Fisher Scientific) and the RNA concentration was measured using Nanodrop. This was followed by cDNA synthesis, for which (if possible) 1µg of RNA was used, otherwise the RNA concentration was adjusted, to have equal input RNA. For cDNA reverse transcription, ProtoScriptII (NEB) and random hexamers were used according to provided protocol. The cDNA was diluted to 50µl (from 20µl) using MilliQ before performing qPCR. For the qPCR, the Luna® Universal qPCR Master Mix (NEB) in 10µL final reaction volume was used (PCR mix and program shown below). It was carried out using the BioRad CFX96 Touch™ Real-Time PCR Detection System.

Luna® qPCR Master Mix		qPCR program			
2X Luna® Master Mix	5µl	Phase	Temp.	Time	Cycles
10 µM Fw & Rv Primer	1µl	Initial Denaturation	95C°	2min	
cDNA	1µl	Denaturation	95C°	5sec	40
Nuclease-Free Water	3 µl	**Target amplification**	60C°	30sec	
Total volume	10µl	Denaturation	95C°	1min	
		Melting curve	50-90C°	2min	
		Target amplification: fluorescence measured after each cycle			
		Melting curve: 0.5C° increment, 1 sec fluorescence measured after each increment			

To analyze the KD efficiency, primers (6.2) to amplify a ~80-150bp long fragments of the gene of interest were selected (designed using Primer3 tool, see 2.2.1). The forward and the reverse primers were diluted to 10µM together in one Eppendorf tube. Triplicate WT cDNA dilutions differing by a factor of 10 (undiluted, 1:10, 1:100) were used to establish a calibration curve for each primer pair. The mean Cq values from each triplicate were scatter-plotted, and the linear trend line equation best fitting the distribution of the Cq values depending on the cDNA template dilution (i.e. $\log_{10}$[DNA concentration]) was calculated in Microsoft Excel. This equation was then used to calculate the relative concentration of the cDNA of interest, using the Cq values of the qPCR performed for KD efficiency evaluation. The DNA concentrations of the shmOrange control and the KD samples were normalized according to the expression of a housekeeping gene glyceraldehyde phosphate dehydrogenase (GAPDH), and then the fold change in the expression of the gene we attempted to knock down was determined in the KD samples in relation to their expression in the shmOrange control.

2.4 Overexpression of *Notum* mRNA

2.4.1 Preparation mRNA in vitro transcription

As templates for the in vitro transcription (IVT) two different plasmids were used generated by Grigory Genikhovich. Schemes can be seen in fig.6. The active construct (fig.6A) contains the SP6 primer site, the *Notum* coding sequence (CDS) followed by a p2A site and an *mCherry* CDS added in frame (*Sp6::Notum::p2A:mCh::SV40*). The putative inactive *Notum* construct (fig.6B) is identical, except for a serine to an alanine substitution (S199A) in the GxSxG motif. The DNA transcription template was cloned from the pJET1.2 plasmid using Sp6 and T7 as primers using Q5 polymerase (standard Q5 procedure- see 2.2.1) A.T. 58°C and 40 cycles. The template was PCR extracted and used for IVT.

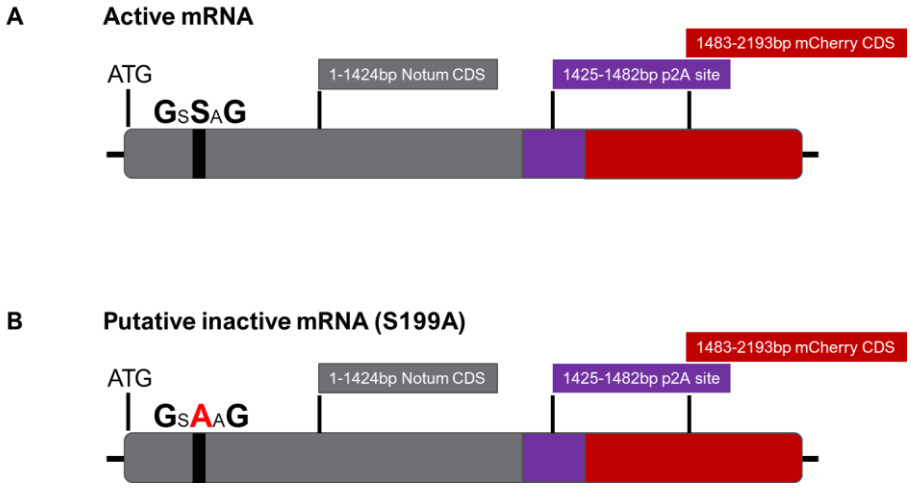

Figure 6 DNA templates for IVT of Notum mRNA constructs. *Wild type Notum construct (A) and the putative inactive form (B). Both sequences have the Notum CDS linked to mCherry CDS using a p2A peptide coding sequence. The inactive form (B) has a single amino acid substitution (S199A) in the GxSxG motif.*

2.4.2 mRNA in vitro transcription

To prepare the mRNA constructs for injection, the PCR templates generated in 2.4.1 were in vitro transcribed using the AMBION mMESSAGE SP6 Transcription Kit according to the provided protocol. Then, the mRNA was purified using the MEGAclear™ Transcription Clean-Up Kit (Ambion) or the Monarch® RNA Cleanup Kit (NEB), eluted in 50µl DEPC water. It was immediately used for injection or stored at -80°C.

2.5 Microinjection of Morpholinos and mRNA constructs

For microinjection, the fertilized eggs were de-jellied (see 2.1.1). The Morpholinos and the mRNA constructs were delivered into the egg using the FemtoJet® electronic microinjector (Eppendorf) and Narishige micromanipulators on Nikon TS100F inverted epifluorescence microscope (Renfer et al., 2010). The final MO concentration was 500ng/µl for the *ß-catenin* MO or 900ng/µl for the *Notum* MO (see 6.3). Standard MO concentrations were adjusted accordingly. The mRNA (*Notum::p2A::mCherry* and *Notum(S199A)::p2A::mCherry*) concentrations varied between 20-150 ng/µl. Same concentrations of both mRNAs were injected on the same day (see details in 2.6). The injection mixes (total volume 3µl) also contained 50ng/µl of Dextran-Alexa Fluor 488 (Invitrogen) to control for injection volume, in MilliQ water. During the injections, the eggs were kept at 14 °C to delay the division, while after injection, the embryos were kept at 21°C until further processing.

2.6 Inhibitor treatments using ABC99 and 1-Azakenpaullone

The fertilized eggs were de-jellied as described in 2.1.1. All treatments (DMSO, ABC99 and AZK)were performed in 12- well plates. For the regeneration experiments, the treatment solutions were prepared in a total of 2ml, while for embryonic treatment post fertilization, the volumes were scaled down to 1.5ml. For 2ml treatments, 1ml of 2X treatment solution was prepared in an Eppendorf tube. For the inhibitor treatments, AZK (stock:5mM) and ABC99 (stock:10 mM) were diluted in NM and for the DMSO control, volumes equal to the inhibitor volumes taken for the highest concentration treatment were used. This was added to 1ml of NM in the 12-well plate and then the bisected body parts were added without adding too much additional medium. For the planarian experiments, PM was used instead of NM. For the 1.5ml embryonic treatments, 500µl of 3X treatment solution was prepared in a separate Eppendorf tube. Then 500µl of NM was added to 12-well plates and 500µl of NM containing the embryos was added. Lastly, the treatment solution was added and mixed in. All animals were kept at 21°C in the dark until further processing.

2.7 Whole mount in situ hybridization

2.7.1 Preparation of digoxigenin (DIG) labelled antisense probes

To prepare the RNA probes, the corresponding fragments were amplified from pJET1.2 plasmids using standard Sp6_pJetR and T7primers. For the amplification, Taq polymerase was used (see standard procedure 2.2.1) in a reaction volume of 50µl (Ta. 53°C, 40 cycles). 3µl of the reactions were loaded on a 1% gel to verify the size of the amplified fragment and the rest was PCR purified (see 2.2.1). For the transcription into an antisense probe either the HiScribe T7 High Yield RNA Synthesis Kit (NEB) or MEGAscript SP6 Kit (Ambion) was used, depending on the orientation of the insert in pJET1.2. The reactions were set up according to protocol (see below) and incubated at 37°C ON. The next day, the template DNA was removed with 1µl TURBO DNase treatment for 30 min at 37°C. Next, the RNA was precipitated by adding 39µl (to 50µl total) of nuclease-free water and 25µL of 7M LiCl solution, followed by an incubation at -20°C for at least 4h (best ON). The samples were centrifuged (4°C for 15 min at 12000g), the supernatant was removed and washed with twice with 70% ethanol (in DEPC water). Then the EtOH was removed and the pellets were air dried. The dry RNA pellets were resuspended in 50µl of nuclease-free water. The RNA concentration was measured using Thermo Scientific™ NanoDrop™ and diluted to a concentration of 100ng/µl with nuclease-free water and then to 50 ng/µl with formamide to be stored at -20°C.

RNA probe transcription	
PCR product	2.5µl
10x reaction buffer	0.5µl
Dig-UTP mix	1µl
RNAseOut	0.5µl
Enzyme mix	0.5µl
Total volume	5µl

2.7.2 Fixation of 30hpf and 2dpf embryos

Prior to the in- situ hybridization, the embryos (inhibitor treated, MO injected or shRNA electroporated) were fixed at 30hpf or 2dpf. The embryos were washed 3 times in NM and then twice in 1x PBS (List of Buffers, in 6.5). Meanwhile 2ml Eppendorf tubes were rinsed with PTw, and the fixation solution was prepared (3.7% FA/1xPBS/MilliQ). The embryos were transferred into the tubes, the remaining PBS was removed, and 2ml fixation solution was added. Fixation took 1h at RT in a rotating mixer. Afterwards the FA was removed, and the embryos were washed 4x using PTw followed by 4x washes of MeOH (100%) and then stored in MeOH at -20°C.

2.7.3 Pretreatment of embryos

To facilitate the handling, the embryos were placed into plastic sieves, which were transferred into washing racks. The protocol is based on previously published protocols (Genikhovich & Technau, 2009) and the washing steps were performed using the Biolane™ HTI 16V machine (Intavis Inc.) (List of Buffers, in 6.5). At first, the embryos stored in MeOH were re-hydrated into PTw using one 50%MeOH/ 50%PTw wash and 3x PTw washes. Then the embryos were digested using Proteinase K (10µg/ml in PTw for 20 min) to increase permeability and the reaction was stopped by glycine treatment (2 washes, PTW and 4mg/ml glycine). Afterwards following washing steps were used to block the charged residues that cause unspecific binding of the probe and to post- fix the embryos: 2 washes of 1% triethanolamine in PTw, followed by one wash using 1% triethanolamine/ 3µl/ml acetic anhydride in PTw and one wash 1% triethanolamine/ 6µl/ml acetic anhydride in PTw. Then the embryos were washed twice using PTw and refixed using 3.7% formaldehyde in PTw (1h) at RT. This was followed by 5X PTw washes, one 50% PTw/ 50% Hybe wash for 10min at RT and a 100% Hybe wash for 10min at RT. Prehybridization with 100% Hybe must be at least 2h but can be extended ON.

2.7.4 Hybridization and Detection of Digoxygenin RNA probe

For the hybridization, the probes were diluted in Hybe (0.5-1ng/µl final probe concentration). Then, 300µl of the probe/Hybe mixture were added into the wells of the Eppendorf tube rack. The sieves were placed into the wells, the racks were sealed and incubated at 62°C in a water bath ON. For the post-hybridization washes the sieves were transferred back into the washing rack with pre-warmed Hybe (incubation: 20 min) followed by washing steps (all at 62°C) with increasingly stringent conditions. Firstly, a 60% Hybe/ 40% 2x SSCT (pH 7) wash for 30min, then 30% Hybe/ 70% 2x SSCT for 30min, followed by 2 washes using 100% 2x SSCT for 30 min and then 3 washes 0.01x SSCT. To detect the labelled probes with the α-digoxygenin antibody coupled to an alkaline phosphatase, the embryos were first washed with 100% PTw for 10 min at RT. Then the unspecific protein binding sites and antibodies were blocked using Roche Blocking reagent (0.5% w/v in 1x maleic acid buffer pH 7.5) and incubated at least 1h at RT. Then the sieves were transferred to a clean Eppendorf tube rack where the Roche AP-coupled-α-Dig antibody diluted in blocking buffer (1:4000) was added and incubated on a rocking plate ON (4°C). Then sieves were transferred back into the washing rack, and 10 PTw washes (for 10 min each) were performed followed by one AP wash. Next, 1ml AP-buffer per

sieve was transferred into the wells of a 48-well plate. The sieves were transferred into the well plate and the embryos were pipetted from the sieves into the wells. Then 800µl of AP were removed and 200µl of 2x staining solution (1x: 1µl/ml NBT and 1.75µl/ml BCIP in AP buffer) was added (final: 400µl total with 1x staining solution). The staining developed in the dark at RT and was stopped by removing the staining solution, followed by an EtOH (99%) wash for at least 1h. The embryos were then rinsed with PTw (at least 3 times), and stepwise infiltrated into 87% glycerol (35% in PTw & 75% in PTw). Then the embryos were mounted for microscopy and imaged using Nikon Eclipse 80i microscope with a Nikon DS-Fi1 camera.

2.8 Regeneration procedure

2.8.1 Regeneration of *Nematostella vectensis*

For the regeneration experiment on adults and primary polyps (PP), different treatment solutions of DMSO, 5µM ABC99 and 10µM ABC99 were prepared in NM (total volume 2ml, for details see 2.6). For the adults, 5 animals per treatment (15 total for all 3 treatments) were cut in the middle of their body column using a scalpel blade. Then the heads and the feet were immediately placed in a marked 12-well plate containing the treatment solutions. This was repeated for all treatment conditions and kept in the dark at 21°C. Their regeneration process was monitored for the following 6 days and the treatment solution was exchanged every second day. When fully regenerated (at 6dpc), they were imaged with a Nikon DS-Fi1 camera under a Nikon SMZ18 binocular. The same procedure was applied to the PP where instead of five, 20 PP per treatment (60 total) were bisected using a microscalpel and imaged after 7 days post cutting.

2.8.2 Regeneration of *Schmidtea mediterranea*

The regeneration experiment using planarians follows the same procedure (2.8.1). The treatment solutions of DMSO and different ABC99 concentrations (2, 5, 10 &15µM) were prepared (2.6). The planarians were bisected using a microscalpel and their tails were immediately transferred into the treatment solutions in a 12-well plate. 10 animals were cut per condition (50 total). The treatment solutions were exchanged every second day, until they were fully regenerated and then imaged with a Nikon DS-Fi1 camera at 14dpc.

2.9 Western blot protocol

2.9.1 Sample lysis and preparation

To prepare the Western blot (WB) samples, approximately 100 embryos (inhibitor treated, MO injected or shRNA electroporated), were transferred into 1.5ml Eppendorf tubes at 30hpf. Any remaining NM was removed and 100µl of cell lysis buffer (Invitrogen™) with added PMSF Protease Inhibitor and Protease and Phosphatase Inhibitor Cocktail (Thermo Scientific™) (1µl of each in 100µl buffer) was added. The embryos were homogenized by pipetting, then centrifuged for 10min at 4°C (max speed). The clear supernatant was transferred into a new tube (around 80-90µl) and the protein concentration was measured using Bradford assay. For this, serial dilutions of BSA (NEB) were prepared to generate a standard curve (10, 5, 2.5 and 0mg/ml BSA in MilliQ). Then the Bradford solution (ROTI®Quant (Roth) 5x solution) was diluted to 1x using MilliQ (500µl/sample). 1.5ml Eppendorf tubes (number of samples + 4 for the quantification curve) were prepared and 500µl of the Bradford solution was added. Then 1µl of each sample (incl. BSA dilutions) were added and vortexed. The concentration was measured using a photometer (BioPhotometer Eppendorf). The samples were then diluted with cell lysis buffer to the lowest measured concentration, and an equal volume of the 2x Laemmli loading buffer (List of Buffers 6.6) was added. For very low protein concentrations, a 6x loading buffer was used to reduce the sample volume. The samples were heated to 95°C for 5 min, chilled on ice, centrifuged at full speed at 4°C for 10 min, and kept on ice until loaded on the gel. In general, around 50µg of total protein were loaded, and when loaded, the solution was taken from the top of the centrifuged Laemmli buffer/ protein mixture.

2.9.2 SDS PAGE preparation and Gel run

To prepare the gels, the glass plates for 1.0 mm thick gels were assembled and fixed using the casting frames in the casting stand (BioRad®). For each WB, two 8% gels were prepared (see below). At first the plastic combs were added to the glass plates and ~1cm below the end of the combs was marked. The combs were removed, and the separating gel was poured until this marked line. Isopropanol (100%) was added immediately on top until the separating gel had solidified (at least 30 min). Then the isopropanol was removed, and the stacking gel was poured on top. The combs were added until completely solidified (30-45min).

Separating gel		Stacking gel	
Milli Q® water	5.3ml	Milli Q® water	1.72ml
37% Acrylamide Mix	2.0ml	37% Acrylamide Mix	0.5ml
1.5M TRIS pH 8.8	2.5ml	1.0M TRIS pH 6.8	0.76ml
10% SDS	0.1ml	10% SDS	0.03ml
10% Ammonium persulfate	0.1ml	10% Ammonium persulfate	0.03ml
TEMED	0.008ml	TEMED	0.003ml
Total volume (for 2 gels)	10ml	Total volume (for 2 gels)	3ml

For the gel run, the running buffer was prepared (see below, details 6.6). 1L was sufficient for one gel run. The gel was placed in the electrode assembly in the tank, using the Mini-PROTEAN® Tetra Cell, then the running buffer was added. The samples were loaded according to a prepared loading scheme (after digestion and centrifugation step) including a color prestained protein standard (NEB).

Running buffer	
10x TRIS/Glycine	100ml
10% SDS	10ml
Elix® water	To 1l
Total volume	1l

The gel run was started using the BioRad® PowerPac Basic Power Supply set at 100V until the samples passed through the stacking gel. Then the voltage was increased to 150V until the proteins were properly separated (~1h).

2.9.3 Transfer of proteins and staining

After the gel run, the proteins were transferred using the Mini Trans-Blot Cell kit (BioRad®). The transfer buffer (see below) was prepared and cooled at -20°C (1.5L is sufficient for one transfer). After the gel run, the tank was rinsed 3x (last rinse with Elix water), the stacking gel was cut off and the separating gel was trimmed to a smaller size, then washed 3x in transfer buffer on a shaker (RT, but on ice package). The Nitrocellulose membrane (Thermo scientific ™) and the filter paper (Thermo scientific™) were cut to fit the gel size. Then the “transfer sandwich” was assembled in a plastic box filled with cold transfer buffer. The gel and the membrane were placed between 3 filter papers and one foam pad on each side. This was clamped together using a gel holder cassette and placed in the Mini-PROTEAN Tetra Cell tank

(BioRad®) filled with transfer buffer. Cooling elements and a magnet were added. The entire tank was placed in an icebox, filled with ice and put on a magnetic rotator plate, to ensure constant circulation of the buffer. For α-active ß-catenin AB, 70V were applied for 3h. Then, the membrane was removed from the sandwich and washed 3x 5min using TBST (details in 6.6) on shaker at RT. 3-5ml of Ponceau staining (Beacle, Inc.) were applied for 1 min to verify whether the transfer was successful. Then the staining was completely removed with Elix water (several rinses). Another 3x 5min washes using TBST (on shaker, RT) followed, then the membranes were blocked using 5% BSA in TBST for 1h at RT on shaker. After that, the blocking solution was removed, and the AB dilutions were added (1:500 for α- ß-actin rabbit and 1:5000 for α-active ß-catenin rabbit in ~2ml, details 6.7). This could be done by mixing both dilutions or by cutting the membranes and adding each dilution individually. The membranes were then incubated at 4°C on a shaker ON. Next day, the primary AB was removed, and the membranes were washed with TBST (3x 5min at RT), then the secondary AB (1:100 000) was added (α-rabbit HRP, details 6.7). They were incubated for 1h at RT, followed by 3x 5min washes using TBST. Then the SuperSignal™ West Femto Maximum Sensitivity Substrate (Thermo Scientific™) was prepared (1:1 mix in total volume of 400µl) and a plastic bag was cut to serve as a folder. The membrane was transferred into this folder and the substrate added on top. The blots were then exposed using the UVP EpiChemi3 Darkroom Gel Imaging System (Cambridge Scientific) using the BioVision software (exposure time between 5-30 min).

Transfer buffer (0.04% SDS)	
TRIS- Base	5.8g
10% SDS	4ml
Glycine	2.9g
EtOH	200ml
Elix® water	To 1l
Total volume	1l

3 Results

3.1 *Notum* expression is highly dependent on canonical Wnt- signaling

Our goal was to identify the function of Notum within *Nematostella* and investigate whether it acts as a Wnt-signaling antagonist. As mentioned in the introduction, *Notum* is highly expressed during embryonic development, with its expression starting as early as 8hpf, reaching its peak between 13 and 24 hpf (see fig.7). After the peak, high expression is maintained throughout early development (100hpf).

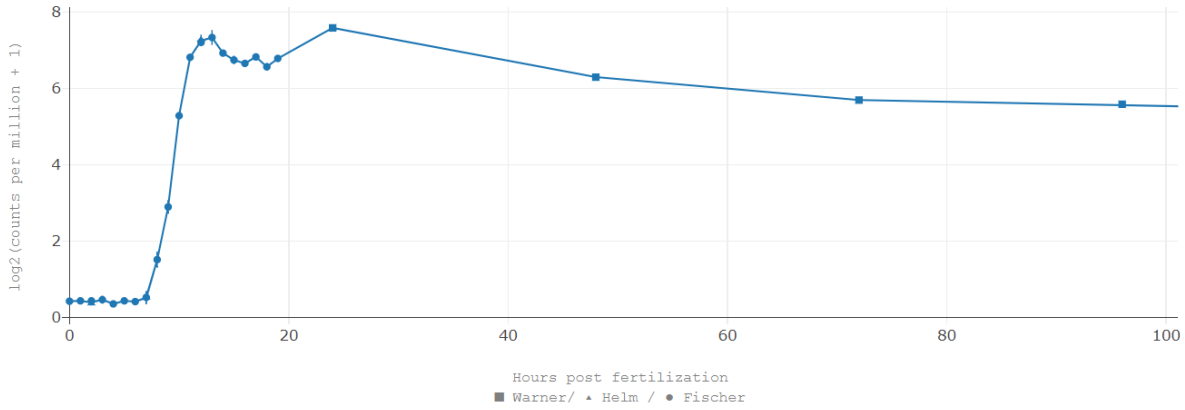

Figure 7 Embryogenesis gene expression plot of Notum using NvERTx transciptome exploration tool (Warner et al., 2017).

Another interesting aspect of Notum is its expression pattern (see fig.5). During embryonic development, its expression can already be seen in the blastula, where its expression forms a ring around the oral pole, surrounding the pre-endodermal plate. During gastrulation, *Notum* mRNA is mainly located in the oral ectoderm in the blastopore lip, with some expression at the aboral end, as well as some single cell expression along the body column. Later in the early planula, its expression becomes restricted to a ring around the blastopore. In this stage, expression also starts in the endoderm close to the pharynx. Moreover, the transcript is asymmetrically expressed along the directive axis.

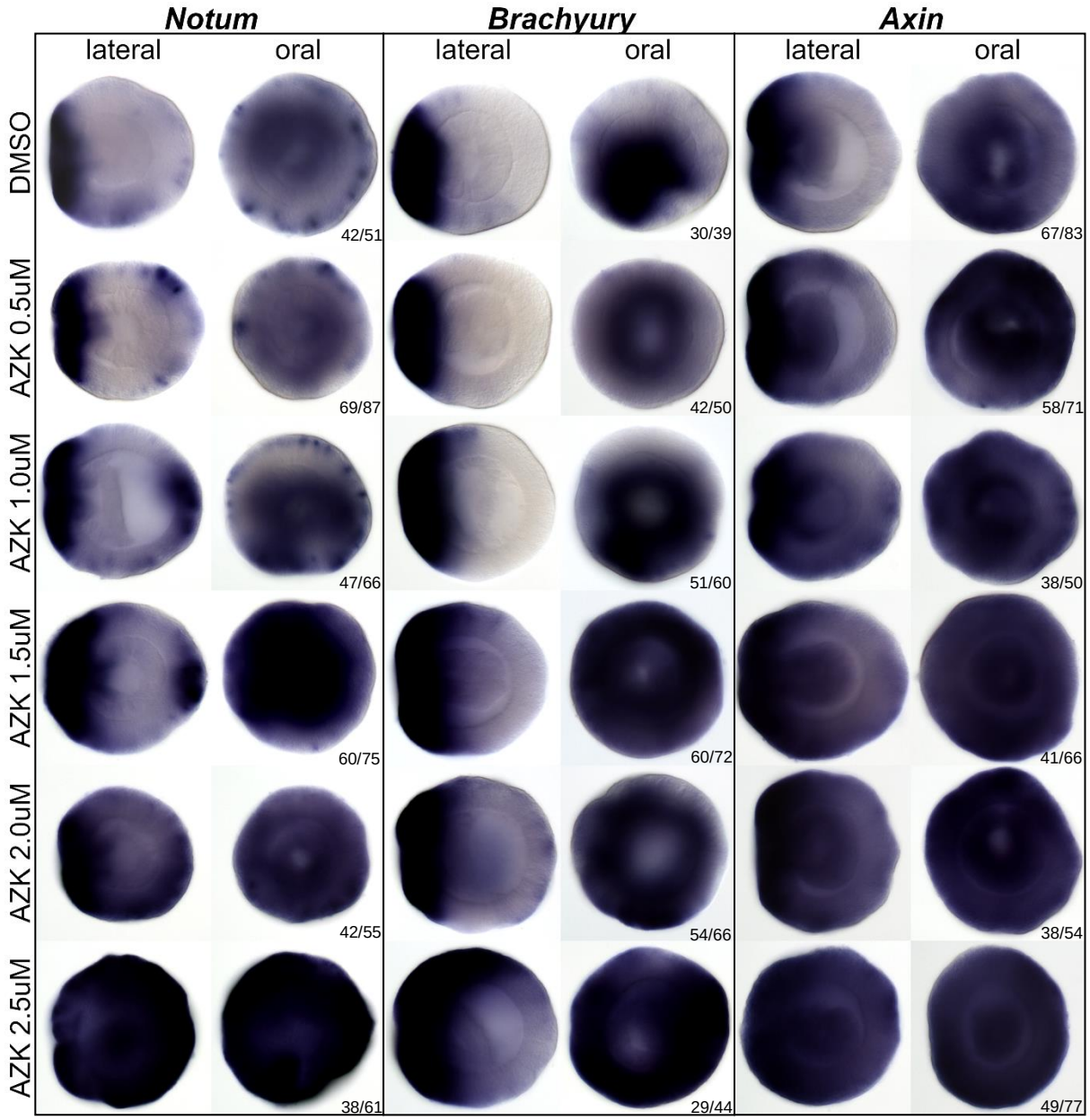

Figure 8 In situ hybridizations using 1-Azakenpaullone (AZK) treated 30hpf embryos illustrates that Notum is highly Wnt-signaling dependent. *The numbers in the bottom left corner of each condition represent the quantification of the expression pattern. Each embryo is shown orally and laterally, in the latter the oral end is oriented towards the left.*

Notum expression is also highly ß-catenin signaling dependent, which can be seen when looking at its expression upon early 1-Azakenpaullone treatment (fig.8). This inhibitor blocks GSK3ß, which leads to an upregulation of ß-catenin signaling within the embryo (Kraus et al., 2016; Marlow et al., 2013). Similar to *Brachyury* and *Axin*, the latter being directly involved in the Wnt signaling pathway, as component of the "destruction complex" and *Brachyury* being one of the main targets, *Notum* is highly upregulated as well, sharing similar expression

domains. It behaves like a typical “saturating” gene: its expression increases throughout the ectoderm with higher ß-catenin signaling intensities, eventually reaching saturation (Bagaeva et al., 2020; Kraus et al., 2016). One can see that upon increasing AZK treatment (see fig.8), the expression of *Notum* is upregulated similar to *Brachyury* or *Axin* expression. What is also notable is that as the oral expression intensifies, the expression at the aboral pole increases drastically as well. At 2.5µM AZK *Notum* and *Axin* expression is completely saturated, while *Brachyury* is less sensitive to the upregulation of ß-catenin signaling.

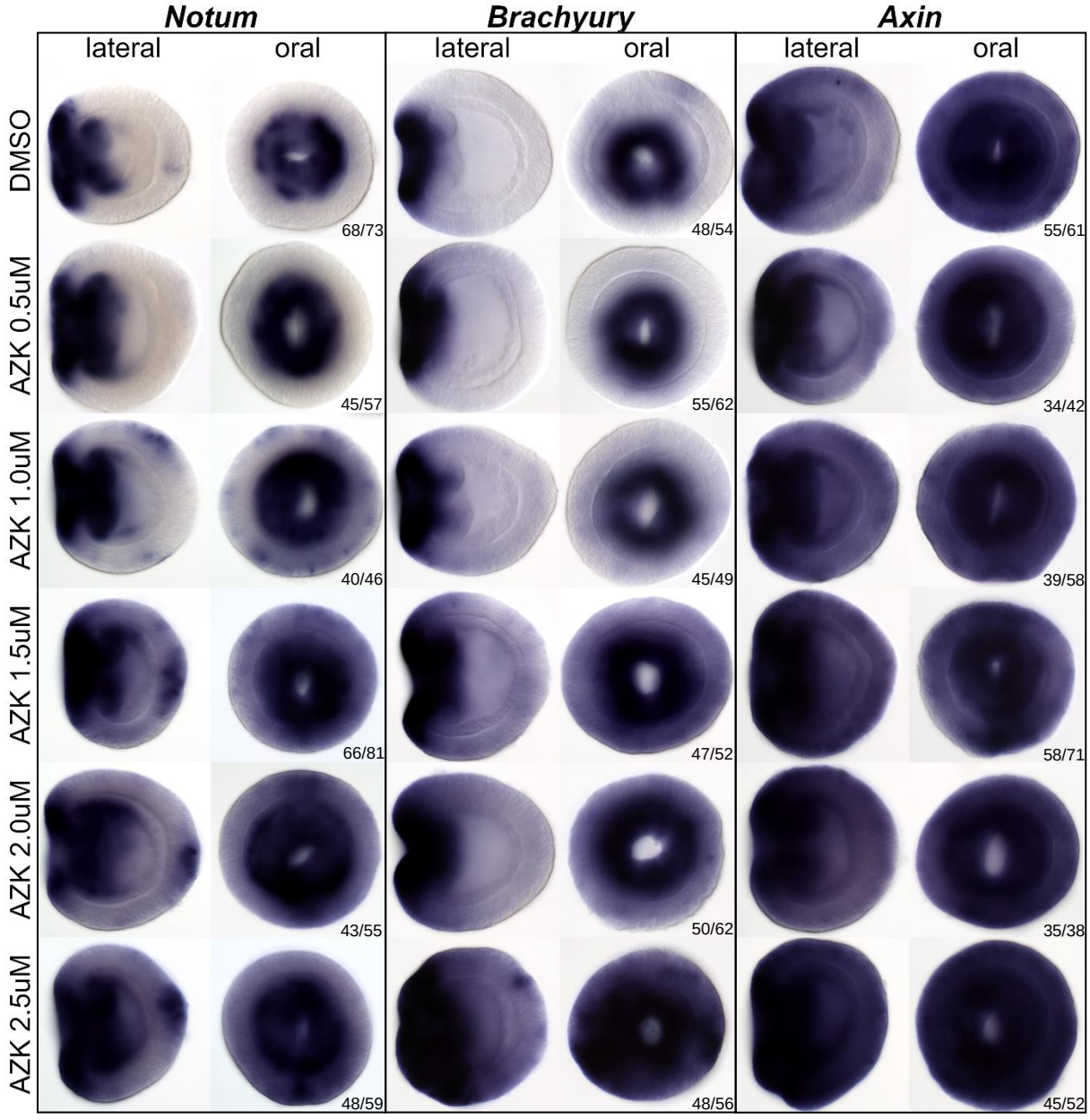

Figure 9 In situ hybridizations using 1-Azakenpaullone treated 2dpf embryos, shows that Notum is highly Wnt-signaling dependent. *Treatment was started right after fertilization. The numbers in the bottom left corner of each condition represent the quantification of the expression pattern. Each embryo is shown orally and laterally, in the latter the oral end is oriented towards the left.*

A similar expression pattern can be seen in 2dpf old embryos (see fig.9). At this stage, the expression of *Notum* is mostly located around the oral opening and the pharynx, with less expression towards the aboral pole when compared to the late gastrula embryos (fig.8). Upon increasing AZK treatment, expression at the aboral pole, however, intensifies similarly to the late gastrula. At this stage one can also see a clear increase in *Axin* and *Brachyury* expression. In both cases, the expression, which in the DMSO control is located around the mouth, extends towards the aboral pole until completely saturated. As already seen in earlier stages (see fig.8) all 3 genes are highly Wnt- signaling dependent.

3.2 Treatment with Notum inhibitor ABC99 has no effect on the regeneration of *Nematostella vectensis* and *Schmidtea mediterranea*

To start off the functional analysis, we used the commercial chemical inhibitor ABC99, which inhibits *Notum* (Suciu et al., 2018). ABC99 was shown to be effective in mammalian intestinal stem cells (Liang et al., 2020; Pentinmikko et al., 2019) and as chemical treatments such as AZK have been proven to work within *Nematostella*, a chemical treatment to investigate *Notum* would be an easy method to investigate any downstream effects. Analysis using the NvERTx database, shows that *Notum* is highly upregulated during regeneration after sub-pharyngeal bisection (see fig.10). At 8 hours post amputation (hpa) *Notum* is clearly upregulated, reaching its peak at 20hpa and then slowly declining again over the following hours. For this reason, the first experiment was focused on the regeneration of PP and adults and whether they were able to regenerate properly when incubated in varying ABC99 concentrations.

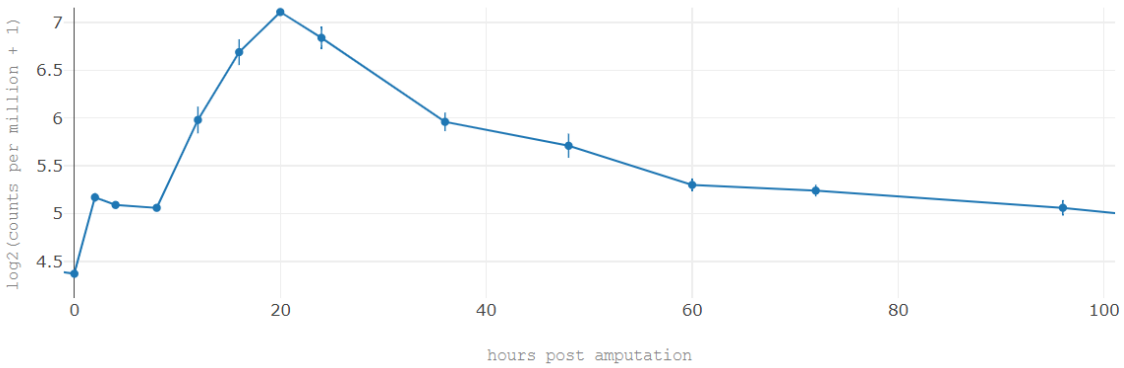

Figure 10 Regeneration gene expression plot of Notum using NvERTx transcriptome exploration tool (Warner et al., 2017).

3.2.1 ABC99 incubation does not affect head and foot regeneration in *Nematostella*

At first, adult animals were cut in the middle of their body column and both body halves could fully regenerate in DMSO control, as well as in 5µM and 10µM ABC99 (5 animals per treatment). The upper row (see fig.11A-C) shows the heads regenerating feet, while the bottom row shows feet regenerating heads (see fig.11D-F). The numbers in the bottom right illustrate how many of the cut animals exhibit the phenotype shown in the illustration. As one can clearly see, all heads were able to regenerate the lower part of the body column as well as their feet. The same applies to the feet regenerating heads. In fig.11 C &D, it is more difficult to tell but these animals were able to form tentacles meaning that they fully regenerated.

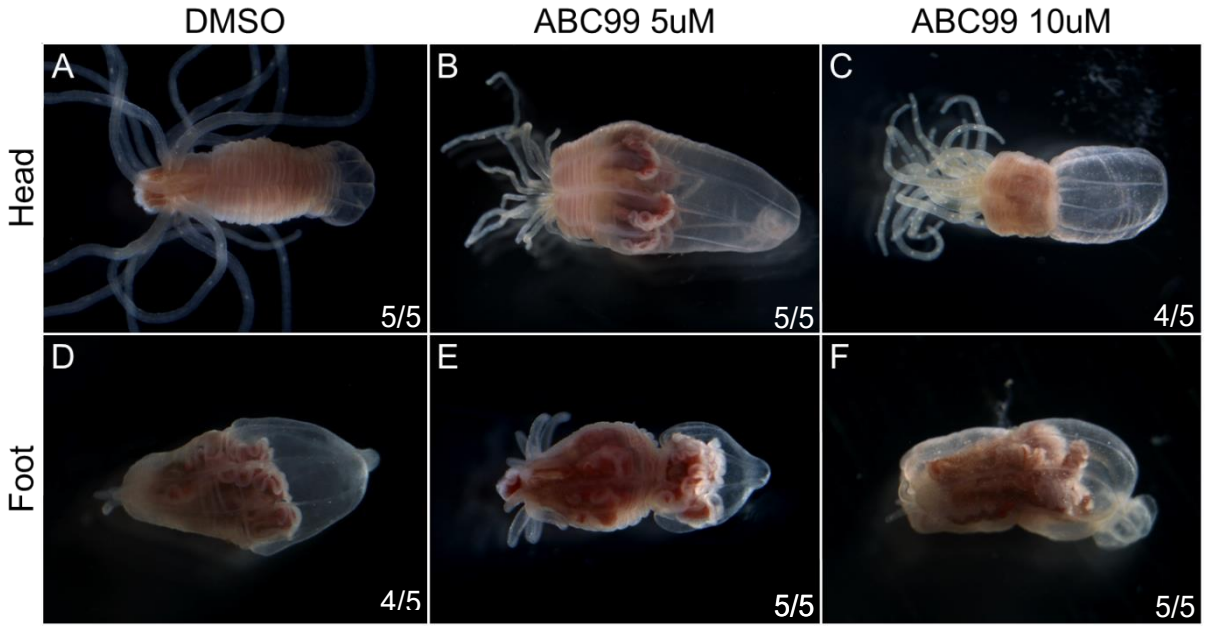

Figure 11 Regeneration of bisected Nematostella adults was not affected by Notum Inhibitor ABC99 treatment. *The treatment started right after bisection until 6 days post cut. The differences in morphology are due to individual differences and the lack of relaxation. The numbers in the bottom left corner of each condition represent the quantification of each outcome. In cases where there are only 4 out of 5, the body half failed to regenerate. All heads are oriented towards the left side.*

After discovering that adults were able to fully regenerate heads and feet at different ABC99 concentrations, this experiment was repeated with primary polyps (PP) (fig.12). For this experiment, 20 primary polyps were used for each condition (DMSO, 5µM & 10µM ABC99), cut in the middle of their body column and incubated in ABC99 inhibitor until fully regenerated. As shown on fig.12A-C, all heads were able to fully regenerate their feet (7d). In contrary to

that, not all feet were able to regenerate their heads. While the DMSO and 10µM ABC99 incubated body halves were able to regenerate and build primary tentacles, the PP in 5µM ABC99 were not. They instead formed an oblong shape, where one can see the pharynx forming, but no tentacles were formed. In this case, the PP were able to re-establish the oral identity as the pharynx region had been removed during the amputation process, but it was not completed. Moreover, in this experiment the survival rate of the regenerates is much lower than in comparison to the adults. In case of fig.12E, there were only 2 surviving animals, which limited the number of phenotypes that can be compared. Nevertheless, as the PP were able to regenerate fully within 10µM ABC99, it is likely that this effect had nothing to do with the Notum inhibitor treatment, but rather being an artefact of the amputation itself. For this reason, we conclude that the treatment of Notum inhibitor ABC99 during regeneration of adult and PP *Nematostella* does not seem to affect regeneration.

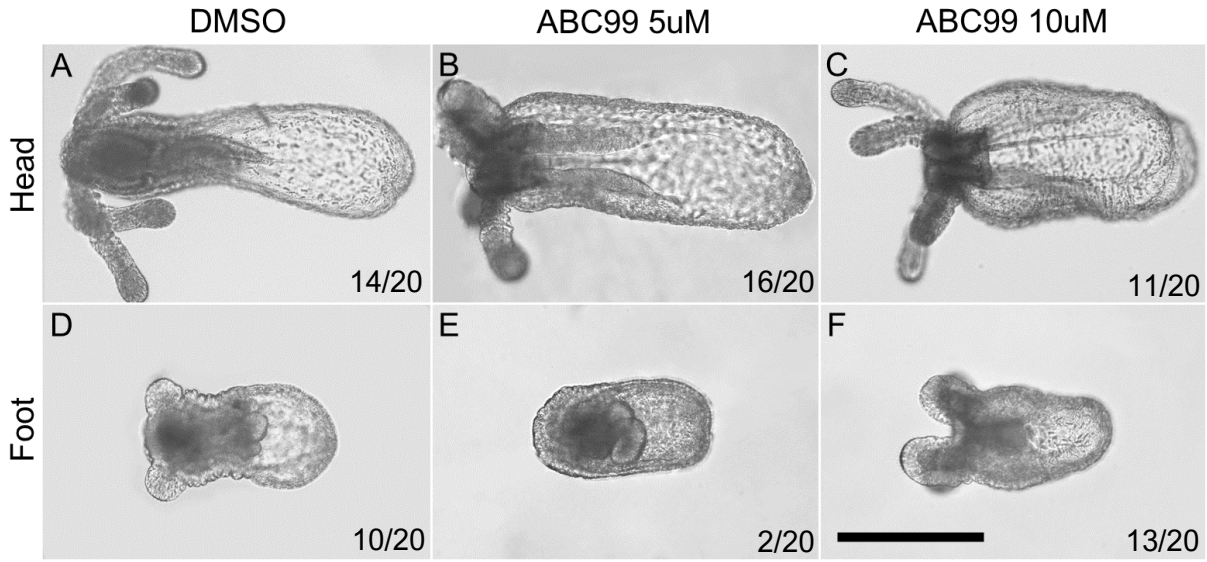

Figure 12 Regeneration of bisected Nematostella primary polyps (PP) was not clearly affected by Notum inhibitor ABC99 treatment. *PPs were cut in the center of the body column and heads (A-C) and tails (D-F) could regenerate in DMSO (A&D) as control and ABC99 at 5µM (B&E) and 10µM (C&F) for 7 days until the entire body axis was re-established. At 5µM ABC99 (E) the foot was not able to regenerate a complete head, but it was able to form a pharynx. The numbers in the bottom left corner of each condition represent the quantification of each outcome, while the remaining ones did not survive the treatment/ regeneration. All heads are oriented towards the left side. Scale bar=2µM.*

3.2.2 ABC99 does not affect head regeneration of *Schmidtea mediterranea*

As the function of Notum is unknown in *Nematostella* and the inhibitor treatment did not affect the regeneration of adults and PP, this experiment was repeated using *Schmidtea mediteranea*, the planarian model organism where Notum acts as the main Wnt-signaling antagonist (Petersen & Reddien, 2011). It is unclear whether the regeneration experiment in *Nematostella* yielded negative results because Notum does not have a role in regeneration or the ABC99 treatment is for some reason ineffective in this organism. To test the inhibitor, the experiment was repeated using planarians, since there is a known RNAi phenotype, which we tried to replicate using ABC99. However, it must be mentioned that we have not found reports of ABC99 being used in *Schmidtea*, where RNAi, understandably, always was the method of choice. In planarians, Notum was shown to play a key part in inhibiting Wnt-signaling at the very anterior end to allow for head regeneration. Upon inhibition of *Notum* using RNA interference (RNAi) it was found that regenerating tails were not able to form a head, but instead formed and an anterior facing tail (Petersen & Reddien, 2011).

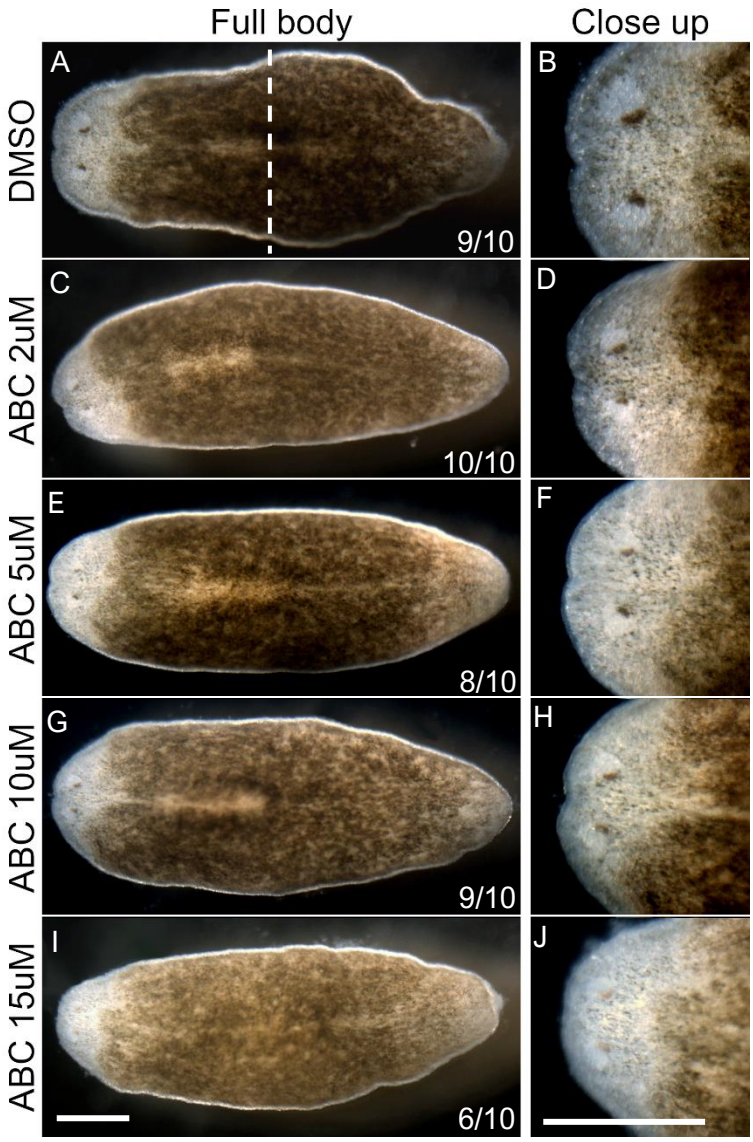

Figure 13 Head regeneration of planarians was not affected by Notum Inhibitor ABC99. *The tail ends of 10 worms per treatment, were incubated directly after being cut in the middle (indicated in A, dashed line). The animals could fully regenerate in 14 days. Shown are full body images (first row) and close ups of the heads of the same animal (second row). All tail ends were able regenerate fully and form eyes. All animals are oriented towards the left. The numbers in the bottom right indicate the quantification of the phenotype shown, others did not survive. Scale bars= 0.5mm.*

For this experiment, 10 animals were cut for each condition: DMSO as control and varying concentrations of ABC99 (2µM, 5µM, 10uM and 15µM). The posterior body halves were placed into the treatment solution directly after being cut, to start the treatment before a blastema could be formed. In this experiment only the posterior halves regenerating heads were observed, as Notum is essential for head formation. All animals were able to regenerate fully upon different inhibitor concentrations (fig.13). This can be clearly seen when looking at the eyes of the planarians, which offer a visible hallmark to assess the anterior identity of the

regenerate (see close ups fig.13). Treatment using 15µM ABC99 caused the eyes of the animals to be less pigmented (see fig.13I&J) in comparison to the other treatments, nonetheless the heads were clearly formed and there was no anterior oriented tail. Higher ABC99 concentrations were also used for this experiment (10µM, 20µM, 30µM, 40µM and 50µM) however, all treatments except for 10µM led to high mortality and regeneration was not possible. To conclude, incubation using ABC99 did not affect the regeneration of the anterior body halves in *Schmidtea mediterranea*. The lack of effect of ABC99 in *Nematostella* and *Schmidtea* may be explained in several ways: i) ABC99 batch we used was non-functional; ii) ABC99 could not penetrate the tissue in *Nematostella* and in *Schmidtea*; iii) *Nematostella* and *Schmidtea* Notum proteins are insensitive to ABC99. It is currently impossible to choose between these options.

3.3 Downregulation of *Notum* has no effect on the gene expression of assayed genes

Since the regeneration experiments using the ABC99 inhibitor were inconclusive, we switched to using embryos for assessing the loss-of-function phenotypes of *Notum*. We reasoned that if Notum acted as a Wnt signaling inhibitor, its knockdown should affect ß-catenin signaling dependent genes involved in patterning the oral-aboral axis in *Nematostella*.

3.3.1 Morpholino KD of *Notum* has little to no effect on the expression of the markers of different embryonic territories.

The first attempt to knock down *Notum* involved the injection of two different *Notum* Morpholinos (MO): the translation-blocking ATG MO and a splice MO, which leads to aberrant splicing. As control, standard MO injected and uninjected wild type embryos were used. We took this approach because prior investigations using these MO were successful (Schauer, 2016) and we wanted to test, whether these results were reproducible. *Notum* was chosen as a control, since it was shown to be affected by morpholino knockdown by Schauer, 2016. In addition, we used an oral marker *Brachyury* and an aboral marker *Six3/6* as known targets of Wnt-signaling, and *Erg* as an endodermal marker expressed in low ß-catenin signaling context (see fig.14) Further *Hedgehog1* (*Hh1*) and *Gli* were chosen as representatives for the Hedgehog signaling pathway and *Dpp* and *Chordin* for the BMP signaling pathway (fig.15).

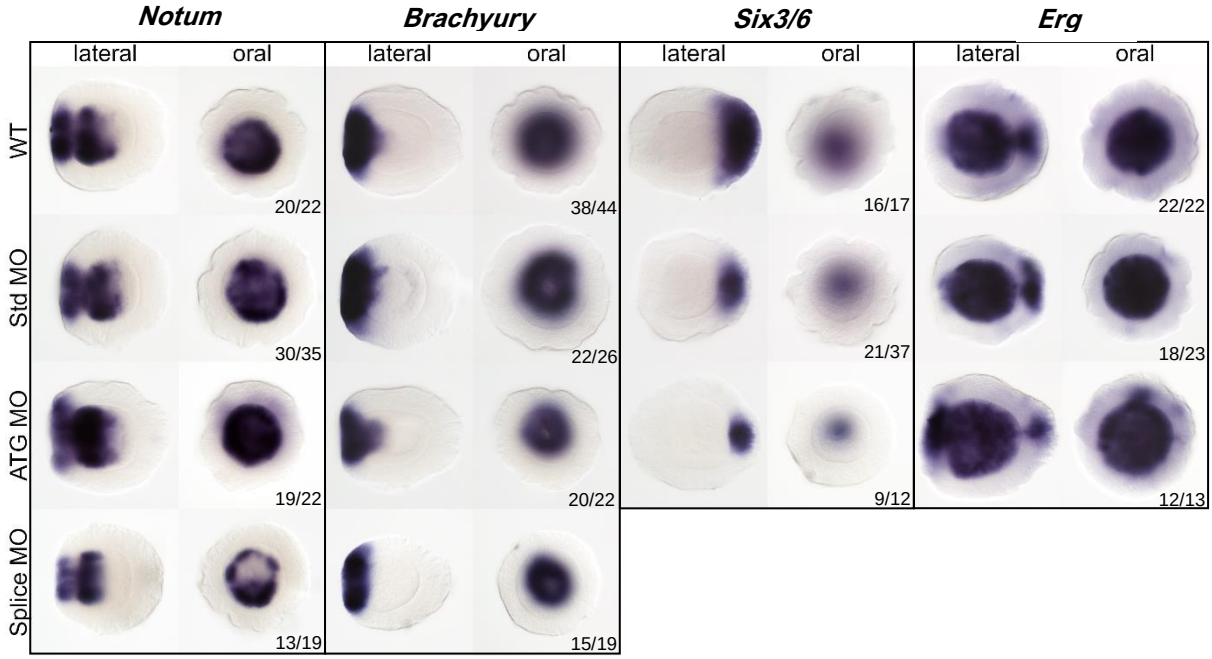

Figure 14 In situ hybridizations using Notum Morpholino injected 2dpf embryos shows that MOs did not KD Notum. *In all 4 genes, there is no change in expression in either condition. The only exception to this, is the Six3/6 expression, where there is stronger expression in the WT than in the Std MO and ATG MO embryos. As this difference is minimal, the Notum MO injection did not knock down Notum, thus not leading to changes in the expression pattern of Notum, Bra, Six3/6 and Erg. The numbers in the bottom left corner of each condition represent the quantification of the expression pattern. Each embryo is shown orally and laterally, in the latter the oral end is oriented towards the left.*

Previous experiments showed that *Notum* KD led to the disappearance of the endodermal *Notum* expression and an expansion of the ectodermal *Notum* domain (Schauer, 2016). In our hands (fig.14), the expression pattern of *Notum* remains the same in the WT and Std MO controls as well as in both *Notum* MO injections. When looking at the gene expression of *Brachyury* there is also no visible change in expression. *Six3/6* expression appears weaker in the ATG MO in comparison so the WT expression, however, when looking at the Std MO, there is also less expression, meaning that this variability is probably unspecific. Lastly, when examining the expression pattern of *Erg*, there is more expression around the oral pole in the MO injected embryos, in comparison to the control embryos. This effect, if specific, speaks in favor of the weaker rather than stronger ß-catenin signaling, which is contradictory to the function of Notum as a Wnt antagonist.

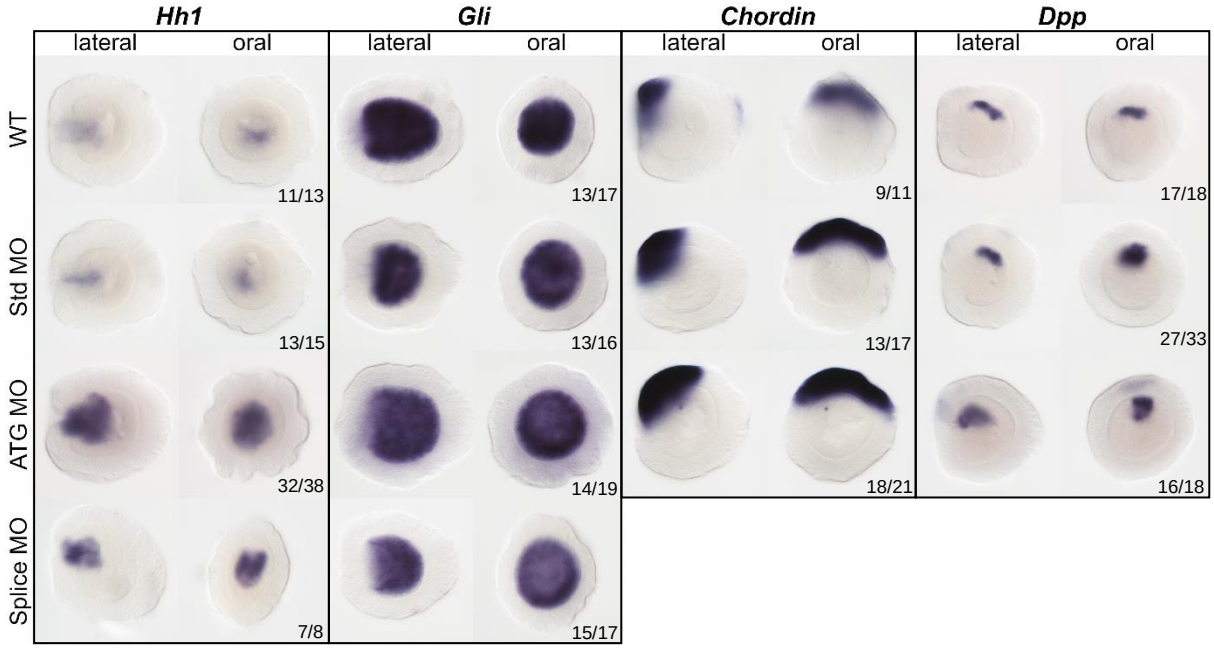

Figure 15 In situ hybridizations using Notum Morpholino injected 2dpf embryos shows no clear effect on assayed genes. *In all 4 genes, there is no obvious change in expression in either condition. The only differences can be seen in Hh1 expression, where there is lower expression in WT and StdMO injections, than in the Notum MO injected embryos. Chordin expression is reduced in the WT than in the MO injected embryos. As variance in gene expression is minimal, the injection of two Notum MO did not affect the expression pattern of Hh1, Gli, Chordin and Dpp. The numbers in the bottom left corner of each condition represent the quantification of the expression pattern. Each embryo is shown orally and laterally, in the latter the oral end is oriented towards the left.*

When examining genes that are involved in different signaling pathways (fig.15) such as the Hedgehog pathway, there is a clear increase of *Hh1* expression in the ATG and Splice MO, when compared to the control embryos. This is the exact opposite for *Gli*, where the expression seems to be slightly reduced in the MO injections. This contradicts the previous observation of Schauer, 2016, who showed the downregulation of *Hh1* transcript and little effect on *Gli* upon MO-mediated *Notum* KD. When looking at *Chordin* and *Dpp*, two genes involved in the BMP signaling pathway, there seems to be no change in expression. Even though one can see some variability in expression patterns, it is not caused by the *Notum* Morpholino injections. Taken together, we conclude, that all changes in expression patterns we observed were unspecific rather than due to knockdown of *Notum*.

3.3.2 Incubation of *Nematostella* embryos using the Notum inhibitor ABC99 has no visible effect on the gene expression of assayed genes involved in certain signaling pathways

As the Morpholino injections were unsuccessful, the second attempt to inhibit Notum was to use the inhibitor ABC99. While there could be several reasons, why there was no observed effect in the regeneration of *Nematostella* and *Schmidtea*, there was still a possibility that ABC99 might affect embryonic development. To test this, fertilized eggs were incubated in DMSO and different ABC99 concentrations, namely 2µM, 5µM and 10µM (see fig.16). To examine the effects, the expression of marker genes was observed using whole mount in situ hybridizations. The marker genes selected were *Notum* to verify the inhibition, *Hh1*, *Gli* and *FoxA* (see fig.16). In all examinations there is some focus on the Hedgehog pathway as it was previously suggested that the KD of *Notum* leads to a reduction of *Hh1* expression (Schauer, 2016). For this reason, in most experiments we assayed genes involved in this pathway. *FoxA* was also included in this an analysis as it is a saturating Wnt-responsive gene co-expressed with *Notum* in the pharynx (Fritzenwanker et a., 2004).

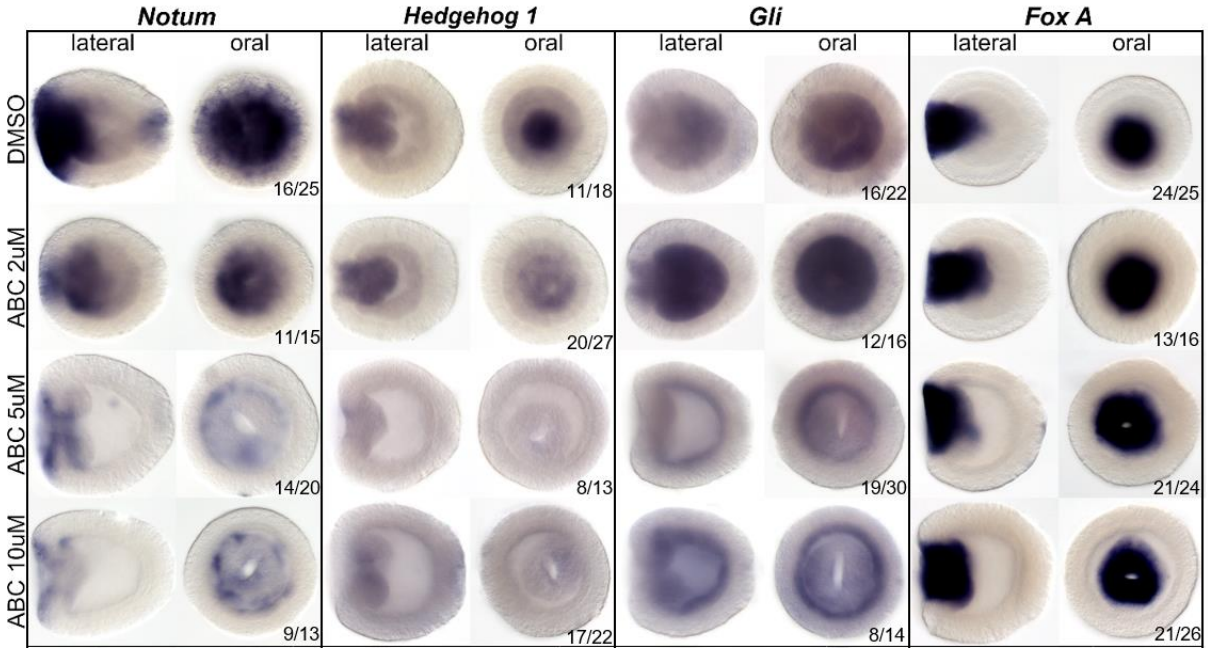

Figure 16 In situ hybridizations using Notum Inhibitor ABC99 treated embryos fixed at 30hpf shows reduced Notum, Hedgehog and Gli expression. *Fox A expression remains completely unchanged in all conditions. For the genes like Hh1and Gli, the results are unclear while FoxA was not affected. The numbers in the bottom left corner of each condition represent the quantification of the expression pattern. Each embryo is shown orally and laterally, in the latter the oral end is oriented towards the left.*

We observed dose-dependent reduction of *Notum* expression in different ABC99 concentrations both in the ectoderm and in the endoderm (fig.16). The aboral expression has completely disappeared and the expression in the pharynx is also reduced. The disappearance of the endodermal expression of *Notum* is in line with the results of Schauer, 2016, but the lack of ectodermal expansion is not. Looking at the *Hh1* expression (fig16), the expression is also rather unusual. The DMSO and 2µM ABC99 treated animals are clearly stained, with expression located in the pharynx, where it is expected. However, at 5µM and 10µM ABC99, the expression is massively reduced, with only faint staining in the pharynx. This expression suggests that *Hh1* is downregulated upon ABC99 treatment, in line with the previous observation of Schauer, 2016. *Gli*, being an effector gene involved in the Hedgehog signaling pathway, also offers an unexpected expression pattern. In the DMSO control, its expression can be found in the pharynx and endoderm. In 2 µM ABC99, the expression appeared stronger than in control, while in 5µM and 10µM ABC99, the staining was comparable to the control suggesting little effect of ABC99. The expression of *FoxA* remains unchanged, independent of the treatment. One can see clear staining of the pharynx, which is unaffected by the treatments.

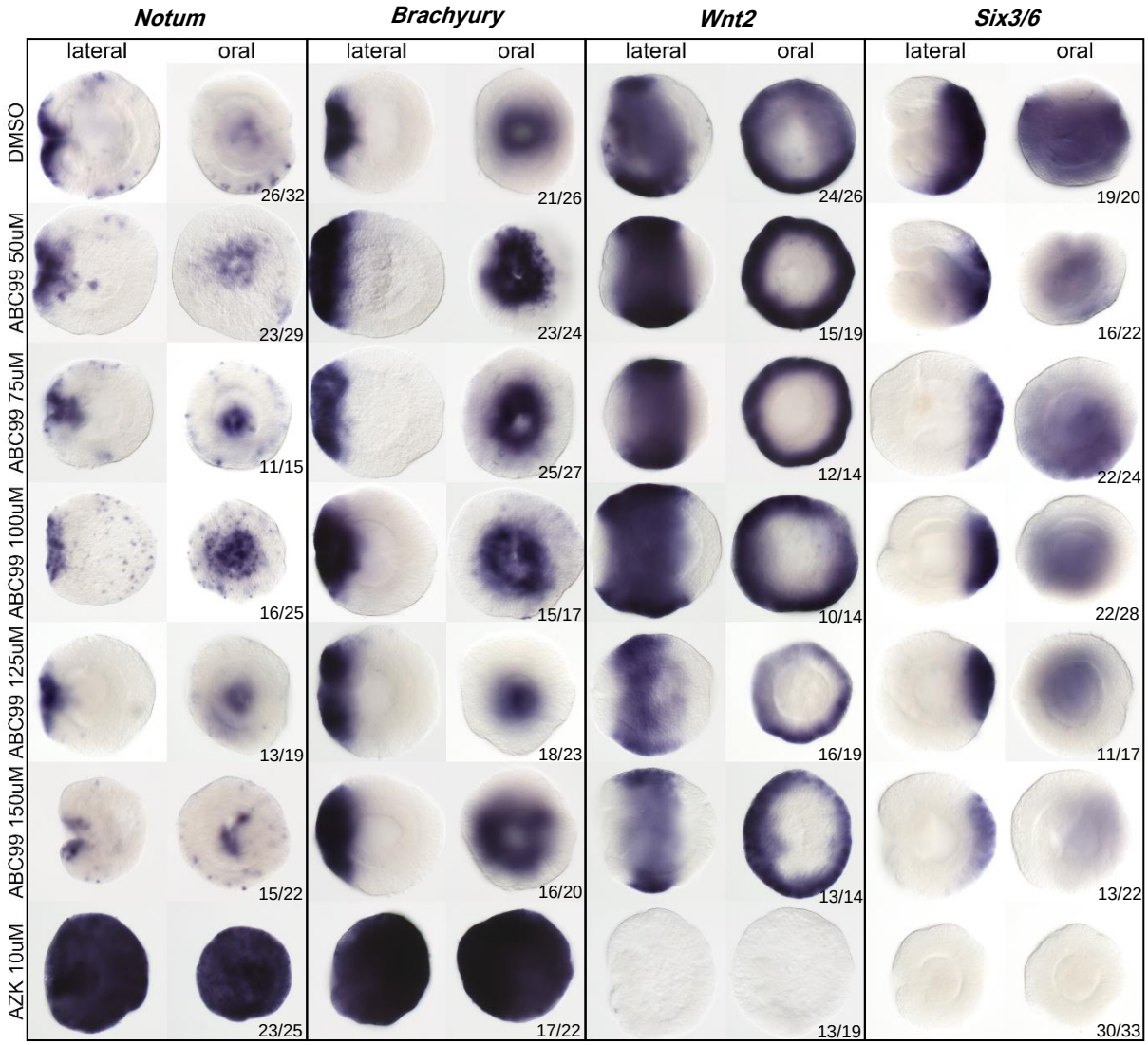

Figure 17 Whole mount in situ hybridization of ABC99 treated embryos fixed at 30hpf shows slight reduction in gene expression of assayed genes. *The treatment was started right after fertilization and ended when fixed. The expression of either gene does not change drastically upon ABC99 treatment. As expected, AZK treatment clearly upregulates Notum and Bra, while Wnt2 and Six3/6 are completely abolished. The numbers in the bottom left corner of each condition represent the quantification of the expression pattern. Each embryo is shown orally and laterally, in the latter the oral end is oriented towards the left.*

As the low concentrations of ABC99 yielded unclear results, the treatment was repeated using higher inhibitor concentrations and a different batch of ABC99 to exclude the possibility of an ineffective batch. For this treatment, the concentrations were increased to 50µM, 75µM, 100µM, 125µM and 150µM ABC99 including DMSO as control and 10µM AZK for comparison (see fig.17 &18). If ABC99 acts as a Notum inhibitor in *Nematostella* and if Notum is a Wnt antagonist, one would expect higher levels of Wnt-signaling upon ABC99 treatment. For this reason, AZK treatment was performed for comparison. *Brachyury*, *Wnt2* and *Six3/6* (see

fig.17) were used as markers of high ß-catenin, medium ß-catenin, a low ß-catenin signaling. As already shown, *Bra* is expressed in the oral most domain and behaves as a saturating gene. In comparison to that, *Wnt2* and *Six3/6* behave as so-called window genes, where *Wnt2* marks the mid body domain and *Six3/6* the aboral domain, subdividing the late gastrula into three axial domains (Bagaeva et al., 2020; Kraus et al., 2016). Also included was *Notum* to verify the effectiveness of the treatment. If ABC99 inhibited Notum, then one would expect an upregulation of Wnt signaling, which in turn upregulates *Notum* expression, similar to the AZK treatment. However, *Notum* expression is centered around the oral pole (fig.17) and with increasing ABC99 concentration, there is a slight reduction of expression. In contrast, in 10µM AZK, *Notum* is distinctly overexpressed, which was expected due to its saturating behavior. The expression pattern of *Brachyury* seems to be unaffected by the varying inhibitor concentrations, as the expression located towards the blastopore remains unchanged. Upon AZK treatment, it is upregulated like *Notum*. In contrary to *Brachyury* and *Notum*, *Wnt2* and *Six3/6* are window genes, meaning that upon increased Wnt-signaling, their expression domain shifts towards the aboral end, until it completely disappears. This can be seen in the AZK treatment (fig.17) where neither gene is expressed. In the ABC99 treatments, the expression domain of *Wnt2* is getting narrower, but there is no shift towards the aboral end. For *Six3/6* the expression appears weaker, however, in this case it is not possible to assess whether it is simply reduced or shifted as well.

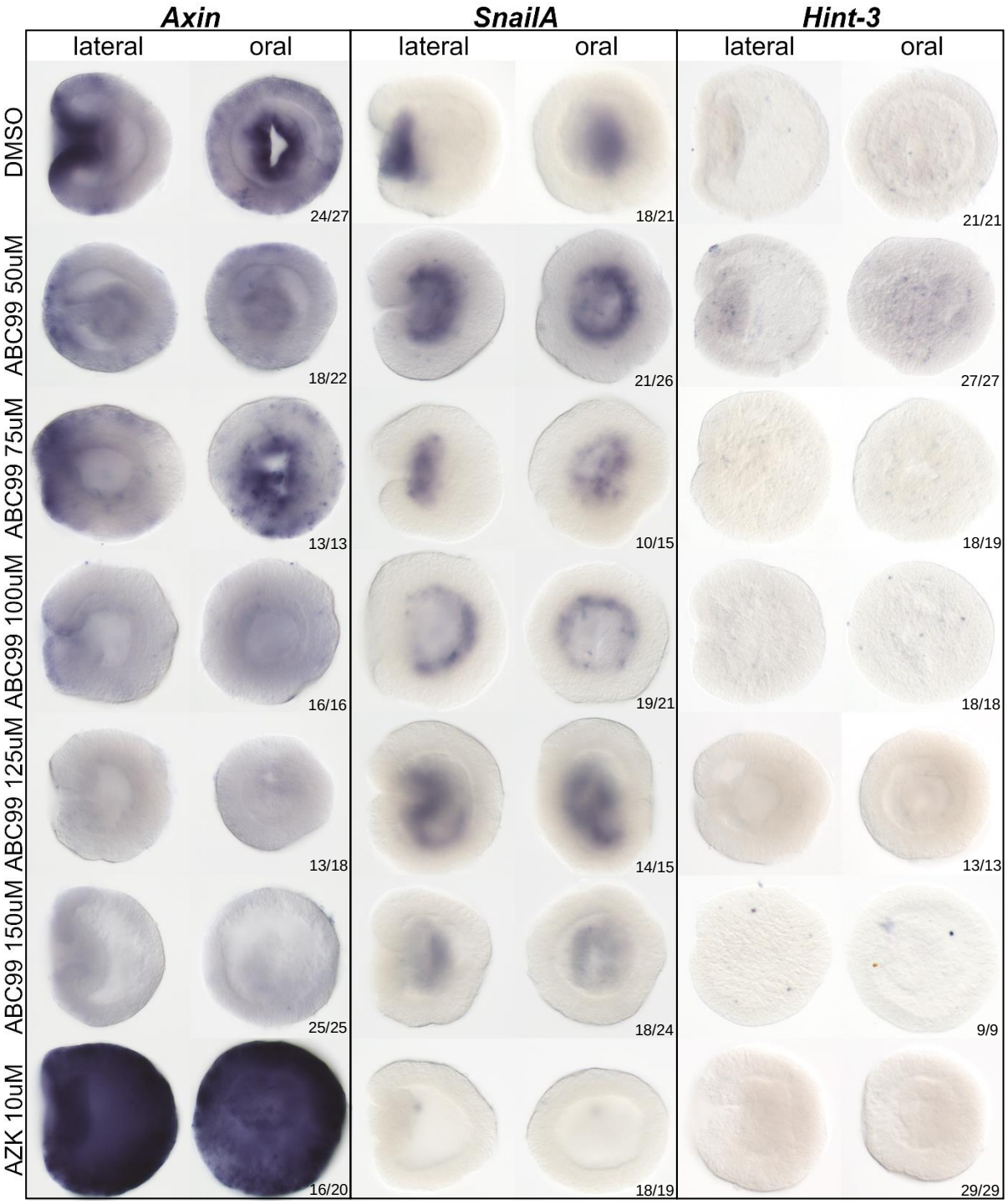

Figure 18 Whole mount in situ hybridization of ABC99 treated embryos fixed at 30hpf shows reduction of Axin expression. *The treatment was started right after fertilization and was ended at fixation. The expression of Snail A and Hint-3 is not affected by ABC99 treatment, while Axin expression seems to be reduced in conjunction with increasing ABC99 concentration. In contrary, AZK treatment clearly upregulates Axin and completely abolishes SnailA and Hint-3. High concentrations of ABC99 only seems to affect Axin but not SnailA and Hint-3 expression. The numbers in the bottom left corner of each condition represent the quantification of the expression pattern. Each embryo is shown orally and laterally, in the latter the oral end is oriented towards the left.*

Other genes included in this analysis were *Axin*, *SnailA* and *Hint3* (see fig.18). The member of the destruction complex *Axin* has been shown to be a direct target of ß-catenin signaling in other systems (Jho et al., 2002) . *Axin* expression is reduced with increasing ABC99 concentrations, which is the exact opposite to our expectation. *SnailA* is one of two *Snail* genes, which is expressed in the endoderm in the low ß-catenin signaling context (Fritzenwanker et al., 2004). As shown, its expression is found in the invaginating endoderm. One can see that there are little changes in *SnailA* expression intensity upon ABC99 treatment. In contrast, upon AZK treatment, *SnailA* expression is abolished, as described previously (Leclere et al., 2016). A Hedgehog-related gene *Hint-3* was the last one to be included in this investigation. It is expressed in single cells in the ectoderm, but at this developmental stage (30hpf) its expression is still rather weak. There is no apparent difference in expression caused by either treatment. In conclusion, the incubation of *Nematostella* embryos in different concentrations of ABC99 did not show any clear effects on gene expression patterns of assayed genes, that would suggest its role as a Wnt-signaling antagonist.

3.3.3 Incubation of *Nematostella* embryos using the Notum inhibitor ABC99 has no effect on the gene expression of a *Notum-like* gene

Previous experiments using ABC99 did not cause any effects on oral-aboral marker gene expression in the embryos or on regeneration of polyps. It remains unclear whether these negative results stem from the ineffectiveness of the method or from Notum not acting as a Wnt signaling antagonist. Upon further analysis, it was found that apart from the previously assayed *Notum*, there are three other *Notum-like* genes in the genome of *Nematostella* (Schauer, 2016). This array of *Notum-like* genes (fig.19) led to the hypothesis, that there might be a certain degree of functional redundancy between the different genes. Assuming this, the loss of function of one *Notum* gene, could be compensated by upregulating a *Notum-like*.

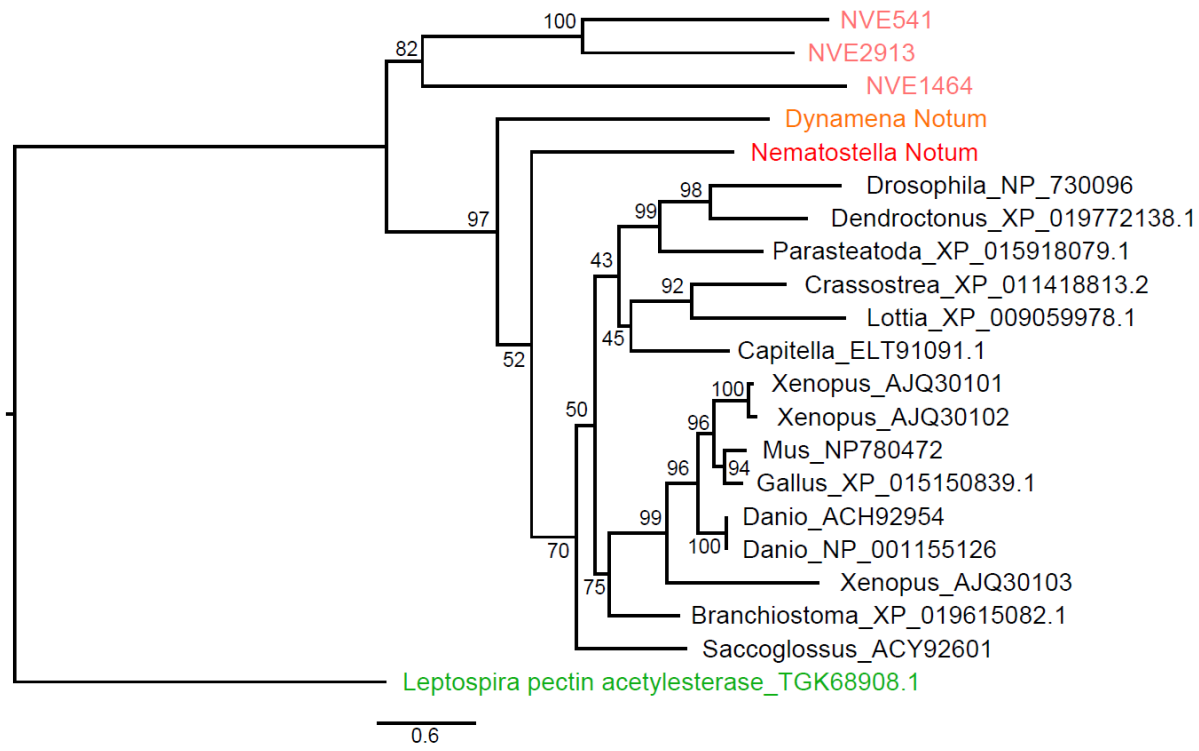

Figure 19 Sequence phylogeny of Notum including Nematostella Notum- like genes (NVE542, NVE1464 and NVE2913)

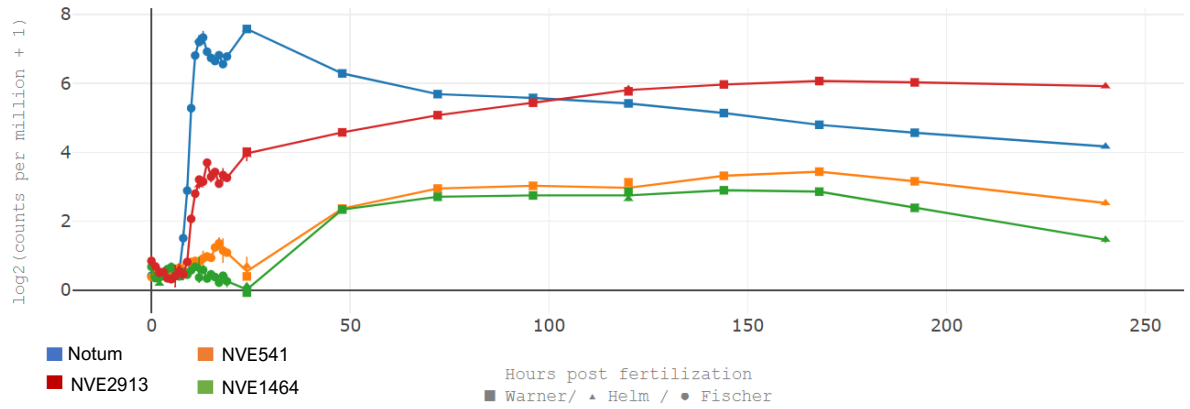

Figure 20 Embryogenesis gene expression plot of Notum and Notum-like genes using NvERTx transcriptome exploration tool (Warner et al., 2017).

The three other *Notum-like* genes are *NVE541*, *NVE1464* and *NVE2913* (fig.19). According to the NvERTx database (Warner et al., 2017), during embryonic development *Notum* (blue) expression is by far the strongest and starts the earliest (fig.20). The *Notum-like* gene *NVE2913* (red) has weaker expression but also starts at 10hpf, which makes it a viable candidate to compensate for *Notum*. The other two genes *NVE1464* (green) and *NVE541* (orange) start to be expressed much later, at around 48hpf with generally weaker expression levels. Upon amputation, *NVE2913* is the only *Notum-like* gene that is upregulated, reaching even higher expression levels than *Notum* and maintaining these levels for longer (fig.21). The other two genes are not expressed and only start being slowly upregulated between 40-60 hpa. For these reasons, any further analyses were focused on *NVE2913*, which will be referred to as *Notum-like*, as the other *Notum* homologs will not be investigated in the following experiments.

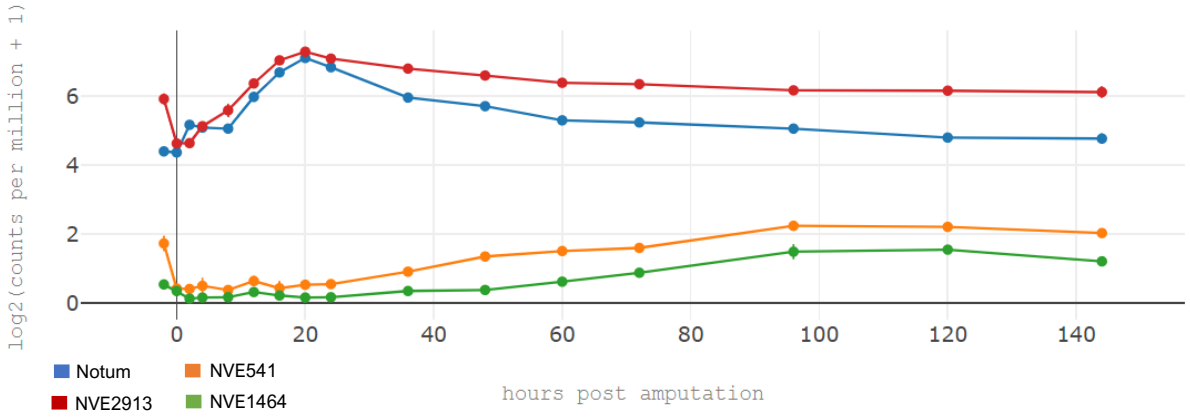

Figure 21 Regeneration gene expression plot of Notum and Notum-like genes using NvERTx transcriptome exploration tool (Warner et al., 2017).

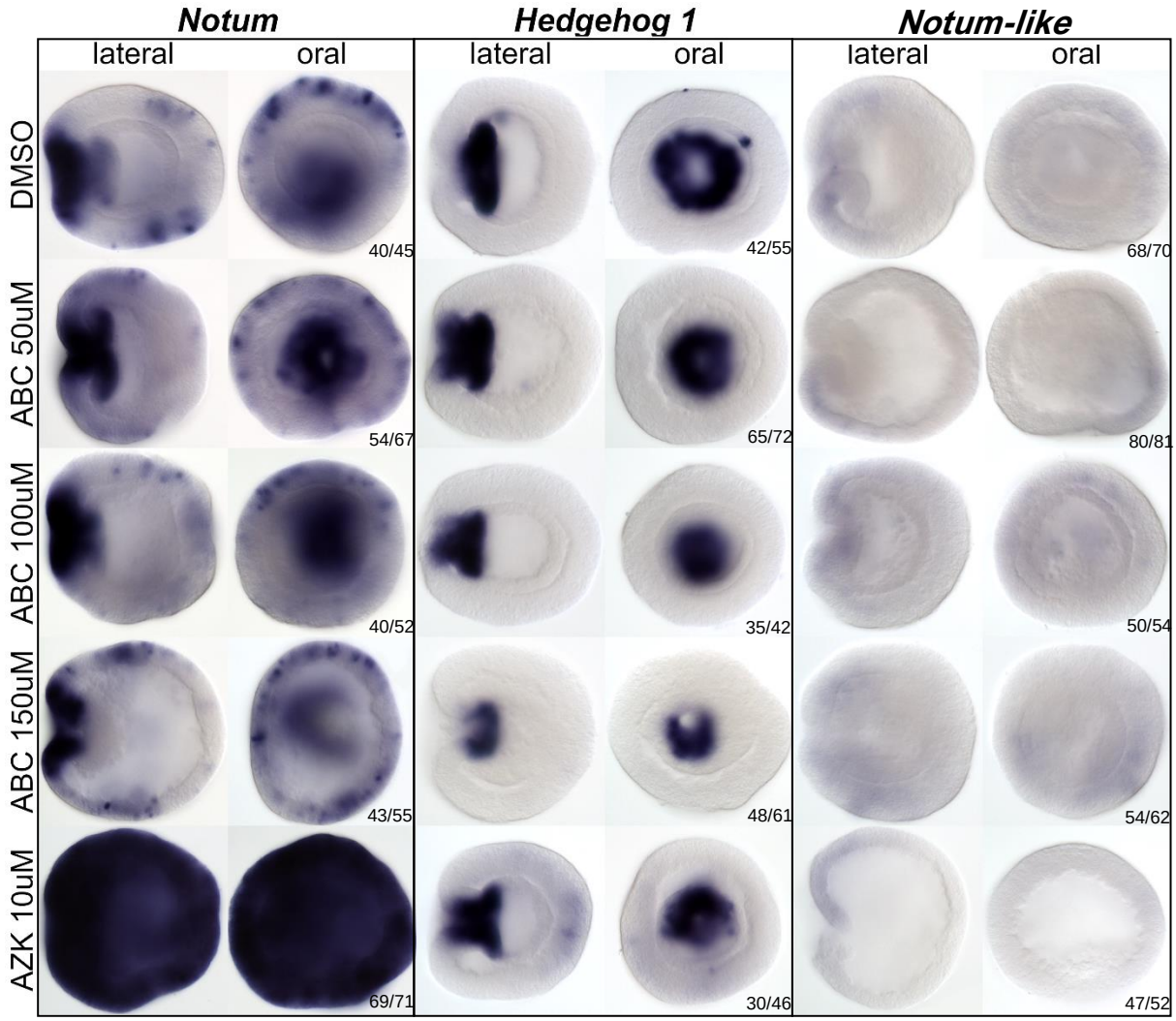

Figure 22 Whole mount in situ hybridization of ABC99 treated embryos fixed at 30hpf shows no change in assayed gene expression. *The treatment was started right after fertilization and ended at fixation. Upon ABC99 treatment, there is no change in expression pattern of either gene. In the AZK treatment, Notum is completely saturated, while Hh1 and Notum-like remain unchanged. The numbers in the bottom left corner of each condition represent the quantification of the expression pattern. Each embryo is shown orally and laterally, in the latter the oral end is oriented towards the left.*

To examine whether the inhibition of Notum using ABC99 incubation, yielded no effects due to compensatory upregulation of the *Notum-like* gene, we treated the embryos in varying high ABC99 concentrations (50µM, 100µM and 150µM), DMSO and 10µM AZK as comparison. We then analyzed the expression of *Notum*, *Notum-like* and *Hh1*. In the animals that were fixed at 30hpf (see fig.22) in late gastrula stage, *Notum* expression is strong and defined. *Notum* is clearly expressed in the oral ectoderm, with expression also reaching into the pharynx. Slight single cell expression can also be seen along the entire ectoderm. Similar to earlier results there was no clear change in the expression pattern found in the ABC99 treatments, while in

the AZK treatment, *Notum* expression was saturated in the ectoderm of the embryo. There might be a slight reduction of *Notum* expression in the 150µM ABC99 but if that is the case, the effect is not strong. *Hh1* is clearly expressed in the pharynx with no obvious change in expression pattern, except for 150µM ABC99, where there is a slight reduction. The *Notum-like* expression is very faint in all conditions (fig.22). It is expressed towards the oral pole, in the same area as *Notum*, which in theory would allow for a functional redundancy. However, neither ABC99 nor AZK treatment does influences *Notum-like gene* expression, which speaks against the possibility that it might compensate for *Notum*.

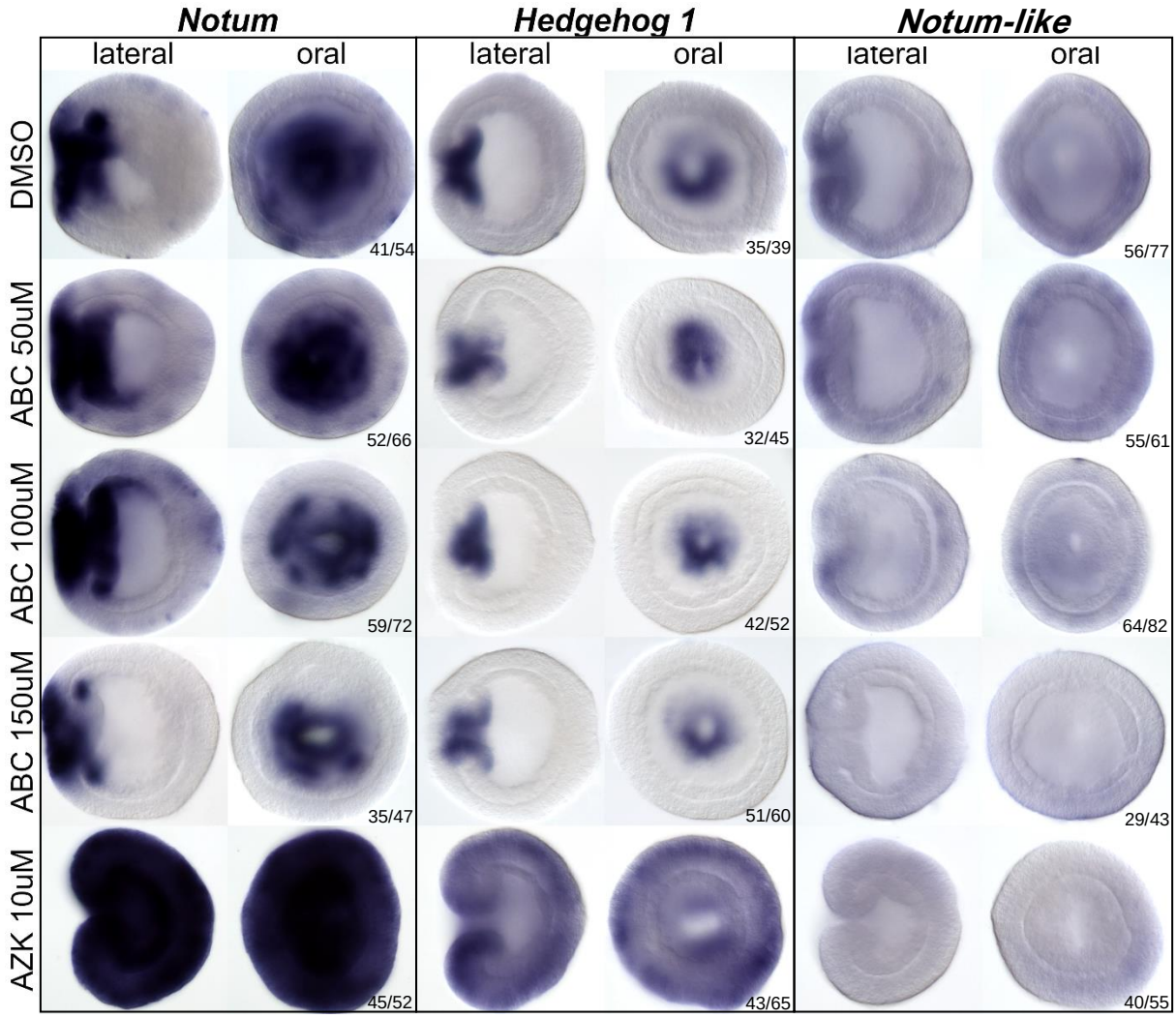

Figure 23 Whole mount in situ hybridization of ABC99 treated embryos, fixed at 2dpf shows reduction of Notum and Notum-like expression. *The treatment was started right after fertilization and was ended when fixed. Upon ABC99 treatment, there is no change in expression pattern of either gene. In the AZK treatment, Notum and Hh1 are completely saturated, while Notum-like appears minimally downregulated. The numbers in the bottom left corner of each condition represent the quantification of the expression pattern. Each embryo is shown orally and laterally, in the latter the oral end is oriented towards the left.*

Investigating the effects of ABC99 incubation on *Notum*, *Notum-like* and *Hh1*, at 2dpf (see fig.23) yielded similar results, as already shown for 30hpf (see fig.22). *Notum* and *Hh1* expressions do not clearly change upon increasing ABC99 treatment. Similar to earlier stages (fig.22), a slight reduction of *Notum* in 150µM ABC99 is observed. *Hh1* expression does not change, except for in the AZK treatment (fig.23). At 2dpf *Hh1* is clearly upregulated upon AZK treatment, while at 30hpf, it is not. The expression of *Notum-like* is stronger in this stage, and more visibly concentrated towards the oral ectoderm. One can also distinguish some slight single cell staining towards the aboral ectoderm, similar to *Notum* expression. An increase in ABC99 concentration, seems to downregulate *Notum-like*, as there is less pharyngeal expression at 100µM and 150µM ABC99. In comparison to that, AZK treatment does not affect *Notum-like* expression, just as observed at 30hpf. Thus, it cannot be excluded that *Notum-like* can functionally compensate for the suppression of *Notum* by ABC99, but if this is the case, it is not reflected in its mRNA expression levels. The lack of the effect of AZK on *Notum-like*, however, can be used as circumstantial evidence against the involvement of *Notum-like* in Wnt signaling.

3.3.4 ABC99 treatment does not increase the amount of active ß-catenin

Since all experiments using the Notum inhibitor ABC99 yielded unclear results, we pursued a different approach to check for its effectiveness. To do so, Western blots were performed to assay the amount of active ß-catenin in the treated embryos. Assuming that Notum acts as Wnt- signaling antagonist, it would directly affect the amount of active ß-catenin. If Notum antagonises Wnt signaling, higher levels of ß-catenin are expected upon ABC99 treatment. Accordingly, fertilized eggs were incubated in different concentrations of ABC99 or DMSO, and after 30hpf, the embryos were lysed, and protein was extracted. Std MO and ß-catenin MO injected embryos, as well as 10µM AZK treated embryos were included to illustrate the effectiveness of the anti-active ß-catenin AB. To verify that for each sample equal amounts of protein were loaded, an antibody against ß-actin was used. Active ß-catenin has a molecular weight of 92kDA while ß-actin has 42kDA, allowing for a clean separation between the two proteins within the same SDS PAGE.

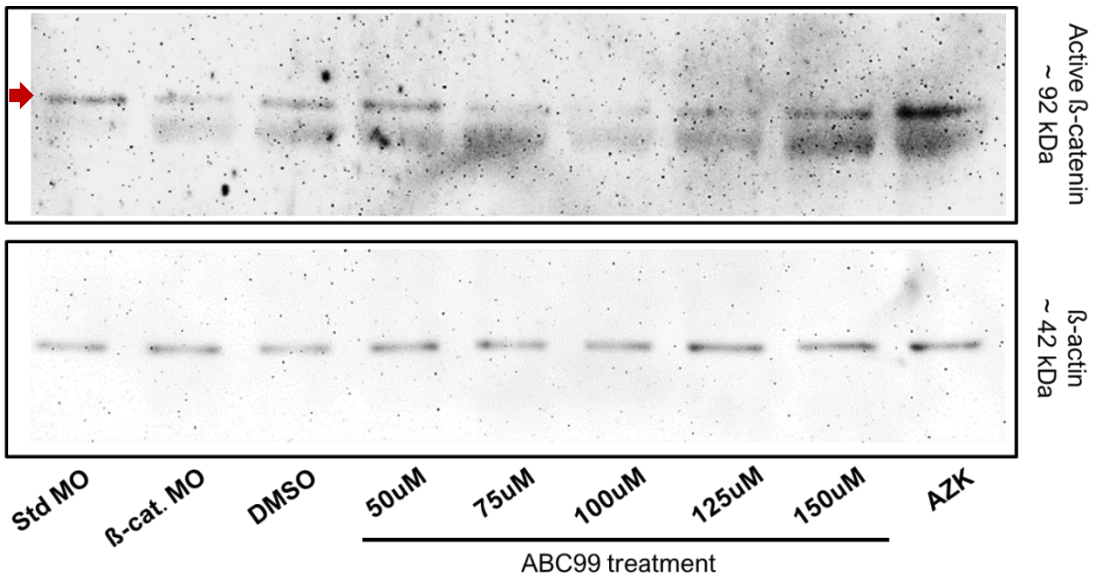

Figure 24 Western blot does not illustrate an increase in active ß-catenin upon ABC99 treatment. *In the ß-cat MO sample, there is less active ß-catenin than in the Std. MO. In the ABC99 treatments, active ß-catenin initially decreases, followed by an increase at 125µM and 150µM. In the AZK treatment, the amount of active ß-catenin is highest, which is expected. There appears to be an effect on the amount of active ß-catenin upon ABC99 treatment. Exposure time: 15 min.*

One can see that in the lower ß-actin panel, serving as the loading control, all samples contain similar amounts of protein (fig.24). An exception to this, are the 125µM ABC99 and AZK samples, where slightly more protein is loaded, than for the other samples. When looking at the amount of active ß-catenin shown in the upper panel, there are clear bands on top marking the ß-catenin whereas there is also a broader, more unspecific protein cloud below each band, which can probably traced back to unspecific binding of the AB. Therefore, we will only discuss the specific bands. When comparing the Std MO to the ß-catenin MO injected embryos, there is a clear reduction of active ß-catenin in the ß-catenin MO sample, suggesting that the AB is properly working. Conversely, ß-catenin band appears much more pronounced in the AZK sample on the right. In the AZK sample, also slightly more protein was loaded, nonetheless, the intensity of ß-catenin is not in relation to the increased load. In ABC99 treated samples (50µM, 75µM, 100µM, 125µM and 150µM), one can see that the DMSO control and 50µM ABC99 have similar levels of active ß-catenin, while in the 75µM and 100µM ABC99 treatments it seems to be reduced, which is exactly the contrary to our hypothesis. In the 125µM and 150µM sample, however, ß-catenin increases again and at 150µM the amount is similar to 50µM ABC99 and DMSO. We conclude that ABC99 treatment does not increase the amount of active ß-catenin in the cytoplasm suggesting that either ABC99 is not actively inhibiting Notum or Notum is not acting as a Wnt antagonist in *Nematostella*.

3.3.5 *Notum* knock-down by RNAi

Since we failed to knock *Notum* down by morpholinos and suppress its function pharmacologically, we switched to using RNAi for gene knockdown. We tested two different shRNAs to target *Notum* (shNot1 & shNot2) including shRNAs against mOrange (shmOr) as control. The efficiency of the KD was verified using qPCR (fig.25). To assay the effect of the knockdowns, we assayed *Notum* and *Hedgehog1* expression, since *Hh1* has been suggested to be affected by *Notum* KD by Schauer, 2016.

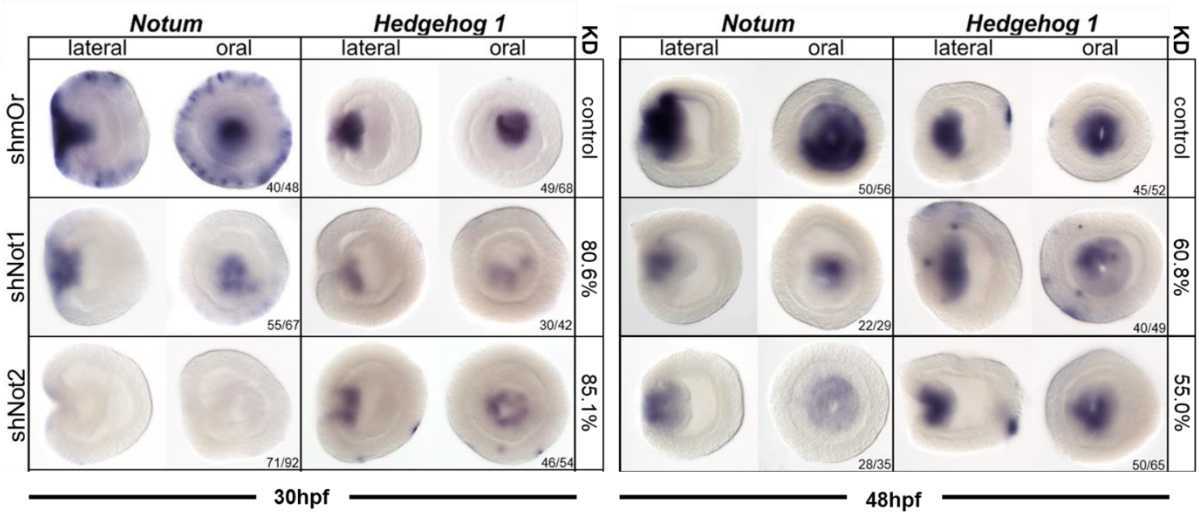

Figure 25 In situ hybridization using shRNA electroporated embryos fixed at 30hpf (left panel) and 48hpf (right panel) illustrates a clear reduction of Notum and Hh1 expression upon Notum KD. *Each panel shows the gene expression pattern of Notum and Hedgehog1 in both lateral and oral view. The numbers on the bottom right of each condition, illustrate the quantification of each expression pattern shown. The electroporated shRNAs are labelled on the left. On the right side of each panel, one can see the knock-down efficiencies (KD) of each electroporation.*

QPCR analysis shows that KD efficiency achieved by electroporation of *Notum* shRNAs, (shNot1 and shNot2) is 80.6% and 85.1%. At the level of in situ hybridization, *Notum* is visibly reduced in both shRNAs (fig.25, left panel). Upon *Notum* KD, expression is mainly reduced in the ectoderm, but remains at the blastopore lip (see shNot1 at 30hpf). Higher KD efficiencies (see shNot2 at 30hpf) also reduced the expression in the blastopore. *Hh1* expression is also slightly reduced, when compared to the mOrange control, in line with the observations of Schauer, 2016. By 48hpf, the effect of the knockdown starts to wear off (fig.25 right panel). After *Notum* shRNA electroporation (shNot1 & shNot2), the amount of *Notum* mRNA was reduced by 60.8% and 55.0% KD in comparison to shmOR. At this point during development,

Notum expression is already restricted to the pharynx and oral endoderm, and the expression appears also appears reduced. *Hedgehog1* expression is not visibly affected, which could be due to the lower KD efficiencies of *Notum*. Thus, we conclude that *Notum* was effectively knocked down by RNAi. The effect of *Notum* KD on *Hh1* expression was comparable to the one reported upon MO-mediated KD by Schauer, 2016.

3.3.6 RNAi against *Notum* does not clearly increase the amount of active ß-catenin

Since the electroporation of shRNAs was effective in knocking down *Notum*, we assayed the amount of active ß-catenin by Western blot. Zygotes were electroporated with shNot1 and shNot2 shRNAs, and protein was extracted at 30 hpf (see fig.26). KD efficiencies were estimated by QPCR. shNot2 electroporation led to a 61.6% downregulation of *Notum*, while shNot1 resulted in its 255.9% overexpression, which is an artefact from time to time occurring after electroporation. However, independent of whether *Notum* was downregulated or upregulated the amount of active ß-catenin appeared to be similar on the Western blot. Due to differences in loading, this experiment needs to be repeated. However, the lack of the correspondence between *Notum* up- or downregulation and the amount of active ß-catenin speaks against the role of Notum as a Wnt-antagonist in *Nematostella*.

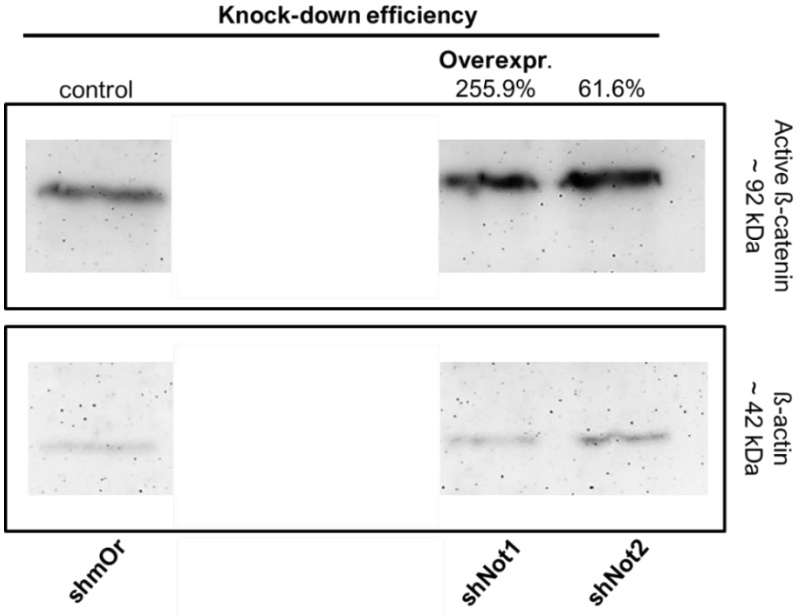

Figure 26 Western blot analysis of active ß-catenin upon Notum RNAi illustrates no effect on the amount of active ß-catenin.

3.4 *Notum* overexpression has no effect on gene expression and amount of active ß-catenin

If Notum acts as a Wnt-signaling antagonist in *Nematostella*, then the overexpression of the protein would lead to a reduction of Wnt-signaling as more Notum is available to deacylate the Wnt-ligands. In other organisms, Notum is α/β hydrolase that contains a conserved GxSxG motif, where the serine is responsible to the hydrolytic activity of the protein (Nardini and Dijkstra, 1999). Therefore, we generated a wild type *Notum* mRNA as well as a putative inactive form of *Notum*, in which the critical serine was replaced by an alanine (S199A), which was previously shown to abolish its enzymatic activity (Zhang et al., 2015). Both, the active and the inactive form of *Notum* were fused to the coding sequence of the *mCherry* reporter via a p2a linker, which results in the translation of two unlinked peptides – the Notum protein with the first 13 amino acids of the p2a peptide and *mCherry* with an additional amino acid on its N-terminus. We injected these mRNAs into *Nematostella* zygotes and confirmed that in both cases mCherry protein was produced (see fig.27), which confirms that Notum is produced as well. Then we analysed the expression *Hh1*, which is affected by *Notum* knockdown, the oral ß-catenin dependent marker *Bra*, and the amount active ß-catenin.

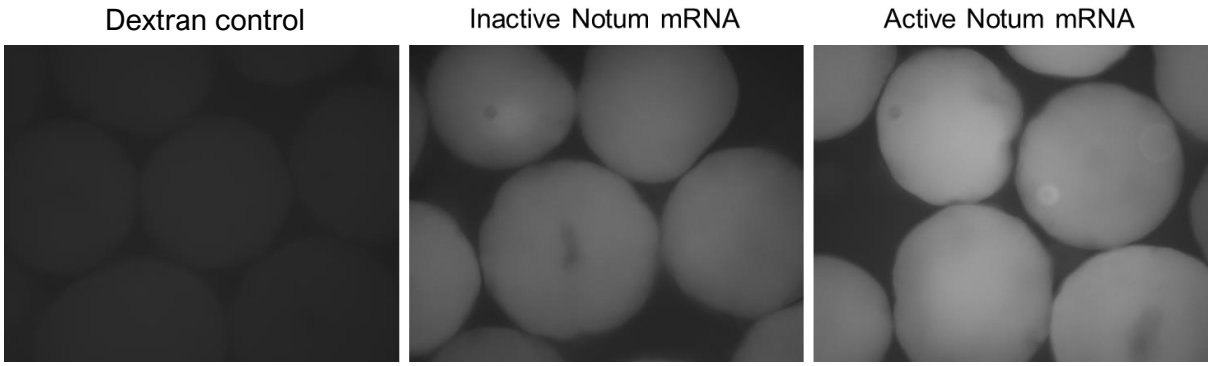

Figure 27 Translation validation of injected mRNAs. *Shown are embryos injected with Dextran-Alexa Fluor 488 as control, 100ng/µl of inactive and active Notum mRNA. The mRNA (incl. mCherry CDS) injected embryos are strongly fluorescent while the control is not, thus the mRNAs were translated.*

In all concentrations (fig. 28), both the active and the inactive form of *Notum* did not seem to result in a change of the *Bra* expression pattern. A slight reduction of the *Hh1* staining observed upon injection of 70 ng/µL solutions of active and inactive *Notum* mRNA does not appear to be significant, and, since it is observed in both cases, is unlikely to be due to the changes in the level of ß-catenin signaling.

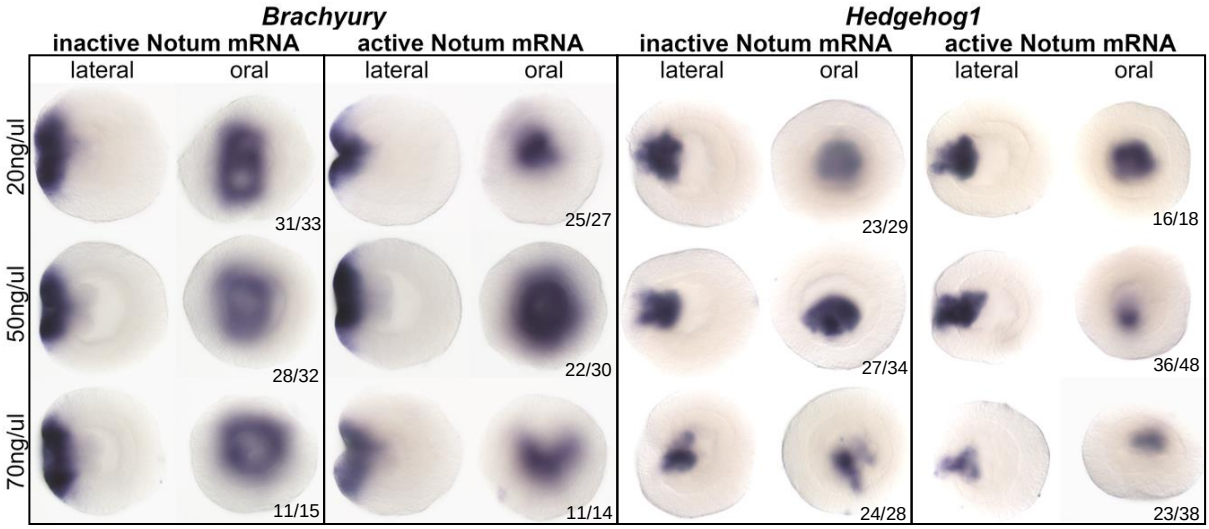

Figure 28 In situ hybridization of Notum mRNA injected embryos at 30 hpf shows no change in gene expression of Brachyury and Hedgehog1*. There is very little change in the expression of both genes under all conditions.*

We then assayed the amount of active ß-catenin in *Notum* mRNA injected embryos by Western blot. If Notum acts as Wnt antagonist, one can expect a reduction in the amount of active ß-catenin in the embryos upon *Notum* overexpression. Therefore, ß-catenin MO injected embryos were used as control (fig. 29).

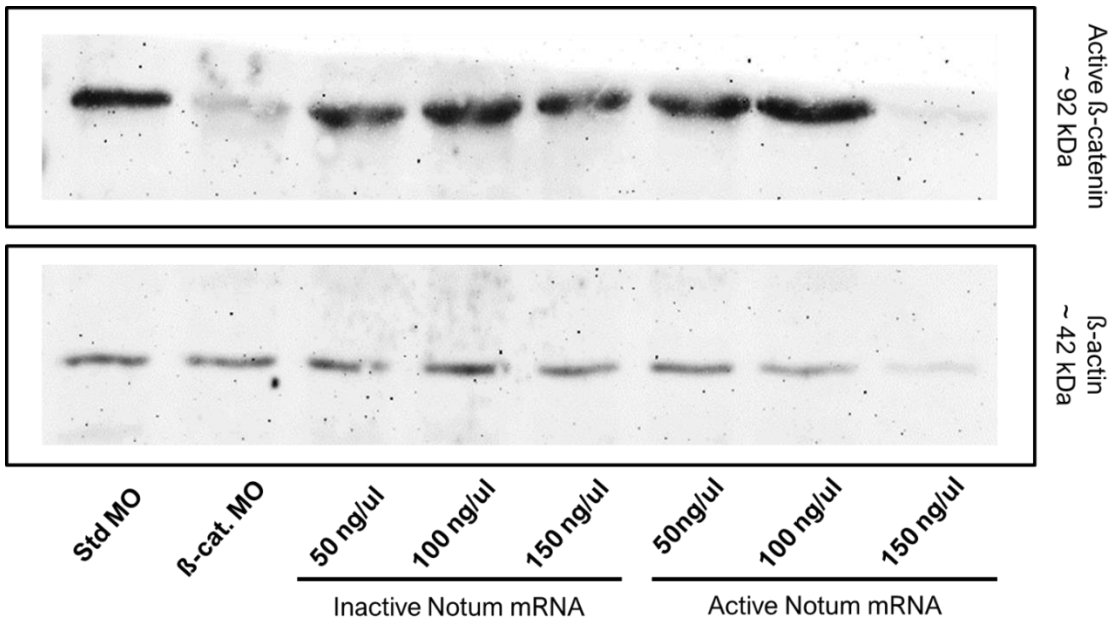

Figure 29 Western blot analysis of active ß-catenin amounts upon Notum mRNA overexpression illustrates no effect. *Protein was extracted at 30hpf. Exposure time: 15 min.*

In contrast to ß-catenin MO injected embryos, in which the amount of active ß-catenin was clearly reduced, the inactive and active *Notum* mRNA injected embryos contained the amount of active ß-catenin comparable to that in the StdMO injected controls. 150 ng/µl active *Notum* mRNA caused increased lethality, which is reflected by the lower amount of protein in the last lane (see anti-ß-actin loading control). Therefore, this lane should be disregarded. However, the comparison of the other lanes clearly indicates that Notum does not reduce the amount of active ß-catenin in *Nematostella*.

4 Discussion

The canonical Wnt-signaling pathway is a crucial component of embryonic development and establishment of the primary body axis in *Nematostella*. Depending on the developmental stage, overactivation of canonical Wnt-signaling can result in the formation of ectopic heads or complete oralization, meaning that this pathway has to be highly regulated to maintain appropriate signaling levels (Bagaeva et al., 2020; Kraus et al., 2016; Marlow et al., 2013; Trevino et al., 2011). In this Master thesis, we perform loss- and gain-of-function experiments to investigate the role of *Nematostella* Notum, which was identified as a Wnt-signaling antagonist in many different organisms and evaluate whether this function is conserved in our model.

4.1 Treatment with the Notum inhibitor ABC99 did not lead to changes in ß-catenin signaling in *Nematostella*

The first approach that we took to downregulate Notum was by using a commercial Inhibitor, ABC99. Although clearly less specific than genetic methods, inhibitor treatments are a common tool in *Nematostella* thanks to their simplicity, low cost and, especially, since they can be applied at any developmental stage, including adults. ABC99 was shown to be effective in mammalian intestinal stem cells (Liang et al., 2020; Pentinmikko et al., 2019) and there is evidence that it is effective in hydroids (Kremnyov et al., personal communication), which is why this was the first method applied.

Initially, we investigated the effects of ABC99 using regeneration experiments in *Nematostella* and *Schmidtea*. However, neither in *Nematostella* adults, nor in primary polyps, ABC99 incubation affected regeneration. As Wnt signaling is a crucial component in the regeneration of cnidarians (Hobmayer et al., 2000; Lengfeld et al., 2009; Schaffer et al., 2016; Trevino et al., 2011), the inhibition of a Wnt antagonist is expected to influence it. However, we did not observe any changes in the regeneration process both in adults and in primary polyps, which may have three possible explanations: i) *Nematostella* Notum does not regulate Wnt signaling during regeneration; ii) ABC99 does not penetrate *Nematostella* tissue; iii) ABC99 penetrates *Nematostella* tissue but does not inhibit *Nematostella* Notum. To test the functionality of ABC99, we used regenerating *Schmidtea mediterranea*, a planarian with a well-characterized RNAi phenotype for *Notum*. We repeated the bisection experiment of Petersen & Reddien, 2011 using ABC99 instead of RNAi. In *Schmidtea mediterranea*, Notum is a crucial antagonist

of Wnt signaling necessary for head formation in the anterior-facing wounds. *Notum* RNAi caused the regeneration of an anterior-facing tail instead of a head following bisection (Petersen & Reddien, 2011). Unfortunately, we could not reproduce the *Notum* RNAi phenotype by ABC99 incubation, leaving us with the same three possible explanations of the lack of ABC99 effect mentioned above.

Since no effect of ABC99 was discovered during the regeneration, we tested ABC99 in embryos, where morpholino mediated knockdown of *Notum* was previously shown not to affect the expression of the Wnt signaling target *Brachyury* but reduce the expression intensity of *Hedgehog1* (Schauer, 2016). Unfortunately, we realized that old *Notum* morpholinos lost their activity, so we could not use them as controls for our inhibitor treatments. For this experiment, embryos were treated in different ABC99 concentrations (2µM to 10µM) starting right after fertilization until fixation at 30hpf (see fig.16) and then used for whole mount in-situ hybridization. There are clear changes in the expression patterns of *Notum*, *Hedgehog1* and *Gli* in the ABC99 treatment, especially in higher concentrations (5µM &10µM), however, these changes are inconsistent with the ones previously reported by Schauer, 2016 in the morpholino experiment. Therefore, we cannot be sure whether the treatment led to inhibition of Notum. In consequence, this experiment was repeated, using higher ABC99 concentrations (50µM to 150µM) and AZK (10µM) as a control (fig.17 & 18). To monitor possible changes in ß-catenin signaling intensity, we performed in situ hybridization with probes against well-characterized markers of the high, medium and low ß-catenin signaling. However, in contrast to the controls treated with the GSK3ß antagonist AZK, there was no sign of upregulation of the Wnt/ß-catenin signaling even in the highest concentrations of ABC99.

Nematostella has three gene models coding for proteins similar to *Notum*, so it is theoretically possible that some of them might compensate for the ABC99-mediated suppression of Notum (unless ABC99 is also capable of suppressing their activity). One of them, *NVE2913*, which we called *Notum-like*, is upregulated during early embryonic development and during head regeneration. We tested whether *Notum-like* expression was upregulated by AZK and by ABC99 treatment, and it was not. Thus, it is quite unlikely that the effect of Notum suppression by ABC99 is compensated for by the upregulation of *Notum-like*. To verify the apparent lack of effect of ABC99 on ß-catenin signaling, Western blots targeting active ß-catenin were performed. If Notum acts a Wnt- signaling antagonist, one would expect more active ß-catenin in the cytoplasm upon Notum inhibition. We confirmed that the anti-active ß-catenin AB is effective, judging by the decreased intensity of the active ß-catenin band in the ß-catenin MO injected embryos, and the increased amount of active ß-catenin in AZK treated embryos.

However, there was no accumulation of active ß-catenin in the ABC99 treated embryos. Thus, ABC99 incubation does not affect Wnt/ß-catenin signaling in *Nematostella*. The failure of any concentration of ABC99 to reproduce the previously reported effect of *Notum* MO on *Hedgehog 1* expression (Schauer, 2016) suggests that Notum is not inhibited in the ABC99 incubated embryos.

4.2 Down- or upregulation of *Notum* expression does not affect ß-catenin signaling

Due to the inconclusive results of the ABC99 treatment and the inefficiency of the MO injections, we also tried to knock-down *Notum* using the electroporation of small hairpin RNAs (shRNAs). The efficiency was validated using qPCR as well as in situ hybridization, and we could see a clear reduction of *Notum* expression using both *Notum* shRNAs at 30hpf and 2dpf. Importantly, similar to the MO-mediated knockdown (Schauer, 2016), *Notum* RNAi reduced *Hedgehog 1* expression. *Notum-like* was also targeted using 2 different shRNAs, however, these shRNAs were less effective and the outcome of the subsequent in situ hybridization was not clearly interpretable. Therefore, we decided to leave *Notum-like* out, and continued with the analysis of the effect of *Notum* RNAi on ß-catenin signaling by Western blot using the α-active ß-catenin antibodies. According to qPCR analysis, in this experiment, electroporation of only one of the two *Notum* shRNAs resulted in a knockdown, while the other caused *Notum* overexpression, which is a common electroporation artefact. In spite of problems with loading, it is clear that the amount of active ß-catenin is unaffected by either the loss of 61.1% of *Notum* transcript or by 256% overexpression of *Notum*.

To evaluate the effect of *Notum* upregulation on ß-catenin signaling we overexpressed it ubiquitously by mRNA microinjection into zygotes. Two different mRNAs were injected, one carrying the wildtype *Notum* CDS linked to *mCherry* via a p2a peptide, and the other one, the putative inactive form to be used as control. This inactive form has a serine-to-alanine substitution in the conserved GXSXG active site motif, which resulted in the loss of Notum activity in in *Drosophila* (Giráldez et al., 2002) and *Xenopus* (Zhang et al., 2015). Although *mCherry* expression confirmed that both our mRNAs were translated, no obvious effect on ß-catenin signaling could be detected both at the level of marker gene expression and by the amount of active ß-catenin. Thus, we conclude that Notum is probably not a Wnt antagonist in *Nematostella*.

4.3 Possible alternative roles for *Nematostella* Notum

While most of this investigation was focused on the effect of Notum on canonical Wnt-signaling, experiments also included the analysis of *Hedgehog1* (*Hh1*). Previous analysis of Notum (Schauer, 2016), have shown that the injection of *Notum* MO (500µM) leads to a reduction of *Hh1* expression. We reproduced this result in our RNAi experiments. *Hedgehog1* is one of 2 *Nematostella* Hh ligands (NvHh1 and NvHh2) that can active the Hedgehog signaling pathway (Matus et al., 2008). The basic molecular mechanism of Hedgehog signaling is best understood in *Drosophila*, as well as vertebrates (Huangfu & Anderson, 2006). When Hedgehog ligands bind the receptor Patched, Patched can no longer inhibit Smoothened, another membrane bound receptor (Lee et al., 2016), of which there are two identified two homologs (NvSmo1 & NvSmo2) in *Nematostella* (Matus et al., 2008). This allows the full-length transcription factor Gli, to accumulate and activate any downstream targets (Lee et al., 2016). Similar to Wnt-ligands, Hh-ligands also have palmitates attached, making up one of its two lipid modifications, the other one being a cholesterol (Willert et al., 2003). While Wnt and Hh are unrelated proteins, there have been speculations about the evolutionary origin of both pathways as lipid modified signaling system based on specific membrane translocators have been reported in the bacterium *Myxococcus*. This suggests a possible common origin of the Wnt and Hh signaling systems (Nusse, 2003).

Recently it was shown that putative primordial germ cells (PGCs) are formed between the expression domains of *Patched* and *Hh1*, which suggests that Hh signaling is needed for PGC formation and specification. Moreover, *Hh1* mutants exhibited broad endomesodermal patterning defects, indicating the conserved role of this pathway during gut and germline development (Chen et al., 2020). It would be, of course, exciting if Notum in *Nematostella*, unlike in Bilateria, were capable of deacylating Hh ligands. However, the connection between Notum and Hedgehog signaling can also be different. In *Drosophila* imaginal disk, Notum appears to cleave the GPI anchor of the membrane-tethered glypican Dally, which in turn, binds Hedgehog. In Hh secreting cells this appears to result in the release of the Dally-Hh complex and its long-range diffusion. In Hh receiving cells, Dally cleavage by Notum seems to promote the internalization of the Hh-Patched ligand receptor complex. Thus, Dally hydrolysis by Notum appears to provide a switch between the short-range and long-range Hedgehog signaling (Ayers et al., 2010, 2012).

In the future, it would be interesting to analyse the possible role of Notum in the regulation of Hedgehog signaling in more detail by checking the expression of Hedgehog pathway

components and target genes upon *Notum* RNAi and in *Notum* CRISPR mutants. Conversely, the expression of *Notum* should be analysed upon Hedgehog signaling inactivation – either in a mutant line (Chen et al., 2020) or in cyclopamine treated embryos.

4.4 Conclusion

In this Master thesis, I tested whether *Nematostella* Notum is involved in regulating ß-catenin signaling, using methods such as Inhibitor treatments, Morpholino injections and shRNA electroporations to achieve a repression or KD, as well as mRNA injections to overexpress *Notum*. In my investigations, I could not confirm that Notum acts as a Wnt-signaling antagonist, or in any way involved in regulating Wnt-signaling, however, it might play a role in the Hedgehog signaling pathway.

5 Bibliography

Ashe, H. L., & Briscoe, J. (2006). The interpretation of morphogen gradients. In *Development* (Vol. 133, Issue 3, pp. 385–394). The Company of Biologists Ltd. https://doi.org/10.1242/dev.02238

Ayers, K. L., Gallet, A., Staccini-Lavenant, L., & Thérond, P. P. (2010). The Long-Range Activity of Hedgehog Is Regulated in the Apical Extracellular Space by the Glypican Dally and the Hydrolase Notum. *Developmental Cell*, *18*(4), 605–620. https://doi.org/10.1016/j.devcel.2010.02.015

Ayers, K. L., Mteirek, R., Cervantes, A., Lavenant-Staccini, L., Thérond, P. P., & Gallet, A. (2012). Dally and notum regulate the switch between low and high level hedgehog pathway signalling. *Development (Cambridge)*, *139*(17), 3168–3179. https://doi.org/10.1242/dev.078402

Bagaeva, T., Aman, A. J., Graf, T., Niedermoser, I., Zimmermann, B., Kraus, Y., Schatka, M., Demilly, A., Technau, U., & Genikhovich, G. (2020). β-catenin dependent axial patterning in Cnidaria and Bilateria uses similar regulatory logic. In *bioRxiv* (p. 2020.09.08.287821). bioRxiv. https://doi.org/10.1101/2020.09.08.287821

Bouldin, C. M., & Kimelman, D. (2012). Taking a bite out of Wnts. *Cell Research*, *22*(12), 1621–1623. https://doi.org/10.1038/cr.2012.104

Capron, A., Chatfield, S., Provart, N., & Berleth, T. (2009). Embryogenesis: Pattern Formation from a Single Cell. *The Arabidopsis Book*, *7*, e0126. https://doi.org/10.1199/tab.0126

Chen, C. Y., McKinney, S. A., Ellington, L. R., & Gibson, M. C. (2020). Hedgehog signaling is required for endomesodermal patterning and germ cell development in the sea anemone nematostella vectensis. *ELife*, *9*, 1–27. https://doi.org/10.7554/ELIFE.54573

Christian, J. L. (2012). Morphogen gradients in development: From form to function. *Wiley Interdisciplinary Reviews: Developmental Biology*, *1*(1), 3–15. https://doi.org/10.1002/wdev.2

Flowers, P. G., Topczewska, J. M., & Topczewski, J. (2012). A zebrafish Notum homolog specifically blocks the Wnt/β-catenin signaling pathway. *Development (Cambridge)*, *139*(13), 2416–2425. https://doi.org/10.1242/dev.063206

Fried, P., & Iber, D. (2014). Dynamic scaling of morphogen gradients on growing domains. *Nature Communications*, *5*(1), 1–12. https://doi.org/10.1038/ncomms6077

Fritzenwanker, J. H., Saina, M., & Technau, U. (2004). Analysis of forkhead and snail expression reveals epithelial-mesenchymal transitions during embryonic and larval development of Nematostella vectensis. *Developmental Biology*, *275*(2), 389–402. https://doi.org/10.1016/j.ydbio.2004.08.014

García de Herreros, A., & Duñach, M. (2019). Intracellular Signals Activated by Canonical Wnt Ligands Independent of GSK3 Inhibition and β-Catenin Stabilization. In *Cell* (Vol. 8, Issue 10). NLM (Medline). https://doi.org/10.3390/cells8101148

Genikhovich, G., & Technau, U. (2009). Induction of spawning in the starlet sea anemone nematostella vectensis, in vitro fertilization of gametes, and dejellying of zygotes. *Cold Spring Harbor Protocols*, *4*(9), pdb.prot5281. https://doi.org/10.1101/pdb.prot5281

Genikhovich, G., & Technau, U. (2017). On the evolution of bilaterality. *Development*

(Cambridge), *144*(19), 3392–3404. https://doi.org/10.1242/dev.141507

Gierer, A., & Meinhardt, H. (1972). A theory of biological pattern formation. *Kybernetik*, *12*(1), 30–39. https://doi.org/10.1007/BF00289234

Giráldez, A. J., Copley, R. R., & Cohen, S. M. (2002). HSPG modification by the secreted enzyme Notum shapes the Wingless morphogen gradient. *Developmental Cell*, *2*(5), 667–676. https://doi.org/10.1016/S1534-5807(02)00180-6

Green, J. B. A., & Sharpe, J. (2015). Positional information and reaction-diffusion: Two big ideas in developmental biology combine. *Development (Cambridge)*, *142*(7), 1203–1211. https://doi.org/10.1242/dev.114991

Guder, C., Philipp, I., Lengfeld, T., Watanabe, H., Hobmayer, B., & Holstein, T. W. (2006). The Wnt code: cnidarians signal the way. *Oncogene*, *25*, 7450–7460. https://doi.org/10.1038/sj.onc.1210052

Gurdon, J. B., & Bourillot, P. Y. (2001). Morphogen gradient interpretation. In *Nature* (Vol. 413, Issue 6858, pp. 797–803). Nature. https://doi.org/10.1038/35101500

Hao, H. X., Jiang, X., & Cong, F. (2016). Control of Wnt receptor turnover by R-spondin-ZNRF3/RNF43 signaling module and its dysregulation in cancer. In *Cancers* (Vol. 8, Issue 6). MDPI AG. https://doi.org/10.3390/cancers8060054

Hill, E. M., & Petersen, C. P. (2018). Positional information specifies the site of organ regeneration and not tissue maintenance in planarians. *ELife*, *7*. https://doi.org/10.7554/eLife.33680

Hobmayer, B., Rentzsch, F., Kuhn, K., Happel, C. M., Von Laue, C. C., Snyder, P., Rothbächer, U., & Holstein, T. W. (2000). WNT signalling molecules act in axis formation in the diploblastic metazoan Hydra. *Nature*, *407*(6801), 186–189. https://doi.org/10.1038/35025063

Holló, G. (2015). A new paradigm for animal symmetry. In *Interface Focus* (Vol. 5, Issue 6). Royal Society of London. https://doi.org/10.1098/rsfs.2015.0032

Huangfu, D., & Anderson, K. V. (2006). Signaling from Smo to Ci/Gli: Conservation and divergence of Hedgehog pathways from Drosophila to vertebrates. In *Development* (Vol. 133, Issue 1, pp. 3–14). The Company of Biologists. https://doi.org/10.1242/dev.02169

Ikmi, A., McKinney, S. A., Delventhal, K. M., & Gibson, M. C. (2014). TALEN and CRISPR/Cas9-mediated genome editing in the early-branching metazoan Nematostella vectensis. *Nature Communications*, *5*(1), 1–8. https://doi.org/10.1038/ncomms6486

Jho, E., Zhang, T., Domon, C., Joo, C.-K., Freund, J.-N., & Costantini, F. (2002). Wnt/β-Catenin/Tcf Signaling Induces the Transcription of Axin2, a Negative Regulator of the Signaling Pathway. *Molecular and Cellular Biology*, *22*(4), 1172–1183. https://doi.org/10.1128/mcb.22.4.1172-1183.2002

Jiang, X., & Cong, F. (2016). Novel Regulation of Wnt Signaling at the Proximal Membrane Level. In *Trends in Biochemical Sciences* (Vol. 41, Issue 9, pp. 773–783). Elsevier Ltd. https://doi.org/10.1016/j.tibs.2016.06.003

Kakugawa, S., Langton, P. F., Zebisch, M., Howell, S., Chang, T.-H., Liu, Y., Feizi, T., Bineva, G., O'reilly, N., Snijders, A. P., Jones, E. Y., & Vincent, J.-P. (2015). Notum deacylates Wnts to suppress signalling activity. *Europe PMC Funders Group*, *519*(7542), 187–192. https://doi.org/10.1038/nature14259

Karabulut, A., He, S., Chen, C. Y., McKinney, S. A., & Gibson, M. C. (2019). Electroporation of short hairpin RNAs for rapid and efficient gene knockdown in the starlet sea anemone, Nematostella vectensis. *Developmental Biology*, *448*(1), 7–15. https://doi.org/10.1016/j.ydbio.2019.01.005

Komiya, Y., & Habas, R. (2008). Wnt signal transduction pathways. In *Organogenesis* (Vol. 4, Issue 2, pp. 68–75). Landes Bioscience. https://doi.org/10.4161/org.4.2.5851

Kraus, Y., Aman, A., Technau, U., & Genikhovich, G. (2016). Pre-bilaterian origin of the blastoporal axial organizer. *Nature Communications*, *7*(1), 1–9. https://doi.org/10.1038/ncomms11694

Kreuger, J., Perez, L., Giraldez, A. J., & Cohen, S. M. (2004). Opposing activities of Dally-like glypican at high and low levels of wingless morphogen activity. *Developmental Cell*, *7*(4), 503–512. https://doi.org/10.1016/j.devcel.2004.08.005

Kusserow, A., Pang, K., Sturm, C., Hrouda, M., Lentfer, J., Schmidt, H. A., Technau, U., Von Haeseler, A., Hobmayer, B., Martindale, M. Q., & Holstein, T. W. (2005). Unexpected complexity of the Wnt gene family in a sea anemone. *Nature*, *433*(7022), 156–160. https://doi.org/10.1038/nature03158

Kutejova, E., Briscoe, J., & Kicheva, A. (2009). Temporal dynamics of patterning by morphogen gradients. In *Current Opinion in Genetics and Development* (Vol. 19, Issue 4, pp. 315–322). Elsevier Current Trends. https://doi.org/10.1016/j.gde.2009.05.004

Layden, M. J., Rentzsch, F., & Röttinger, E. (2016). The rise of the starlet sea anemone Nematostella vectensis as a model system to investigate development and regeneration. In *Wiley Interdisciplinary Reviews: Developmental Biology* (Vol. 5, Issue 4, pp. 408–428). John Wiley and Sons Inc. https://doi.org/10.1002/wdev.222

Layden, M. J., Röttinger, E., Wolenski, F. S., Gilmore, T. D., & Martindale, M. Q. (2013). Microinjection of mRNA or morpholinos for reverse genetic analysis in the starlet sea anemone, Nematostella vectensis. *Nature Protocols*, *8*(5), 924–934. https://doi.org/10.1038/nprot.2013.009

Leclère, L., Bause, M., Sinigaglia, C., Steger, J., & Rentzsch, F. (2016). Development of the aboral domain in Nematostella requires β-catenin and the opposing activities of Six3/6 and Frizzled5/8. *Development (Cambridge)*, *143*(10), 1766–1777. https://doi.org/10.1242/dev.120931

Lee, P. N., Kumburegama, S., Marlow, H. Q., Martindale, M. Q., & Wikramanayake, A. H. (2007). Asymmetric developmental potential along the animal-vegetal axis in the anthozoan cnidarian, Nematostella vectensis, is mediated by Dishevelled. *Developmental Biology*, *310*(1), 169–186. https://doi.org/10.1016/j.ydbio.2007.05.040

Lee, R. T. H., Zhao, Z., & Ingham, P. W. (2016). Hedgehog signalling. *Development (Cambridge)*, *143*(3), 367–372. https://doi.org/10.1242/dev.120154

Lengfeld, T., Watanabe, H., Simakov, O., Lindgens, D., Gee, L., Law, L., Schmidt, H. A., Özbek, S., Bode, H., & Holstein, T. W. (2009). Multiple Wnts are involved in Hydra organizer formation and regeneration. *Developmental Biology*, *330*(1), 186–199. https://doi.org/10.1016/j.ydbio.2009.02.004

Liang, S. jie, Zhou, J. yi, & Wang, X. qi. (2020). Signaling Network Centered on mTORC1 Dominates Mammalian Intestinal Stem Cell Ageing. In *Stem Cell Reviews and Reports* (pp. 1–8). Springer. https://doi.org/10.1007/s12015-020-10073-y

MacDonald, B. T., Tamai, K., & He, X. (2009). Wnt/β-Catenin Signaling: Components, Mechanisms, and Diseases. In *Developmental Cell* (Vol. 17, Issue 1, pp. 9–26). Cell Press. https://doi.org/10.1016/j.devcel.2009.06.016

Marlow, H., Matus, D. Q., & Martindale, M. Q. (2013). Ectopic activation of the canonical wnt signaling pathway affects ectodermal patterning along the primary axis during larval development in the anthozoan Nematostella vectensis. *Developmental Biology*, *380*(2), 324–334. https://doi.org/10.1016/j.ydbio.2013.05.022

Matus, D. Q., Magie, C. R., Pang, K., Martindale, M. Q., & Thomsen, G. H. (2008). The Hedgehog gene family of the cnidarian, Nematostella vectensis, and implications for understanding metazoan Hedgehog pathway evolution. *Developmental Biology*, *313*(2), 501–518. https://doi.org/10.1016/j.ydbio.2007.09.032

Niehrs, C. (2010). On growth and form: A Cartesian coordinate system of Wnt and BMP signaling specifies bilaterian body axes. In *Development* (Vol. 137, Issue 6, pp. 845–857). Development. https://doi.org/10.1242/dev.039651

Niida, A., Hiroko, T., Kasai, M., Furukawa, Y., Nakamura, Y., Suzuki, Y., Sugano, S., & Akiyama, T. (2004). DKK1, a negative regulator of Wnt signaling, is a target of the β-catenin/TCF pathway. *Oncogene*, *23*(52), 8520–8526. https://doi.org/10.1038/sj.onc.1207892

Nusse, R. (2003). Wnts and Hedgehogs: Lipid-modified proteins and similarities in signaling mechanisms at the cell surface. In *Development* (Vol. 130, Issue 22, pp. 5297–5305). The Company of Biologists Ltd. https://doi.org/10.1242/dev.00821

Peifer, M., Sweeton, D., Casey, M., & Wieschaus, E. (1994). *Wingless signal and Zeste- white 3 kinase trigger opposing changes in the intracellular distribution of Armadillo*. Development. https://www.researchgate.net/publication/15049171_Wingless_signal_and_Zeste-_white_3_kinase_trigger_opposing_changes_in_the_intracellular_distribution_of_Armadillo

Pentinmikko, N., Iqbal, S., Mana, M., Andersson, S., Cognetta, A. B., Suciu, R. M., Roper, J., Luopajärvi, K., Markelin, E., Gopalakrishnan, S., Smolander, O. P., Naranjo, S., Saarinen, T., Juuti, A., Pietiläinen, K., Auvinen, P., Ristimäki, A., Gupta, N., Tammela, T., … Katajisto, P. (2019). Notum produced by Paneth cells attenuates regeneration of aged intestinal epithelium. *Nature*, *571*(7765), 398–402. https://doi.org/10.1038/s41586-019-1383-0

Petersen, C. P., & Reddien, P. W. (2011). Polarized notum activation at wounds inhibits Wnt function to promote planarian head regeneration. *Science*, *332*(6031), 852–855. https://doi.org/10.1126/science.1202143

Renfer, E., Amon-Hassenzahl, A., Steinmetz, P. R. H., & Technau, U. (2010). A muscle-specific transgenic reporter line of the sea anemone, Nematostella vectensis. *Proceedings of the National Academy of Sciences of the United States of America*, *107*(1), 104–108. https://doi.org/10.1073/pnas.0909148107

Restrepo, S., Zartman, J. J., & Basler, K. (2014). Coordination of patterning and growth by the morphogen DPP. In *Current Biology* (Vol. 24, Issue 6, pp. R245–R255). Cell Press. https://doi.org/10.1016/j.cub.2014.01.055

Rogers, K. W., & Schier, A. F. (2011). Morphogen gradients: From generation to interpretation. *Annual Review of Cell and Developmental Biology*, *27*, 377–407. https://doi.org/10.1146/annurev-cellbio-092910-154148

Röttinger, E., Dahlin, P., & Martindale, M. Q. (2012). A Framework for the Establishment of a

Cnidarian Gene Regulatory Network for “Endomesoderm” Specification: The Inputs of ß-Catenin/TCF Signaling. *PLoS Genetics*, *8*(12), e1003164. https://doi.org/10.1371/journal.pgen.1003164

Ryan, J. F., & Baxevanis, A. D. (2007). Hox, Wnt, and the evolution of the primary body axis: Insights from the early-divergent phyla. In *Biology Direct* (Vol. 2, p. 37). BioMed Central. https://doi.org/10.1186/1745-6150-2-37

Sagner, A., & Briscoe, J. (2017). Morphogen interpretation: concentration, time, competence, and signaling dynamics. In *Wiley Interdisciplinary Reviews: Developmental Biology* (Vol. 6, Issue 4, p. 271). John Wiley and Sons Inc. https://doi.org/10.1002/wdev.271

Sánchez, A., & Howard, A. (2008). *Practical lab: The planarian Schmidtea mediterranea*. http://planaria.neuro.utah.edu

Schaffer, A. A., Bazarsky, M., Levy, K., Chalifa-Caspi, V., & Gat, U. (2016). A transcriptional time-course analysis of oral vs. aboral whole-body regeneration in the Sea anemone Nematostella vectensis. *BMC Genomics*, *17*(1), 1–22. https://doi.org/10.1186/s12864-016-3027-1

Schauer, A. (2016). *Analysis of BMP signaling targets in Nematostella vectensis*. University of Vienna.

Schwaiger, M., Schönauer, A., Rendeiro, A. F., Pribitzer, C., Schauer, A., Gilles, A. F., Schinko, J. B., Renfer, E., Fredman, D., & Technau, U. (2014). Evolutionary conservation of the eumetazoan gene regulatory landscape. *Genome Research*, *24*(4), 639–650. https://doi.org/10.1101/gr.162529.113

Sebé-Pedrós, A., Chomsky, E., Saudememont, B., Mailhe, M. P., Pleisser, F., Renno, J., Loe-Mie, Y., Lifshitz, A., Mukamel, Z., Schmutz, S., Nouvault, S., Spitz, F., Tanay, A., & Marlow, H. (2017). Cnidarian cell type diversity revealed by whole-organism single-cell RNA-seq analysis. In *bioRxiv* (p. 201103). bioRxiv. https://doi.org/10.1101/201103

Suciu, R. M., Cognetta, A. B., Potter, Z. E., & Cravatt, B. F. (2018). Selective Irreversible Inhibitors of the Wnt-Deacylating Enzyme NOTUM Developed by Activity-Based Protein Profiling. *ACS Medicinal Chemistry Letters*, *9*(6), 563–568. https://doi.org/10.1021/acsmedchemlett.8b00191

Trevino, M., Stefanik, D. J., Rodriguez, R., Harmon, S., & Burton, P. M. (2011). Induction of canonical Wnt signaling by alsterpaullone is sufficient for oral tissue fate during regeneration and embryogenesis in Nematostella vectensis. *Developmental Dynamics*, *240*(12), 2673–2679. https://doi.org/10.1002/dvdy.22774

White, B. D., Chien, A. J., & Dawson, D. W. (2012). Dysregulation of Wnt/β-catenin signaling in gastrointestinal cancers. In *Gastroenterology* (Vol. 142, Issue 2, pp. 219–232). W.B. Saunders. https://doi.org/10.1053/j.gastro.2011.12.001

Willert, K., Brown, J. D., Danenberg, E., Duncan, A. W., Weissman, I. L., Reya, T., Yates, J. R., & Nusse, R. (2003). Wnt proteins are lipid-modified and can act as stem cell growth factors. *Nature*, *423*(6938), 448–452. https://doi.org/10.1038/nature01611

Winston, J. T., Strack, P., Beer-Romero, P., Chu, C. Y., Elledge, S. J., & Harper, J. W. (1999). The SCF(β-TRCP)-ubiquitin ligase complex associates specifically with phosphorylated destruction motifs in IκBα and β-catenin and stimulates IκBα ubiquitination in vitro. *Genes and Development*, *13*(3), 270–283. https://doi.org/10.1101/gad.13.3.270

Wlkramanayake, A. H., Hong, M., Lee, P. N., Pang, K., Byrum, C. A., Bince, J. M., Xu, R., &

Martindale, M. Q. (2003). An ancient role for nuclear β-catenin in the evolution of axial polarity and germ layer segregation. *Nature*, *426*(6965), 446–450. https://doi.org/10.1038/nature02113

Zhang, X., Cheong, S. M., Amado, N. G., Reis, A. H., MacDonald, B. T., Zebisch, M., Jones, E. Y., Abreu, J. G., & He, X. (2015). Notum is required for neural and head induction via wnt deacylation, oxidation, and inactivation. *Developmental Cell*, *32*(6), 719–730. https://doi.org/10.1016/j.devcel.2015.02.014

Zhou, Y., & Nathans, J. (2014). Gpr124 controls CNS angiogenesis and blood-brain barrier integrity by promoting ligand-specific canonical Wnt signaling. *Developmental Cell*, *31*(2), 248–256. https://doi.org/10.1016/j.devcel.2014.08.018

6 Supplement

6.1 Short hairpin RNA primers

Name	Target sequence
T7 forward	TAATACGACTCACTATA
shmOr reverse (control)	AAGCGAGTTCTTCTACAAGGTGACTCTTGATCACCTTGTAGA AGAACTCGCTTTATAGTGAGTCGTATTA
shNot1 reverse	AATGAAGTCATCAGATAACGCTCTCTTGAATGA AGTCATCAGATAACGCTATAGTGAGTCGTATTA
shNot2 reverse	AAGGAATAGTCCCTGAGAATTTCTCTTGA AAATTCTCAGGGACTATTCCTATAGTGAGTCGTATTA

6.2 qPCR Primers

Gene	Primer name	Sequence
GAPDH	qGAPDH_F	TATGACTCCACCCATGGCA
	qGAPDH_R	GAGTCCACTGGCGTCTTCAC
NVE7485	NVE7485_qF	GTGCTACTTTGGCGAAACTGTC
	NVE7485_qR	TCAGGTCGATCGTTTGAATACC

6.3 Morpholino sequences

Morpholino oligo	Concentration	Sequence
Std MO	500 or 900µM	CCTCTTACCTCAGTTACAATTTATA
ß-catenin MO	500µM	GCATCCCCATACCGTGTGTCTCCAT
Notum ATG MO	900µM	AGGCTCCACAAAGTATCCATTCTTA
Notum Splice MO	900µM	GCGCGGTGCTACATACCTTCCAGGT

6.4 List of hybridization probes and primers for additional probes

Gene name	NVE Accession number
NvNotum	NVE7485
NvBrachyury	NVE3568
NvWnt2	NVE21992
NvSix3/6	NVE12346

NvAxin	NVE14577
NvFoxA	NVE20630
NvSnailA	NVE13986
NvErg	NVE25536
NvHedgehog1	NVE18028
NvGli	NVE3641
NvHint-3	NVE6291
NvChordin	NVE22735
NvBmp2-4 (Dpp)	NVE963
Probes and templates were provided by Paul Knabl, Isabell Niedermoser, Tatiana Lebedeva, Alexandra Schauer and Grigory Genikhovich	

Gene	Primer name	Sequence
NVE2913	2931F1_	ACCGCGGACTCTGTGTATAGACTC
	2931R1_	AGCGGGCAGAGCTACTACAATG

6.5 In-situ hybridization buffers

Buffers and reagents	Composition
10x PBS (Phosphate Buffer Saline) pH 7.4	18.6 mM NaH2PO4 84.1 mM Na2HPO4 1.75 M NaCl
1x PTw	1xPBS 0.1% Tween20 (stock=100%) Elix water
Proteinase K /PTw	1xPTw 80µg/ml Proteinase K (20mg/ml)
Glycine/PTw	1xPTw 4mg/ml Glycine
1%Triethanolamine/PTw	1xPTw 1%TEA (Triethanolamine)
Acetic anhydride/1%TEA/PTw	1xPTw 1%TEA (Triethanolamine) -3µl AA per ml 1%TEA/PTW -6µl AA per ml 1%TEA/PTW
FA/PTw	3.7% FA (formaldehyde) (Stock: 37%) PTw
Hybe	50% formamid (stock=100%) 5xSSC pH4.5 (stock=20x) 5mg/ml torula RNA 1%SDS (stock=10%) 100µg/ml Heparin (stock=20mg/ml)

	0.1% Tween20 (stock=100%) Elix water For probes add 5% Dextran sulfate
Alkaline Phosphatase Buffer ph9.5	100 mM NaCl (stock=5M) 50 mM MgCl2 (stock=1M) 100 mM Tris (pH 9.5) (stock=1M) 0.5% Tween-20 Elix water

6.6 Additional Western blot buffers

Buffers and reagents	Composition
10x TRIS/Glycine Buffer	30.3g TRIS Base 144g Glycine Elix water to 1L
2x Laemmli loading buffer	4% SDS (Stock: 10%) 20% Glycerol (Stock: 86%) 120mM Tris-Cl (pH 6.8) 10% 2-mercaptoethanol Elix water add bromophenol blue to a final conc. of 0.04% (w/v)
1x TBST pH 7.4	137 mM NaCl 2.7 mM KCl 19mM TRIS Base 0.1% Tween

6.7 List of Antibodies for WB and Immunostaining

Primary antibodies	
α-active ß-catenin AB	Non-phospho (Active) β-Catenin (Ser33/37/Thr41) Rabbit mAb (Cell signaling Technology®) Working dilution 1:5000 for WB
α-ß actin AB	β-Actin Rabbit mAb (Cell signaling Technology®) Working dilution 1:500 for WB
α-TCF AB	Custom made, pAbs (BioGenes). Peptides used for immunization were prepared by Vienna Biocentre Core Facility (VBCF). Working dilution: 1:1000 for IS

Secondary antibodies	
α-rabbit Alexa 488	Goat anti-Rabbit IgG (H+L) Cross-Adsorbed Secondary Antibody, Alexa Fluor 488 (Invitrogen) Working dilution 1:1000 IS
A-rabbit HRP	Anti-Rabbit IgG (H+L), HRP Conjugate (Promega) Working dilution: 1:100 00 WB

7 Appendix

7.1 *ß-catenin* CRISPR/ Cas9 Knock-In animals

7.1.1 Generation of Knock- in template fragment

We wanted to generate a CRISPR/ Cas9 *Nematostella* knock-in line, where we integrate a *mCherry* CDS and a *V5* Tag into the N- terminus of the genomic *ß-catenin* locus. For this, the genomic sequence flanking the start codon of *ß-catenin* was amplified using Q5 polymerase (for protocol see 2.2.1- Ta. 63°C, 35 cycles, 3mM MgCl) from genomic DNA (provided by Tatiana Lebedeva). In this PCR, we used primers that flanked the start codon ~900bp upstream & downstream, bcat_g_F4 and bcat_g_R4 (sequences below). The genomic fragment including parts of the 5'UTR was gel extracted (2.2.1) and ligated into pJET1.2. The ligation reaction was transformed into competent cells as described in 2.2.3 and mini prepped as in 2.2.4. The plasmid was then sent for sequencing. To produce the knock-in DNA template, we assembled the fragment using template switching PCR (TS-PCR). The left homology arm was amplified using bcat_g_F4 & Chbcat_R as primers in a Q5 polymerase reaction (see 2.2.1, Ta. 63°C, 35 cycle) using the genomic *ß-catenin* fragment as template. The same reaction was set up for the right homology arm, however other primers were used (bcatV5RHA_F & bcat_g_R4). For the middle part of the fragment, the *mCherry* CDS was amplified from a clone bank plasmid (CB646) SnailAP2::mcherry(D-stopp)-p2A-mef2(D-stopp)-V5 using bcat_ChF & bcatV5Rp2A_R primers (Q5 polymerase, Ta. 65°C, 35 cycles) (all primer sequences below).

The fragments were gel extracted using the peqlab kit and used for TS-PCR. First, the left homology arm and the *mCherry* sequence were combined using both fragments (1+3) as template (Q5 polymerase Ta. 65°C, 35 cycles, master mix see below) and the bcat_g_F4 and bcatV5Rp2A primers. Then the right homology arm was combined with the *mCherry* fragment (2+3) applying the same procedure but using bcat_ChF and bcat_g_R4 primers. These TS-PCR products were gel extracted and the resulting products were further combined using TS-PCR. Here, the products of 1+3 and 2+3 were used as templates and amplified using the bcat_g_F4 and bcat_g_R4 primers, to combine all three fragments into one piece, which was then gel extracted and ligated into pJET1.2 (see 2.2 for procedures) and sequenced. A scheme of the PCR template is shown in figure 30A. It includes the tag (red/ purple/ green) with the homology arms (grey). The genomic *ß-catenin* fragment that was amplified (bcat_g_F4 &bcat_g_R4) spans the gRNA site 879bp upstream and 905bp downstream.

TS-PCR Mastermix using Q5 polymerase	
2x Q5 Mastermix	20µl
Template 1 (gel extracted, diluted 1:100)	1µl
Template 2 (gel extracted, diluted 1:100)	1µl
Forward primer (10µM)	2,5µl
Reverse primer (10µM)	2,5µl
Milli Q water	13µl
Total volume	40µl

This plasmid was used to generate the DNA template fragment for injection (see fig.30A) using ubiquitinated primers (Sigma Aldrich) UHbcatFbio & UHbcatRbio and the standard Q5 polymerase protocol (see 2.2.1. Ta. 65°C, 35 cycles). The product was PCR extracted and the concentration was measured using Nanodrop. The eluate was reduced in volume by incubating it at 37°C for 2-3h (to increase the concentration of the DNA template). The product using the ubiquitinated primers (fig.30A) is indicated by the thicker bar and the red arrows, to illustrate where they bind our template.

Gene	Primer name	Sequence
Genomic *ß-catenin* fragment	bcat_g_F4	GGTCGTAGATGGTACCCTAAG
	bcat_g_R4	CAACTCTGGGATAGCACGTGTAG
Left homology arm	bcat_g_F4:	GGTCGTAGATGGTACCCTAAG
	Chbcat_R	TCCTCGCCCTTGCTCACCATGGTA ACTGGCAAATAAATAG
Right homology arm	bcatV5RHA_F	TTCTACGGAaACcCAtGGgATGGGGA TGCAGCAGGGGCGGGACAT
	bcat_g_R4	CAACTCTGGGATAGCACGTGTAG
mCherry fragment	bcat_ChF	CTATTTATTTGCCAGTTACCATG GTGAGCAAGGGCGAGGA
	bcatV5Rp2A_R	ATCCCATGGGTTTCCGTAGAATCGA GACCGAGGAGAGGGTTAGGGATAGG CTTACCAGGGCCGGGGTTTTCTTCCACA
Injection fragment	UHbcatFbio	ATTCGCAGCATTTCTCA
	UHbcatRbio	GATGGCTCAGCAAGC

To integrate the *mCherry* CDS and the *V5* tag into the genome, the genomic *ß-catenin* locus was targeted using the CRISPR/ Cas9 (Alt-R CRISPR-Cas9 crRNA:tracrRNA) gRNA system of IDT. A guide RNA was chosen, with the PAM site located directly upstream of the start codon

of *ß-catenin* (see fig.30B- gRNA sequence: CTATTTATTTGCCAGTTACC). By cutting this site between the 5'UTR and the start codon and adding the DNA template, there was a chance, that the cutting site would be repaired through homology-directed repair, using the DNA fragment as template, thus integrating the tag and *mCherry* sequence. To avoid that the gRNA also targets the DNA we tried to knock-in, we integrated silent mutations into it making it unrecognizable for the gRNA. *Nematostella* embryos were injected with a mix containing the CRISPR/Cas9 system as well as the DNA template. The gRNA duplex was prepared according to the manufacturers protocol (ribonucleoprotein delivery using 2-part guide RNAs (crRNA:tracrRNA duplex)). The detailed injection mix is shown below:

CRISPR/ Cas9 injection mix	
crRNA	1µl
tracrRNA	1µl
Duplex buffer	0.5µl
Mix and heat to 95°C for 5 min	
gRNA duplex (see above)	1.5µl
Cas9 (3µg/µl)	0.6µl
10x Injection buffer	1µl
Dextran 488	0.5µl
DNA template (~500ng/µl)	2.5µl
Total volume	5µl

Embryos were injected and incubated at 21°C ON. The next day, they were screened for red fluorescence. As *mCherry* CDS was included in the template fragment, embryos that were glowing red, were likely to have integrated the tag into their genome. The animals were raised and regularly observed under fluorescent light. Many animals lost their fluorescence after some time, but a few had clear glowing patches (see fig.31). These animals were raised to adulthood.

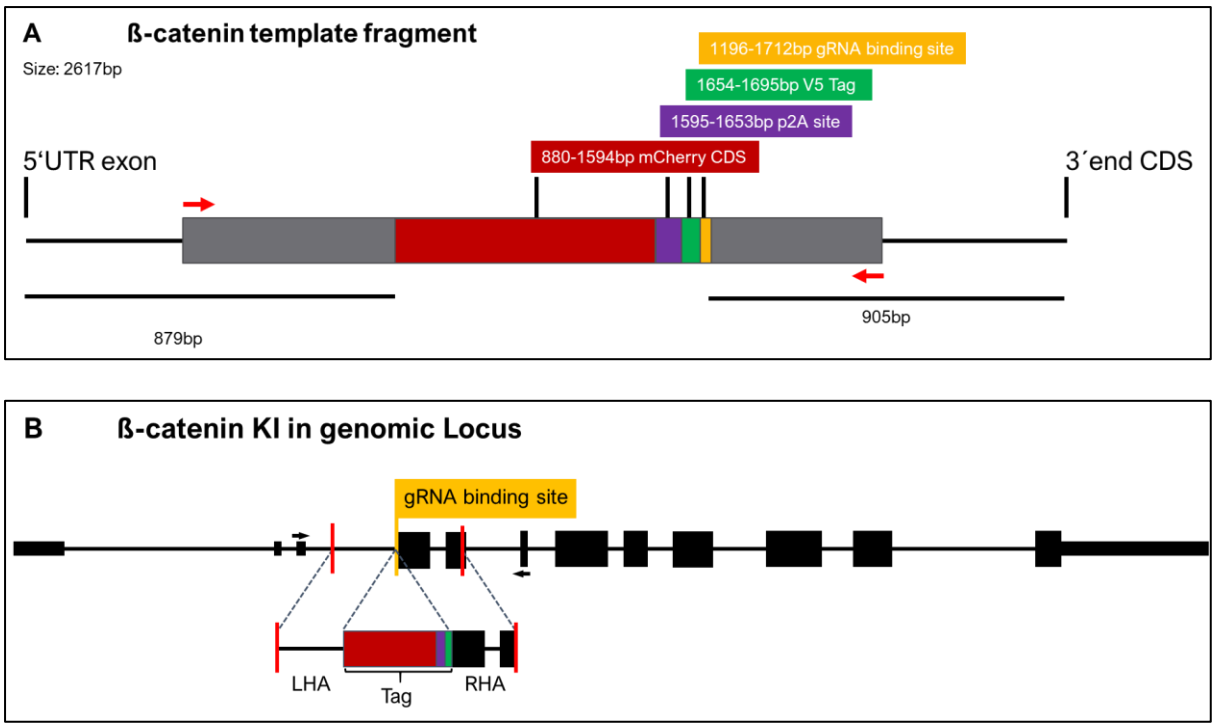

Figure 30 Schemes of the ß-catenin fragment used to amplify the DNA template for microinjection (A) and the position of the KI in the genomic locus of ß-catenin (B). *(A) The product of TS-PCR that was cloned into pJET1.2. Shown is the injection fragment (thick bar) with the KI components mCherry (red), p2A site (purple) and the V5 Tag (green). Also shown is the gRNA binding site (yellow). The KI fragment was amplified from this template using ubiquitinated primers (shown in bright red). (B) Illustrated is where the tag was integrated within the genomic ß-catenin locus. The tag (mch::p2A::V5) follows the same color code as in (A) and the gRNA binding site is also illustrated in yellow. Marked are also the left homology arm (LHA) and the right homology arm (RHA) and where their sequences overlap (red lines). The arrows in black mark the genomic ß-catenin primers used to generate the PCR template and to verify the KI.*

7.1.2 DNA extraction and genotyping of glowing tentacles

To verify that the glowing patch, was indeed the result of the knock-in of *mCherry* and *V5* into the *ß-catenin* locus, the animals were genotyped. For this, animal with a glowing patch in their tentacles (Felicity, Suzie, Ned and Ned Jr.) were used, and one tentacle each was cut off using a microscalpel. Each tentacle was placed in a PCR tube, the NM was removed and the tentacles were washed 5x using 100% MeOH. MeOH was then aspirated, and the remaining MeOH was evaporated by placing open PCR tubes into an open Thermocycler (Biometra Ltd) for 20min at 50°C. Next, 25µl of DNA extraction buffer (10mM TRIS pH8, 1mM EDTA pH8, 25mM NaCl and 200µg/ml Proteinase K) was added to each tube and incubated in a closed thermocycler with heated lid at 50°C for 2h followed by 5 min at 95°C to deactivate the

proteinase K. The digested tentacles were directly used as template for a PCR (2µl template for a 20µl Taq polymerase PCR) using the genomic *ß-catenin* primers (bcat_g_F4 & bcat_g_R4).

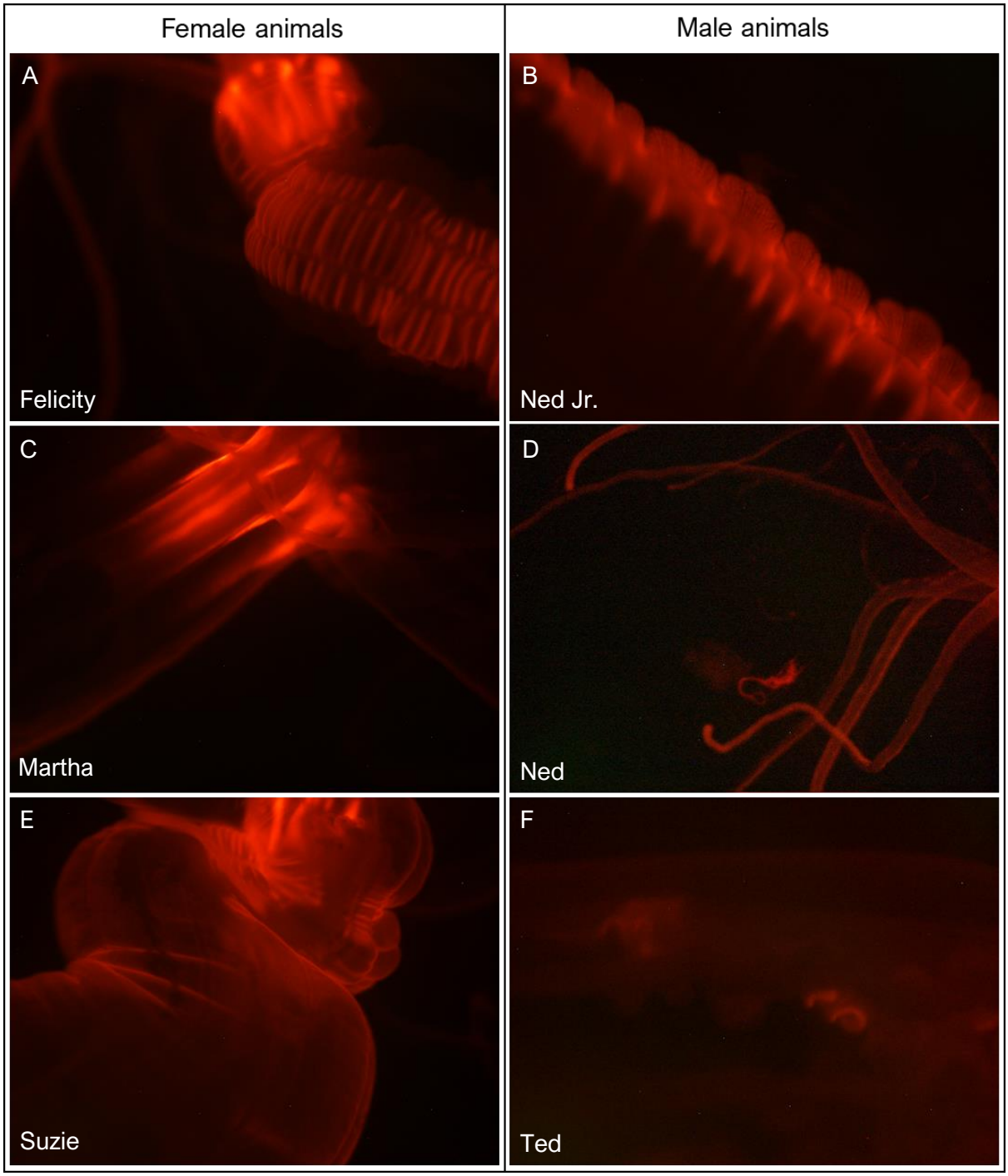

Figure 31 Images of glowing mCherry patches of KI animals. *Shown are 3 females (Felicity, Martha and Suzie) and 3 males (Ned Jr., Ned and Ted). Most animals have a KI patch in their ectoderm, but Ted (F) has a patch in his endoderm. Martha (C) has a patch in the ectoderm towards the pharynx, however, no glowing tentacles, which is why Martha and Ted were not included in the sequencing, as we were not able to dissect parts of the tissue without severely affecting the animal or KI patch.*

The PCR products were purified and directly sequenced. As sequencing primer, a reverse primer, binding at the beginning of the *mCherry* CDS (ER22: TTGGCGGTCTGGGTGCCCTCGTAG) was used, meaning that the sequencing would start in the mCh sequence and go into the genomic *ß-catenin* locus. The alignment of the sequencing results of Felicity, Suzie and Ned Jr. (for Ned, the DNA extraction was unsuccessful, therefore it is not included) is shown in figure 32. One can see the *ß-catenin* and *mCherry* sequence, as well as the position of the sequencing primer (dark blue). Also illustrated is the ubiquitinated primer (UHbcatFbio) used to generate the KI DNA template fragment (bright red). The sequences of Felicity and Ned Jr. span over this primer, meaning that the KI indeed occured in the genomic locus of *ß-catenin*. For Suzie, this is not the case, however, the DNA fragment that was sequenced, was prepared with the genomic primers, which are located outside the homology arms of our KI fragment. As the *mCherry* CDS is clearly found in this PCR product, one can assume that the Tag was integrated in the correct position as well. As we could verify that the KI was indeed successful, the animals can be used to generate a F1 generation. If the knock-in occured also in the cells giving rise to the germ line, some of the F1 animals will be heterozygous for the knock-in, which will make the generation of the homozygous F2 generation possible.

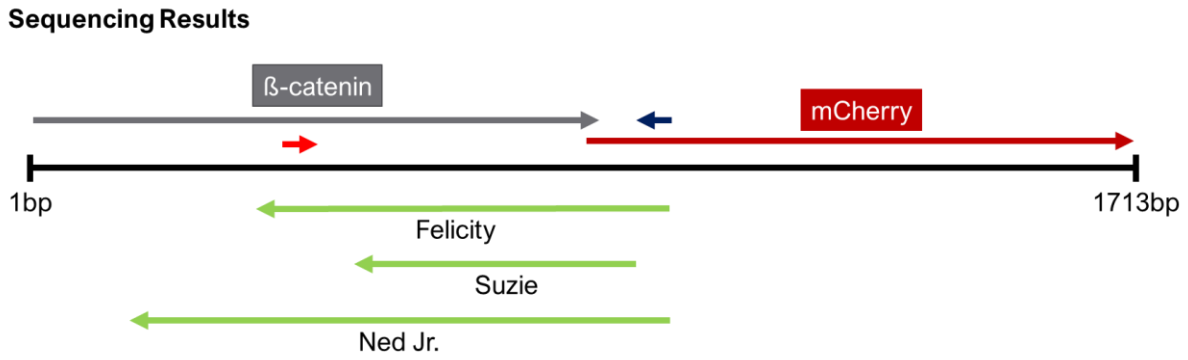

Figure 32 Alignment of sequencing results of KI animals Felicity, Suzie and Ned Jr. with the genomic ß-catenin sequence and mCherry. *Also included is the sequencing primer (dark blue) and the ubiquitinated primer used to generate the DNA KI template (bright red). All three animals carry the mCherry sequence in their genomic ß-catenin locus.*

7.2 Generation of α-TCF Antibody

7.2.1 Production of tagged TCF

To produce αTCF antibodies, it was first necessary to produce *Nematostella vectensis* TCF proteins. To do so, we first amplified TCF coding DNA sequence using Q5 polymerase (see 2.2.1 for details- Ta. 65°C with 40 cycles) using following primers from mixed cDNA (cDNA production described in 2.3.3):

TCF5'UTRF: GCCGCATCTACTTTGGCTCCT
TCF3'UTRR: AACATAGCCCTGGCGTTCAT

The PCR product was loaded on a gel (1% in TAE) and gel extracted (2.2.1). The fragment was ligated into pJET1.2 (see 2.2.3) and transformed using TOP10 cells. After the Miniprep (2.2.4), the plasmid containing the TCF CDS was sent for sequencing to verify that the correct sequence was amplified. Then, another PCR (Taq polymerase 2.2.1) was set up using this plasmid as template with following primers, carrying added restriction sites of BamHI and NotI (Ta. 53°C and 35 cycles):

Bam-TcfF1: GGATCCATGCCTCAGCTTCCTAGGAA
NotI-TcfR1: GCGGCCGCCTAAGTGTCTGATGTAACTGG

The product was again loaded on a gel (1% in TAE) and gel-extracted, ligated into pJET1.2 and transformed, as already described before. The inserts were then digested with BamHI and NotI and subcloned in frame into a pHis.Parallel2 expression vector, which added and N-terminal His-tag to the Tcf protein. The plasmids were miniprepped and sequenced. After the sequence was verified, the construct was sent to the VBCF, where they expressed and purified the TCF protein using the poly-histidine tag.

7.2.2 Preparation for Mass spectrometry analysis

To verify that the produced protein was indeed NvTCF, MS/MS spectrometry was performed and analyzed at the department of Molecular Systems Biology University of Vienna, by Dr. Stefanie Wienkoop. For this, 100µg (50µl) of protein (stored at 2µl/µl in 20mm TRIS pH 8.5/200 mM NaCl) were transferred into an Eppendorf tube and 250µl of 20mM TRIS pH 8 was added. This was precipitated by adding 700µl of ice-cold acetone (70% final in 1ml) and 5µl of ß-

mercaptoethanol (0.5% final) and centrifuged for 5 min at 10000g at 4°C. Next, the supernatant was removed, and the pellet redissolved in 100µl of 8M Urea/ 50mM HEPES (pH 7.8). DTT was added (5mM final concentration) and incubated at 37°C for 45 min at 700rpm in the Eppendorf Thermoshaker. Afterwards, it was diluted to 4M Urea using 105 µl of MilliQ and then 210µl of 20% Acetonitrile (ACN)/ 10mM $CaCl_2$/ 20% Ammonium Bicarbonate (AmBic) was added to get a final buffer of 2M Urea/ 10%ACN/ 5mM CaCl2 /10mM AmBic.

This acetone purification was then followed by a trypsin digest and column purification. For this, 1µg of Trypsin in 1mM HCl (1mg/ml stock) was added to the reduced protein. This mixture was incubated at 37°C and digested ON. The next day, another 1µl of Trypsin/HCL (1mg/ml) was added, mixed and incubated at 37°C for 4h. The digestion was stopped using formic acid (final conc. 5% v/v). Next, Pierce™ C18 Spin Columns (Thermo Scientific™) were lightly tapped so that the resin settled. The top and bottom lid was removed and carefully placed into a 2ml Eppendorf tube. The column was rinsed 2x using 200µl of 50%ACN/ MilliQ, by loading the solution and centrifuging for 1min at 1500g. This wash step was repeated using 200µl of 0.1% formic acid/ MilliQ water (also twice). After the columns were prepped, the peptides were loaded by centrifuging for 1min at 1500g (flow through was loaded twice, to ensure proper loading). Once the peptides were loaded, the column was washed 4x using 0.1% formic acid/ MilliQ water by centrifugation (1min, 1500g). After that, the 2ml collection tube was replaced with a fresh low bind tube. This was followed by an initial elution using 50µl of 60% ACN/ 0.1% formic acid, and a second elution using 30µl of 100% ACN/ 0.1% formic acid. The eluate was then dried using the Concentrator Plus (Eppendorf) using the V-AQ setting at RT. The peptides were then stored at -80°C until further processing.

For MS/MS, the peptides (100µg) were re-hydrated using 100µl ACN/ 0.1% formic acid and mixed by pipetting, followed by centrifuging for 1min at 10 200 rpm. Then 15µl of the ACN buffer was added to the mass spectrometry vial and 5µl of the re-hydrated peptides were pipetted on top. This again was mixed and then the lid was added and placed into the UltiMate™ 3000 HPLC system (Thermo Scientific™). Further processing and computational work were all performed by Stefanie Wienkoop. She was able to verify that our protein was indeed NvTCF. Therefore, we were able to send this protein to BioGenes GmbH for rabbit immunization.

7.2.3 Pre-Immune serum and α-TCF antibody tests

Overall serum collected from 4 different unimmunized rabbits (pre-immune serum) were screened by immunofluorescence. For this, *Nematostella* embryos were fixed at 30hpf following the protocol in 2.7.2, but instead of 3.7%, the embryos were fixed in 4% paraformaldehyde for 1h at 4°C on a rotator. After that, the embryos were washed 5x in PTx (1xPBS/ 0.2% TritonX100). Then the embryos were blocked for at least 1h (RT) in 5% sheep serum/ 1%BSA in PTx (blocking solution). For the initial screen dilutions of the pre- immune serums (Pre-IS) were prepared (in blocking solution), one containing no primary AB (just blocking solution), one αFoxA AB dilution (a working rabbit antibody against *Nematostella* FoxA produced by BioGenes and provided by Patricio Ferrer) 1:500 as a positive control, and each Pre- IS was diluted 1:100 and 1:1000. The incubation using the Pre-IS was performed in 50µl total, thus 25µl of 2x dilutions were prepared and added on top of 25µl embryos in blocking solution. They were incubated ON at 4°C. The next day, the embryos were washed 5x using PTx and then incubated in blocking solution for 1h at RT. Afterwards, the secondary AB (Alexa Flour™ 488 Goat anti-Rabbit IgG (H+L)) was diluted 1:1000 using blocking solution and added to the embryo and incubated for 3h (RT). Afterwards, the unbound antibodies were washed 5x using PTw for 10 minutes each and infiltrated in VECTASHIELD® Antifade Mounting Medium (VectaLaboratories) ON. The embryos were mounted on glass slides and imaged Nikon Eclipse 80i microscope with a Nikon DS-Fi1 camera. Based on the weakest fluorescence of the embryos stained with the preimmune serum, two rabbits were chosen for antibody production. Once the ABs arrived, they were again tested using immune fluorescence as already described using 1:100, 1:500 and 1:1000 dilutions (fig.33). We did not observe any specific staining in the immune serum from the rabbit 30754, therefore it was terminated, but obtained some weak but promising oral staining with the serum from rabbit 30753. Rabbit 30753 was boosted by a second injection of the purified NvTcf and bled according to the antibody production scheme of the company.

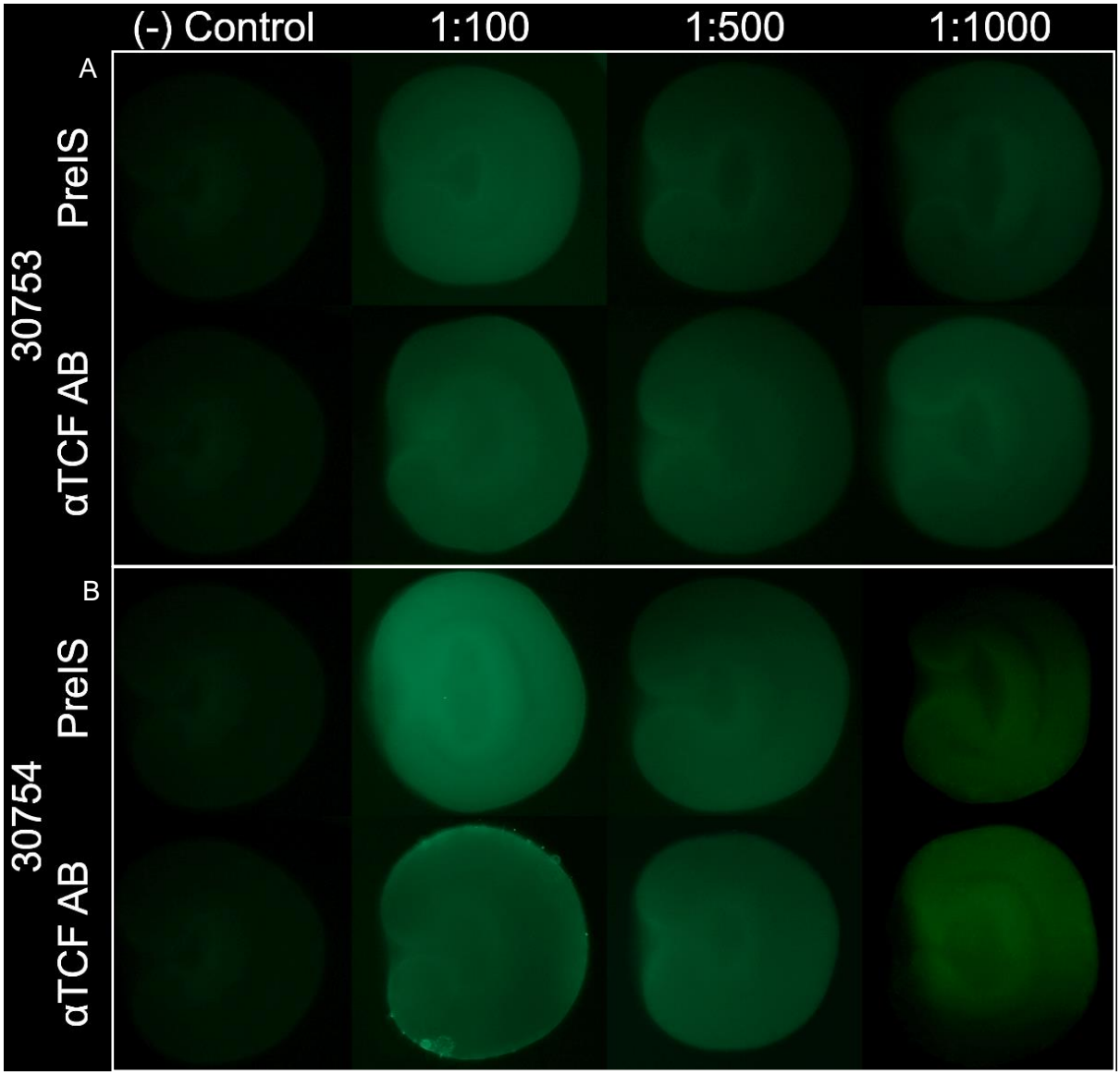

Figure 33 Immunostaining using the first batch of αTCF antibodies of rabbits 30753 (A) and 30754 (B). *Shown are the immune and their corresponding pre-immune sera at different dilutions. Also included is the control, where there was no primary AB added. Lateral views, oral to the left.*

7.2.4 Immuno- staining using boosted αTCF antibodies

Once we received the ABs, they were also tested using immunostaining, as already described in 7.2.3. The primary α-TCF AB was diluted 1:1000 and imaged with Leica TCS SP8 confocal microscope and processed with Gimp2.10.14 and Adobe Photoshop CS5 software. At dilution 1:1000, there is clear staining in the nuclei located around the blastopore (fig. 34), which perfectly corresponds to the TCF mRNA expression domain (Kraus et al., 2016). In conclusion, we were able to generate a αTCF AB, which can be used for future projects targeting canonical Wnt-signaling.

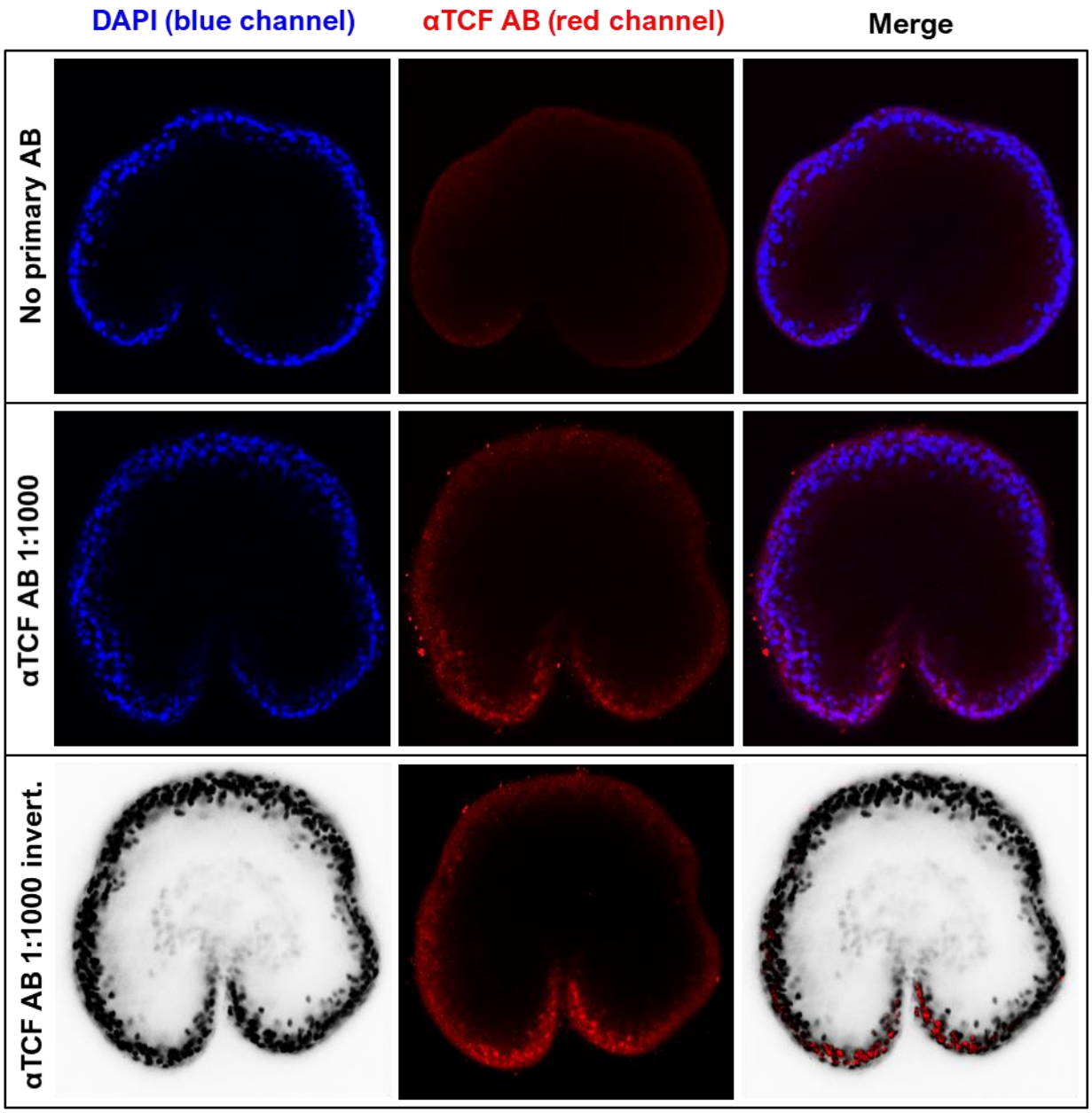

Figure 34 Immuno- staining using the boosted αTCF antibody. *Shown is the control with no primary AB (top row) and αTCF dilution 1:1000 (middle row), which is also shown inverted to make the staining more visible (bottom). Shown is the DAPI staining in the blue channel, to mark the nuclei and the TCF staining in the red channel. The last row illustrates the merge of both images. One can see that the staining of this AB is much more specific than the previous IS. It clearly marks the nuclei around the blastopore, with less background staining than before.*

8 Abstract / Zusammenfassung

8.1 Abstract

The ancient Wnt/ß-catenin signaling pathway plays a major role in different mechanisms such as cell-fate specification, proliferation, and differentiation throughout all Metazoa. In the anthozoan *Nematostella vectensis*, a bilaterally symmetric cnidarian, Wnt-signaling is also a crucial component of embryonic development and the establishment of the primary body axis. Depending on the developmental stage, overactivation of canonical Wnt-signaling can result in the formation of ectopic heads or complete oralization, meaning that this pathway has to be highly regulated to maintain appropriate signaling levels. In this Master thesis, I investigate the function of Notum, a deacylase that acts as an extracellular Wnt-signaling antagonist within a variety of different organisms. To test whether *Nematostella* Notum is also involved in regulating ß-catenin, I first performed loss-of-function experiments using inhibitor treatments, Morpholino injections and shRNA electroporations to achieve a repression or knock-down. In contrary to that, also gain-of function experiments were performed by injecting mRNA to overexpress *Notum.* The effects of these experiments were then assayed using whole mount in situ hybridizations of Wnt-responsive genes or Western blot analysis targeting active ß-catenin. In my investigations, I could not confirm that Notum acts as a Wnt-signaling antagonist or is in any way involved in regulating Wnt-signaling. However, I could recreate the previously described downregulation of *Hedgehog1* upon *Notum* RNA-interference, which suggests that Notum might play a role in the Hedgehog signaling pathway.

8.2 Zusammenfassung

Der hoch konservierte Wnt/ß-catenin Signalweg spielt eine wichtige Rolle bei vielen verschiedenen Mechanismen wie der Spezifikation, Proliferation oder Differenzierung des Zellschicksals in allen Metazoen. Bei der Seeanemone *Nematostella vectensis*, ein bilateral symmetrisches Nesseltier, ist der Wnt-Signalweg ebenfalls ein entscheidender Bestandteil der Embryonalentwicklung und der Etablierung der primären Körperachse. Abhängig vom Entwicklungsstadium, kann eine Überaktivierung des kanonischen Wnt-Signalwegs zur Bildung ektopischer Köpfe oder zur vollständigen Oralisation führen. Dies bedeutet, dass dieser Signalweg stark reguliert werden muss, um angemessene Signalintensitäten aufrechtzuerhalten. In dieser Masterarbeit untersuche ich die Funktion von Notum, einer

Deacylase, die als extrazellulärer Wnt-Signalantagonist in einer Vielzahl von verschiedenen Organismen fungiert. Um zu testen, ob *Nematostella* Notum auch an der Regulierung von ß-catenin beteiligt ist, wurden zunächst Funktionsverlust (Loss-of-Function) Experimente mit Inhibitor-Behandlungen, Morpholino-Injektionen und shRNA-Elektroporationen durchgeführt, um eine Repression oder einen Knock- Down zu erreichen. Zusätzlich dazu, wurde *Notum* als Gain-of-Function Experiment, mithilfe von mRNA- Injektionen auch überexprimiert. Der Effekt dieser Experimente wurde danach unter Verwendung von Whole- mount In situ Hybridisierungen mehrerer Wnt- Zielgenen oder Western Blots, die auf aktives ß-catenin abzielen, untersucht. In meinen Untersuchungen konnte ich nicht bestätigen, dass Notum als Wnt-Signalantagonist fungiert oder an der Regulierung des Wnt-Signalwegs in *Nematostella vectensis* beteiligt ist. Ich konnte jedoch die bereits beobachtete Herabregulierung von *Hedgehog1* nach *Notum* RNA Interferenz reproduzieren, was möglicherweise darauf hindeutet, dass Notum eine Rolle im Hedgehog-Signalweg spielt.